Evaluation of dendritic polyglycerol sulfate as inhibitor of sonic hedgehog and further pro-tumorigenic factors

Inaugural-Dissertation to obtain the academic degree

Doctor rerum naturalium (Dr. rer. nat.)

submitted to the Department of Biology, Chemistry, Pharmacy

of Freie Universität Berlin

by

Serena Rossi

Berlin, November 2019

The work presented in this thesis was carried out at the Institute of Laboratory Medicine, Clinical Chemistry and Pathobiochemistry Charité – Universitätsmedizin Berlin under the supervision of Dr. Jens Dernedde and in collaboration with the research group of Prof. Dr. Rainer Haag at the Institute of Chemistry and Biochemistry of the Freie Universität Berlin from October 2015 until November 2019.

1st Reviewer: Dr. Jens Dernedde, Charité-Universitätsmedizin Berlin

2nd Reviewer: Prof. Dr. Rainer Haag, Freie Universität Berlin

Disputation: 24.02.2020

Index

Abbreviations

ALP	alkaline phosphatase
BCC	basal cell carcinoma
BMPs	bone morphogenetic proteins
c/w	cells per well
Control CM	control conditioned medium
CW	cardin weintraub motif
DISP	dispatched protein
DMEM	dulbecco´s modified eagle medium
dPG	dendritic polyglycerol
dPGS	dendritic polyglycerol sulfate
dPGTPs	dpg-thioglyceryl pentanoatyl sulfate
ECM	extracellular matrix
ECs	endothelial cells
FBS	fetal bovine serum
FGF1	acidic-fibroblast growth factor
FGF2	basic-fibroblast growth factor
FGFs	fibroblast growth factors
GAGs	glycosaminoglycans
GlcA	glucuronic acid
Hh	hedgehog protein
HS	heparan sulfate
HSPGs	heparan sulfate proteoglycans
HUVECs	human umbilical vein endothelial cells
IC_{50}	50% inhibitory concentration
IdoA	L-iduronic acid

k_a	association rate constant
K_D	equilibrium dissociation constant
k_d	dissociation rate constant
MB	medulloblastoma
MMPs	matrix metalloproteases
Nrp-1	neuropilin-1
PTCH	patched receptor
SCK	single-cycle kinetics
SD	standard deviation
SE	standard error
SEM	standard error of the mean
Shh	sonic hedgehog
Shh CM	sonic hedgehog conditioned medium
SMO	smoothened receptor
SPR	surface plasmon resonance
TME	tumoral microenvironment
UFH	unfractionated heparin
VEGF	vascular endothelial growth factor

1 Introduction

1.1 The hallmarks of cancer

"Nothing in cancer makes sense except in the light of evolution"[1]. With this controversial sentence, paraphrasing Dobzhansky's famous dictum, Mel Greaves describes how the study of cancer in evolutionary terms has transformed our understanding over its complexity. As a matter of fact, cancer results from the unregulated proliferation of any kinds of cells in the body; as a result there are more than a hundred distinct types of cancer and for each many subtypes, implying a high degree of variability and complexity in behavior and treatment´s response [2]. Tumor growth in the host body, resembling Darwin´s model of evolution, is provoked by several progressive genetic and epigenetic mutations, which confer differential cellular advantages in terms of adaptive capabilities that progressively support the transformation from a normal cell to a malignant one. These alterations, which often include DNA mutations, but as well rearrangements, deletions, and amplifications, are largely neutral (called "passenger" mutations), whether some provide a selective growth advantage, and therefore are called "driver" mutations [3]. The driver mutations involve gain-of-function of proto-oncogenes, which turn into oncogenes, and loss-of-function of tumor suppressor genes [4]. These alterations can be inherited, caused by environmental factors such as physical (UV, ionizing radiations), chemicals (tobacco smoke, aflatoxins as food contaminant components) or biological carcinogens (virus, bacteria, and parasites), or occur as errors during natural cell´s division.

The National Cancer Institute reports that the incidence of cancer generally increases tenfold between ages 45 and 54 years with a later tenfold increase between 55 to 64 years. This trend reflects the multistep nature of cancer development as a result of the accumulation of several abnormalities over time [5]. The microevolution theory of cancer bases on the clonal evolution model of tumor proposed by Peter Nowell published in Science in 1976 [6], which in turn constitutes one of the bases of the "Hallmarks of Cancer" published by Hanahan and Weinberg in 2000 [7]. This review, which persists at the core of cancer literature, attempted to contain the complexity of cancer as a manifestation of six

essential cellular changes, which support tumor transformation. These gained capabilities, which lately in 2011 the authors updated to eight, include: functional capabilities as sustaining proliferative signaling, evasion of growth-inhibitory signals, circumvention of cell apoptosis, limitless replicative potential, induction of angiogenesis and activation of tumor invasion, and metastasis. Additional enabling characteristics include genome instability and tumor-promoting inflammation (**Figure 1**).

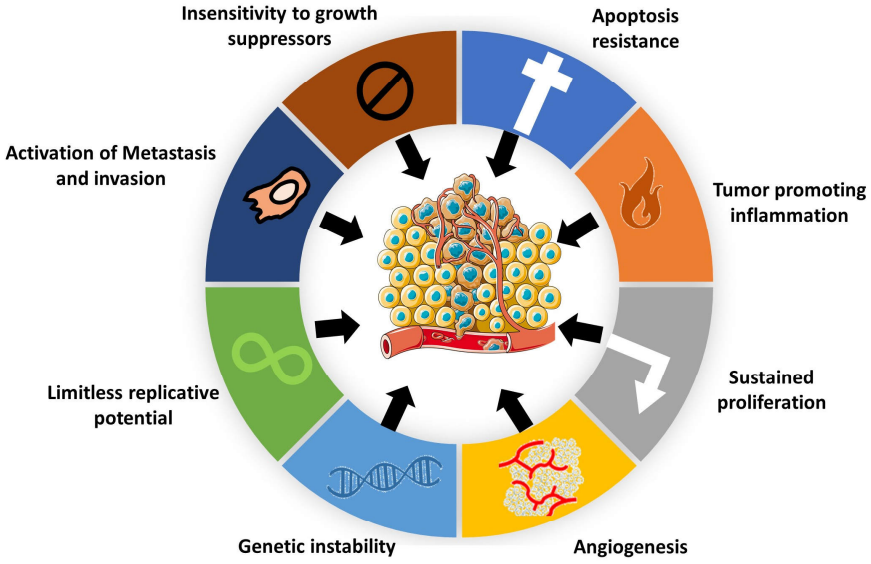

Figure 1: "The Hallmarks of cancer". The eight shared capacities acquired by the most types of tumors during neoplastic transformation, as proposed by Hanahan and Weinberg [8].

Hanahan and Weinberg successfully provided a simplified framework for describing and studying tumorigenesis by looking to its underlying principles. However, cancer is still recognized as being a highly complex and heterogeneous disease with a high degree of variability within individual tumors and within and between tumor types [9]. Its overall complexity has been challenging the researchers since the beginning of the 20th century and still today cancer is worldwide the second cause of death, with an estimated 9,6 million deaths in 2018 [10].

1.2 The tumoral microenvironment (TME)

Nowadays it is clear that carcinogenic cells are alone unable to progress toward tumor formation but must receive active support by cellular and non-cellular components of the tumor niche, which constitute the tumoral microenvironment (TME). The TME, which is constituted by stroma cells such as cancer associated fibroblasts (CAFs), endothelial cells (ECs), pericytes, leukocytes, immune cells, tumor associated macrophages and extracellular matrix (ECM). The stroma contributes to tumorigenesis by providing to cancer a permissive environment [11,12]. During tumor progression, tumor and stroma cells within the TME reciprocally communicate: cancer cells activate ECM cells by secreting signaling factors (growth factors, chemokines, and cytokines), in turn, TME cells feedback to the tumor sending growth-promoting factors, and additionally, activate extensive remodeling of ECM architecture, to favor cancer growth and spread.

1.2.1 The extracellular matrix (ECM)

The extracellular matrix (ECM) constitutes the non-cellular component of the TME, composed by a heterogeneous and dynamic complex of water, minerals, and proteins, including collagens, proteoglycans, elastin, and cell-binding glycoproteins as the major components [13]. The function of the ECM is to provide both a physical and a biochemical support structure to the resident cells [14]. In contrast to the earlier concept, which would relate the ECM to a merely passive function, we know today that ECM plays an active role in regulating cell physiology and homeostasis, being actively involved in controlling intracellular communication, cells adhesion, proliferation, differentiation, and migration [15,16].

Yet, cancer cells usurp the ECM to favor its own progression. In tumorigenic tissues, the ECM undergoes continuous structural remodeling, and its abnormal dynamics, resulting in increased stiffness, are reported as a hallmark of cancer [17,18]. During tumorigenesis, the deregulated composition and over-production of ECM components support the upregulation of many signaling pathways involved in tumor progression. Moreover, cancer cells alter the ECM arrangement via enhancing the secretion

of ECM-modifying enzymes, which enable cell infiltration through the ECM, as required during metastatic processes.

1.2.1.1 Heparan sulfate proteoglycans (HSPGs) and heparin

Diverse proteoglycans are components of the ECM and consist of a "core protein", where one or several sulfated glycosaminoglycan (GAG) side chains are covalently attached [19]. Proteoglycans are involved in the regulation of many relevant biological functions as well as several pathological processes, such as inflammation [20], angiogenesis [21], neurodegeneration [22], and cancer [23]. Notably, these functions are mainly regulated via the binding of proteins, bacteria, and viruses to distinct GAG sequences. The GAGs are unbranched highly sulfated polysaccharides consisting of several repeats of anionic disaccharide units. Depending on the different disaccharide units, the GAGs can be as well categorized into four main groups: hyaluronic acid, keratan sulfate, chondroitin/dermatan sulfate, and heparin/heparan sulfate (HS) [24].

Heparin is probably the most famous GAG, mainly concerning its anticoagulant capacity. Heparin and heparan sulfate (HS) present highly related structures (**Figure 2**). Both carbohydrate polymers derive from the same bio-precursor, the *N*-acetylheparosan (-GlcA-GlcNAc)$_n$, and are composed by α-linked repetitions of disaccharide units comprising an amino sugar (D-glucosamine (*D*-GlcN) or *N*-acetyl-*D*-glucosamine (*D*-GlcNAc) and an uronic acid (*D*-glucuronic acid (*D* -GlcA) or *L*-iduronic acid (*L*-IdoA) [25]. However, during their synthesis, they undergo epimerization and sulfation at differential positions (primarily on GlcN and IdoA) [26].

Heparin has a more homogeneous structure and is mainly composed of regular trisulfated disaccharide units (IdoA2S and GlcNS6S), eventually interrupted by uronic acid residues or undersulfated hexosamines. The high degree of sulfation and content of carboxyl groups turns heparin to the highest negatively charged known biological molecule. HS are, in contrast, more heterogeneous and, as undergo diverse post-translational modifications to generate various HSPGs, are involved in differential biological functions [27]. Furthermore, HS are characterized by lower iduronic acid (IdoA) content, a greater portion of glucuronic acid (GlcA), and overall a reduced degree of sulfation. Although both are polydisperse polymers, HS present longer chains (~30 kDa) compared to heparin (~15

kDa). Nevertheless, given the structural similarity and the reduced heterogeneity, heparin has been extensively used as an analogue of HS for functional studies [28].

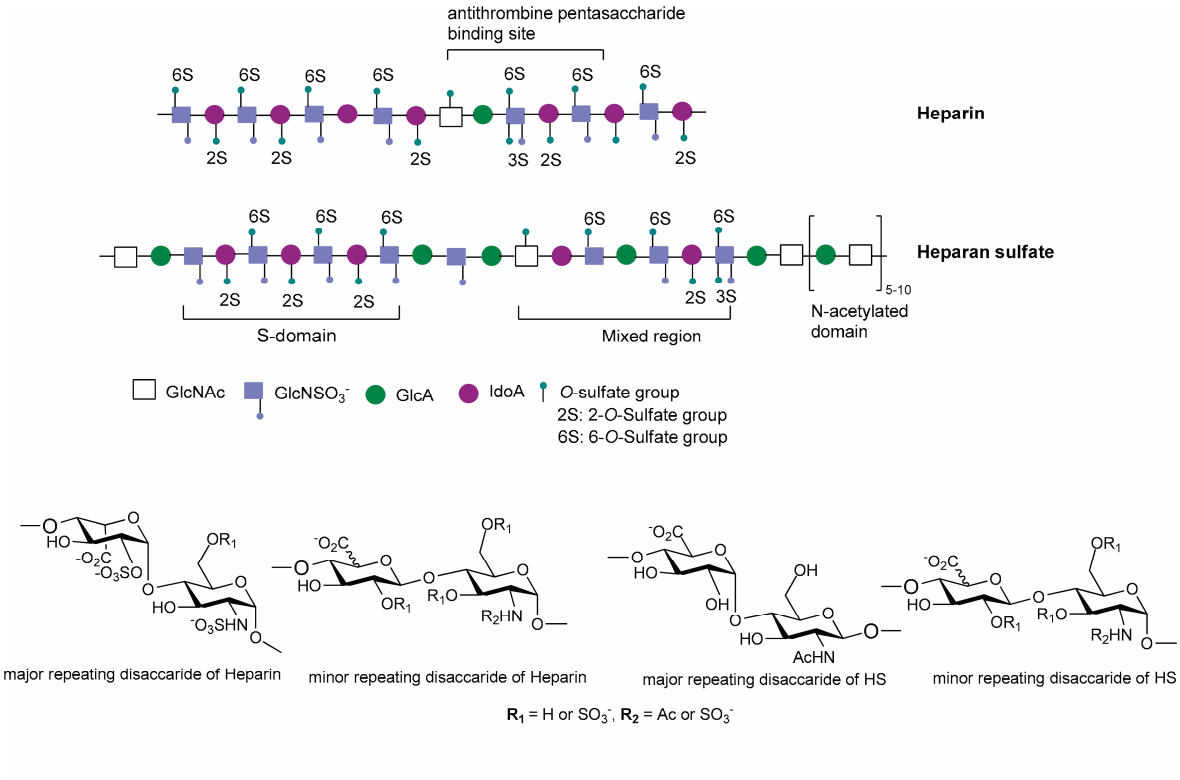

Figure 2: Heparin and HSPGs structure. Illustration of heparin and HS structure, their major and minor disaccharide repeats and binding interactions. Reprinted under the permission of Shifaza M. and Coombe D. R. [26].

While the structures show similarities, the biosynthesis of the two molecules differs substantially. HS are virtually expressed by every cell and can be located at the cell surface (as syndecans and glypicans) or found as free diffusible proteoglycans in the basement membrane and ECM (agrin, perlecan, type XVIII collagen). Heparin is indeed primarily synthetized by mast cells and found in the connective tissues; here it is stored in the granules in complex with histamine and mast-cells proteases [29,30].

1.2.1.2 Heparin/HS signaling in cancer

Functionalities of HS and heparin differ as well. HS bind to at least 300 proteins, including growth factors, morphogens, cytokines, chemokines, enzymes, enzyme inhibitors, and ECM structural proteins [31]. Via binding to the growth factors, HS regulates their activity, thereby influencing autocrine and paracrine signaling loops

involved in several physiological and pathological processes, such as cancer. The binding to HS controls mainly ligands localization and availability via protecting the growth factors from degradation, establishing a gradient in the ECM, and acting as extracellular ligand storage. Besides, HS may function as a co-receptor, directly regulating the cellular signaling controlled by the growth factors. Some HS binding growth factors elicit mitogenic and pro-angiogenic functions as fibroblast growth factor (FGF) and heparin-binding EGF-like growth factor (HBEGF), others promote tumor survival and metastasis, such as Hedgehog (Hh), whereas vascular endothelial growth factor (VEGF) has both, pro-angiogenic and metastatic functions. A comprehensive list of HS binding growth factors and cytokines is given in **Table 1**.

Receptor (HSPG)	Cytokines	Growth factors
Unspecified HSPG	IL-5, IL-6, IL-8, IL-10, CXCL12/SDF-1, TNF-α, and PF-4	**FGF1, FGF2, FGF4, FGF7, FGF8, FGF10, and FGF18; HGF, PDGF, HBEGF, Neuregulin-1, VEGF, BMP-7, Noggin, Hh**
SDC1–4	CXCL12/SDF-1	**FGF2, HGF, VEGF, HBEGF, Hh**, Midkine, Pleiotrophin, TGF-β, Wnt
GPC1–8		**FGF1, FGF2, HGF, VEGF, BMP-7, Hh**, Wnt, TGF-β, Midkine, IGF
Agrin		**FGF2**
Perlecan		**FGF2,** FGF7
TβRIII		**FGF2,** TGF-β1, TGF-β2, TGF-β3, inhibin, **BMP-7**, BMP-2, BMP-4, GDF-5
CD44	MCP-1	**FGF2, VEGF, HBEGF, HGF**
Nrp1–2		**FGF2, FGF4, VEGF**, PIGF, PDGFB, semaphorins, TGF-β

Table 1: HSPGs and their binding interactions. In bold are highlighted the growth factors with confirmed affinity to both HS and heparin. Table reprinted under permission of Knelson E. H. et al. [27]. The references can be found in the original work.

The HS-binding proteins constitute the "heparin interactome", as most of the proteins have been identified via heparin-affinity chromatography. Considerably, the majority of the proteins bind to HS mainly via electrostatic interaction mediated by their positively charged Arg/Lys residues. In addition, the basic sequence is often aligned in an evolutionary conserved motif as the "Cardin Weintraub" motif [CW: XBBBXXBX, where B are a basic Arg/Lys residues and X stands for hydropathic residues (Ala, Gly, Ile, Leu or Tyr)], discovered as a proteins consensus sequence for heparin recognition [32,33]. Nevertheless, the binding of HS/heparin to proteins depends as well on the binding to

further accessible basic residues outside the consensus motif, which contribute to tightly regulate the protein functionalities, in a context and protein-specific manner.

Besides growth factors and cytokines, HS is the native substrate for enzymes as extracellular endosulfatases (Sulf-1 and Sulf-2) and the endoglucoronidase heparanase, which can degrade or alter the structure of HS, not only supporting the tumor invasiveness but also increasing the availability of the bound growth factors. Relevantly, both HS and heparin share the same recognition sites on the heparanase sequence [34].

Regarding heparin, its physiological role remains mostly unclear, but its storage within specific granule in mast cells points to a regulatory role during inflammation [35,36]. As animal-derived material, commonly purified from porcine intestine, unfractionated heparin (UFH) has been used since 1935 extensively in the clinic as anticoagulant for treating clotting disorders and after surgery. Its anti-thrombotic potential relies mostly on its high affinity for the serine protease inhibitor antithrombin III (AT). Independently on anticoagulation and giving its high affinity to a wide variety of proteins (i.e., heparanase and HS-binding proteins), more therapeutic functionalities ranging from anti-tumorigenic [37], anti-angiogenic [38], anti-inflammatory [39–41] and antiviral [42]. Nevertheless, heparin suffers from some limitations: high polydispersity and, due to its animal origin, the risk of contamination and disease transmission.

Based on the affinity for heparin/HS to proteins relevant in tumorigenic cascades, the following chapters focus on the description of two major tumoral processes: the hedgehog signaling pathway and angiogenesis and their relation to HS/heparin interactions.

1.3 The Hedgehog (Hh) signaling pathway

As previously mentioned, the morphogen Hedgehog (Hh) interacts with HSPGs expressed on the cell surface and located in the ECM. Hh is the ligand responsible for the initiation of the Hh pathway, and it has been shown that the interaction with HSPGs plays an essential role in pathway regulation [43].

The evolutionary conserved Hh signaling pathway is one of the diverse signaling pathways physiologically operating in embryogenesis and organogenesis. During early

mammalian embryonic development, the Hh ligand expressed and released by the cell, acts as a morphogen, thus forming long-range concentration gradients by which regulates differential cells fate decisions. In embryos, Hh signaling controls cell proliferation, survival, tissue patterning, and vascularization. Notably, in adult tissue, the Hh pathway is mostly inactive or poorly activated and maintains the homeostasis of stem cells and pluripotent cells involved in tissue repair as mammary, skin, nervous system, lung stem cells and intestine [44–48].

Over the last decades, growing evidence suggests that mutations within the cascade lead to aberrant Hh pathway activation involved at various stages during initiation, progression, and invasion of several types of tumors [49]. Aberrant Hh signaling activation is commonly associated with basal cell carcinoma (BCC), the most common type of skin cancer, medulloblastoma (MB), the most common type of pediatric malignant primary brain tumor, and rhabdomyosarcoma, a sarcoma of skeletal muscles cells [50–52]. Despite these well-recognized cancers, Hh aberrant activation is implicated in the development of other cancer types such as glioma, breast, ovarian, colon, gastric, pancreatic, prostate, and small-cell carcinoma [53,54].

1.3.1 Sonic hedgehog (Shh) ligand

Mutations in the *Hh* gene were first discovered in 1980 by Nüsslein-Volhard and Wieschaus with the aim to identify genetic alterations affecting segmentation and polarity during the development of larval bodies in *Drosophila melanogaster* [55]. As the name suggests, the Hh mutations are responsible for the generation of a “spiked” phenotype of the Hh mutant *Drosophila* larvae, where full body-denticles resemble the spines of a hedgehog. In contrast to *Drosophila*, which possesses only one Hh gene, higher organisms have several, and in mammals, three orthologous are conserved: Sonic hedgehog (*Shh*), Desert hedgehog (*Dhh*) and Indian hedgehog (*Ihh*). All three ligands bind equally strong to their receptors but elicit different biological activities [56]. Among those, Sonic hedgehog has gathered the highest interest due to its expression and central role in the development of various organs during embryogenesis.

The first key component of the pathway is the Shh ligand that is initially synthesized as 46 kDa precursor protein consisting of two units: an N-terminal signaling element domain and a C-terminal protease domain. In the endoplasmic reticulum, the N-terminal domain undergoes autocatalytic cleavage operated by the C-terminal domain and releases a 19 kDa active unit, called Shh-N (**Figure 3**). The nascent peptide is further modified via two post-translational lipid modifications. The first modification is operated by the catalytic C-terminal domain and consists of an intramolecular cholesterol transfer on the carboxyl end of the N-terminal fragment [57]. The second modification is catalyzed by a O-acyltransferase (Hhat), which modifies the peptide by the addition of a palmitoyl group at the Cys-24, resulting in an extremely hydrophobic molecule (Shh-Np, standing for Shh-N processed) [58]. The hydrophobic nature of the dually modified Shh-N enhances the membrane tethering of the protein, whereas the form of Shh that lacks cholesterol modification (Shh-Nu, Shh-N unprocessed) is easily expressed and released in the cell medium [59].

Several studies showed that cholesterol modification is essential during development for both long-range signaling and pathway maximal activity [60–63]. The palmitoyl modification seems in addition being determinant for the signaling functionality. Mutations resulting in Shh-N lacking the palmitoyl group showed reduced pattern activity both in the mouse and *Drosophila* [62,64–66]. Curiously, the highly lipidated nature of Shh may seem to be in contrast with its morphogenic character; to form a concentration gradient, Shh should freely diffuse instead lipid modifications seem to decrease the ligand solubility. However, it is today clear that the modifications are parts of a tightly regulated process in which proteins like Dispatched (DISP), which binds to Shh in a cholesterol-dependent manner via a sterol sensor domain, are responsible for the release of the ligand (**Figure 3**) [49,67]. An additional secreted protein, the soluble glycoprotein Scube2, is implicated in Shh ligand release via alternative affinity to the cholesterol motif [68,69]. Additionally, the release of Shh is shown to be operated via proteolytic cleavage by cellular sheddases, the ADAMs (a disintegrin and metalloproteases), which remove the palmitoyl lipidated terminal peptide, enabling ligand solubilization [70]. Furthermore, Shh ligands are known to self-associate and multimerize at the cell surface membrane via both lipid modifications. Nevertheless, the exact contribution of each modification is still not clear [64,65]. The multimeric complexes at the membrane become diffusible via complex

formation with lipoproteins and micelles, alternatively there are internalized into intraluminal vesicles, which are lately secreted as exovesicles (**Figure 3**) [71].

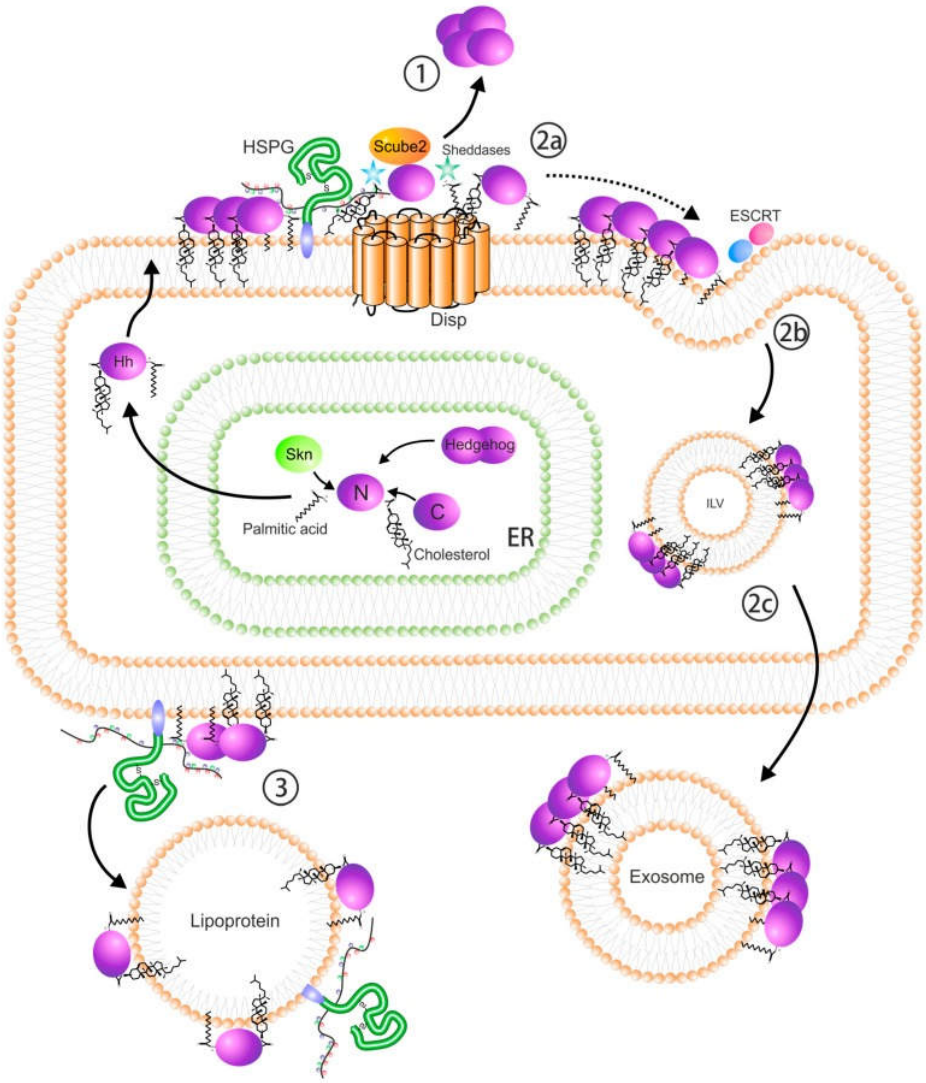

Figure 3: Shh-N ligand synthesis and releasing routes. In the endoplasmatic reticulum, the Shh precursor undergoes autocatalytic cleavage followed by lipid post-translational modifications resulting in Shh-N terminal fragment carrying cholesterol and palmitoyl motif. Shh-N is released extracellularly via diverse mechanisms: **1**: Disp and Scube2 enable the cleavage of monomeric Shh-N via cholesterol removal, whether sheddases remove the palmitoyl motif. HSPGs act as protein scaffolds and participate in regulating the protein cleavage and facilitating Shh-N multimerization. **2**: Lipidated membrane-bound Shh-N can be alternatively internalized into intraluminal vesicles (2b) which subsequently fuse with the plasma membrane and are released as exosomes (2c). **3**: Binding of Shh to HSPGs might regulate the localization of Shh proteins into secreted lipoproteins. Picture reprinted from Ramsbottom et al. [72] licensed under Creative Commons Attribution 4.0 International License.

The interaction of Shh to HSPGs is known to play a central role in pathway activation, although the mechanism remains partially unclear. In 1998, Bellaiche and

colleagues provided in *Drosophila* the first confirmation of the role of HSPGs in Shh signaling. Mutation in the genes codifying for enzymes required in HS synthesis resulted in altered Hh signaling [73]. In 2008, Vyas and colleagues confirmed the colocalization of Hh nanoscale oligomers with HSPGs at the surface of the ligand producing cells [74]. Following, several studies described the binding of Shh to heparin/HS [75–77]. The interaction between Shh and HSPGs counts on the electrostatic binding between HS chains and the N-terminal region of Shh carrying the heparin-binding Cardin-Weintraub (CW) motif (Lys 32-38 for the human sequence). Experimental evidence suggests that HSPGs act as a scaffold, allowing Shh ligand accumulation at the surface of the ligand-producing cell, which enables Shh multimerization and release as diffusible multimeric complexes [64]. Speculations about the activity of HSPGs as Shh co-receptor, concern prevention and promotion of signaling by stabilizing the ligand/receptor complex [78]. In addition, the CW motif of Shh seems to be the recognition site for Shh sheddase-dependent cleavage and release [70]. In this perspective, several studies support the idea that the HSPGs via binding to the CW motif would compete with the sheddase for Shh release, thus regulating the ligand solubilization and thereby signaling activity [68,79]. Finally, a recent *in vivo* and *in vitro* study confirmed the relevance of CW binding to HSPGs to control ligand release and showed that soluble heparin and HS, via binding to Shh, inhibit its interaction to the receptor in a charge degree-dependent manner [80]. Intriguingly, other *in vitro* studies reported that the deletion of the CW reduces but does not eliminate the interaction between Shh and HS/heparin and does not alter Shh-induced embryonic patterning *in vivo* [81]. In this context, Chang et al. showed that also the Lys 178 (human sequence) is involved in the binding to heparin and that its deletion results in reduced pathway activity [82]. Moreover, a recent study examining the crystal structure of complexes formed by Shh and heparin revealed the presence of an evolutionary conserved GAG-binding site (Lys 87, Arg 123, Arg 153, and Arg 155- human sequence), which besides the CW motif, contributes to the interaction of Shh with HSPGs and additionally localizes in the proximity of the receptor-recognition site [83].

1.3.2 Shh signaling cascade

The Shh-signaling cascade, as described in **Figure 4**, is initiated by the binding of processed Shh-N to the transmembrane receptor Patched 1 (PTCH). In the absence of the ligand, PTCH acts as an inhibitor on a seven transmembrane-span receptor called Smoothened (SMO), a G-protein coupled receptor, preventing its activity, probably via preventing its localization on the cell surface [85]. However, the binding of Shh ligand to PTCH resolves its inhibitory activity on SMO, leading to SMO activation. At this point, while active-SMO and other down-stream pathway components translocate to a non-motile primary cilium structure on the cell membrane, the complex PTCH-Shh is internalized and degraded in the lysosomes [86]. The most relevant components at this stage are the zinc finger glioma-associated (GLI)-transcription factors GLI1, 2, and 3. The GLI factors are located at the top of the primary cilium and are activated upon SMO activation [87]. While GLI2 primarily functions as an activator and GLI3 mostly as a repressor [88], GLI1 acts only as an activator. GLI1 is negatively regulated by the binding to the Suppressor of Fused (SuFu), which prevents GLI1 from entering the nucleus [89]. Upon Shh pathway activation, SuFu-GLI complex dissociates allowing GLI to enter the nucleus [90]. In the nucleus, GLI activates the expression of the Shh pathway target genes via binding to the respective promoters. Transcription permits not only the perpetuation of the positive Shh-pathway feedback (i.e., *GLI1*, *PTCH1-2*) [91] but also promotes proliferation and tumorigenesis (i.e., *Cyclin-D1*, *MYCN*) [92], apoptosis (i.e., *BCL-2*) [93], angiogenesis (i.e.*, VEGFA*) [94], epithelial-to-mesenchymal transition in metastasis (*SNAIL*) [95], stem cell self-renewal (i.e., *NANOG*, *SOX2*) [96], Notch signaling pathway (*JAG1*) [97] and tissue repair (*FGF4*) [98]. As well, the existence of crosstalk between the Hh pathway and Wnt signaling has been shown [99]. Recently, two GLI transcript isoforms have been identified: an N-terminal deletion (GLI1ΔN) [100] and a truncated GLI1 variant (tGLI1) [101]. Notably, tGLI1 is expressed only in cancer cells and tissues and acts as a GLI1 gain-of-function variant, activating target genes (i.e., Heparanase 1 (*HPA1*), *VEGFR2* and *CD24*) not regulated by GLI1, thereby supporting the development of more aggressive cancer phenotypes [101,102].

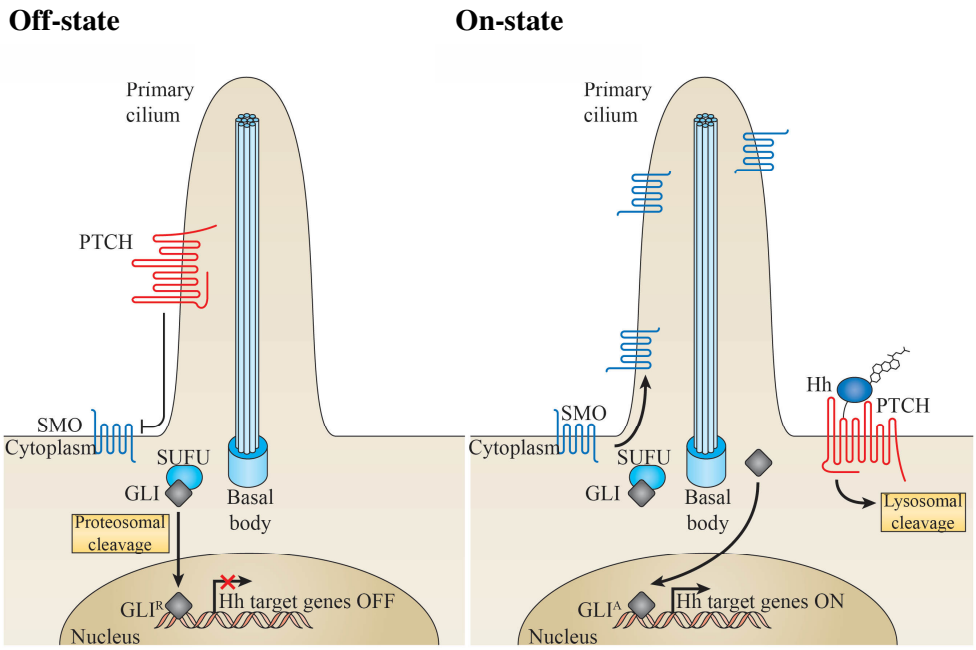

Figure 4: Shh signaling cascade. Shh-pathway cascade activated upon binding of Shh to PTCH receptor (on state). The binding releases the inhibitory activity operated by PTCH on receptor SMO (off-state). SMO moves into a primary cilium structure along the membrane and activates GLI-transcription factors, which translocate to the nucleus and activate the transcription of Shh-pathway target genes. Reprinted under the permission of Amakye D. et al., 2013 [84].

1.3.3 Models of signaling cascade activation in cancer

The cascade model described above mostly refers to the canonical, classical pathway activation via Shh ligand binding to the PTCH receptor. In cancer, a total of four basic models of Shh signaling pathway activation have been proposed [103].

The type I pathway cancers are characterized by non-classical signaling that harbors Shh-pathway driven mutations. They can be loss-of-function mutations of PTCH or SUFU and gain-of-function of SMO, leading to permanent ligand-independent cascade activation. The type I cancers are strongly associated with BCC [104], MB, and occasional rhabdomyosarcoma [105,106]. In addition to genetic mutations affecting the members of the cascade, multiple crosstalk pathways can lead to Shh pathway activation ligand-independently. Examples for these interactions are reported for tumor necrosis factor-α and interleukin-1β, which upregulate GLI1 through the NF-κB pathway in pancreatic and breast

cancer [107,108] and the upregulation of GLI activity by RAS/RAF/MEK/ERK and PI3K/AKT pathways [109].

In the type II autocrine-juxtracrine model, there is an over-expression of Hh ligand, both produced and returned to the same or nearby located tumor cells, supporting cancer cell proliferation and survival. Additionally, high Shh ligand expression associates with upregulated *PTCH* and *GLI* expression [110]. In the last decades, the type II Shh pathway activation has been associated with a wide variety of tumors, including lung, stomach, breast, pancreas, prostate, liver, and brain [47,111–117].

In type III paracrine signaling, the Shh ligand produced by the tumor cells is received by the stroma cells, which then feedback the tumor cells by producing and secreting signaling molecules (such as VEGF, IGF, PDGF, and BMPs) that further support cancer cells growth. Recent evidence suggests that Shh ligand overexpressing cancers might be refractory to the ligand while the tumoral stroma is ligand-responsive [118,119]. Fan and colleagues showed that prostate cancer activates paracrine Shh mechanism [120]. Additionally, Theunissen and Sauvage support this finding [121]. More evidence suggested that in pancreatic ductal adenocarcinoma (PDAC) the paracrine activation Shh signal might be the principle mechanism supporting tumor growth, whether tumor cells might not be responsive to Shh ligand themselves [119,122–124]. Lately, it has been also recognized a further model of Shh signaling, called type III reverse paracrine, in which Shh is secreted from the stroma and targets back the tumor cells. However, so far, the inverse paracrine model has been only observed in hematological cancers [118].

1.3.4 Shh signaling inhibitors

In **Table 2** are reported some of the most common Shh inhibitors as part of a long list, including more than 50 drugs with diverse targets within the signaling cascade. The most common targets for inhibitors design are Shh ligand, SMO receptor, and GLI transcription factors. To date, only three SMO-specific inhibitors, Vismodegib, Sonidegib, and Glasdegib, received the US Food and Drug Administration (FDA) approval. Cyclopamine derives from the corn lily *Veratrum californicum*, belongs to the family of

steroidal alkaloids and was the first SMO inhibitor discovered in 1998 [125]. Lately, the potential of cyclopamine in cancer treatment has been reported, and cyclopamine became a model drug for studying the Shh-signaling pathway [54,126]. However, low oral solubility, reduced potency, and associated toxicity limited its progress in clinics [127].

Target	Drug
Shh ligand	Neutralizing antibodies (5E1) [128] Robotnikin[129] RU-SKI 43[130]
SMO	Cyclopamine [125] Saridegib (IPI-926)[131] Vismodegib (GDC-0449)[132] Sonidegib (LDE-225)[133] Taladegib (LY2940680)[134] Glasdegib (PF-04449913)[135] Itraconazole[136]
Gli factors	GANT58/GANT61[137] Arsenic trioxide (ATO)[138]

Table 2: Shh pathway inhibitors.

Vismodegib, a cyclopamine derivative, was the first specifically designed Shh-inhibitor synthesized in 2009. In 2012, Vismodegib received FDA approval for the treatment of metastatic basal cell carcinomas (BCCs) [139,140]. To date, 42 clinical trials using Vismodegib have been completed, and many of them investigated the anticancer potential of Vismodegib in various types of cancer as pancreatic (NCT01088815)[1], ovarian (NCT00739661), colorectal (NCT00636610), prostate (NCT02115828), lung (NCT00887159), to mention some. However, limitations related to SMO antagonists are represented by the development of therapeutic resistance linked to acquired mutations in

[1] Clinical trial NCT identification number

the drug-binding pocket of SMO, amplification of downstream GLI transcription factors, or upregulation of the Hh pathway by synergistic SMO-independent signals [127,141,142].

GLI inhibitors represent an emerging alternative therapy. These inhibitors not only act downstream of SMO, and therefore are effective likewise in tumors carrying SMO mutations but acting directly on GLI factors, result successful in inhibiting also the non-canonical Hh pathway activation by other oncogenic pathways [54]. GANT58 and GANT61 are two small synthetic inhibitors targeting GLI. GANT61 is the most studied and efficient GLI antagonist. GANT61 binds to the zinc finger regions 2 and 3 of GLI1 and GLI2 and thereby interferes with GLI nuclear translocation and GLI-to-DNA binding, [143]. The anti-tumorigenic efficiency of GANT61 has been reported for several cancer types such as lung, breast, pancreatic cancer, and acute myeloid leukemia both *in vitro* and *in vivo* [137,144–146]. So far, GANT61 did not reach clinical trials.

Direct targeting of Shh ligand, is also an emerging therapeutic strategy. Petrova and colleagues discovered in a screen for inhibitors of the hedgehog acyltransferase (Hhat), an enzyme responsible for Shh palmitoylation, the compound RU-SKI 43. [130]. The authors demonstrated the anti-tumorigenic potential of RU-SKI 43, also *in vivo* in a mouse xenograft model of pancreatic cancer [147]. Instead, the monoclonal inhibitory Shh antibody 5E1 binds to Shh with a low nanomolar affinity, preventing its interaction with the PTCH receptor and thereby blocking the cascade activation [148]. 5E1 caused growth inhibition of medulloblastoma, as well as reduces pancreatic tumor growth in mouse xenografts [149,150]. However, none of these Shh-inhibitors reached clinical trials so far. Only recently, Manikowski et al. studied the capacity of heparin and HS oligosaccharides to inhibit Shh-pathway activation and to reduce ligand solubilization [80]. Nevertheless, to date, no heparin/HS mimetics have been described as Shh signaling inhibitors.

1.4 Tumor Angiogenesis

As previously mentioned, HSPGs bind to several growth factors and enzymes, which are involved in activating and supporting angiogenesis. In a physiological context, angiogenesis, as a coordinated and complex process, regulates the formation of new blood vessels from the pre-existing ones in response to certain stimuli in the body. In cancer, this

process is known as tumor angiogenesis and represents a key factor for supporting tumor growth, proliferation and metastasis [151,152].

The first confirmation of the interconnection between angiogenesis and tumorigenesis was discovered in 1945 when Algire and Chalkey first concluded that the growth of a solid tumor must be closely connected to the development of a rich vascular network [153]. Almost 20 years later, in 1971, the surgeon Folkman first hypothesized that targeting neovascularization would block or even reduce tumor growth. His hypothesis based on the findings that most tumors stop growing when they reach 1-2 mm^3 in size in an avascular state and enter a dormant viable state [154].

1.4.1 Molecular mechanism of angiogenesis: the "angiogenic switch"

The induction of tumor vasculature is also known as the "angiogenic switch" that follows the "tumor dormancy" phase, which can last over the years. The angiogenic switch is regulated by the equilibrium between positive (pro-angiogenic) and negative (anti-angiogenic) factors that control tumorigenic homeostasis [155]. The induction of the angiogenic switch occurs when the "balance" tips in favor of pro-angiogenic molecules, as schematically shown in **Figure 5**; at this point, the tumor assumes the angiogenic phenotype and neovascularization is induced.

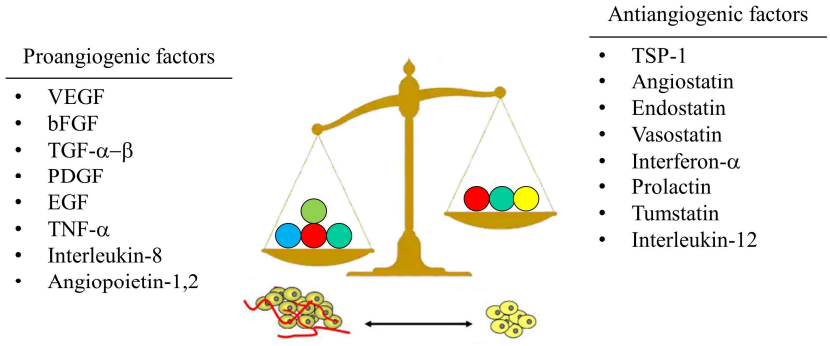

Figure 5: The "angiogenic switch". Schematic representation of the "angiogenic switch" as a balance of pro- and anti-angiogenic molecules.

The difference between physiological angiogenesis during body development and pathological angiogenesis in tumors lies in the tight regulation of the angiogenic balance. In tumors, in fact, the balance between pro and anti-angiogenic factors is lost, leading to the constant growth of new tumor vasculature and loss of vessel quiescence, overall resulting in a highly disorganized blood vessel architecture [156]. The dysregulated angiogenic signals act in response to the demand of nutrients and oxygen to support tumor growth.

Several stimuli contribute to the angiogenic switch. These are not only genetic mutations, leading to expression of oncogenic proteins and loss of tumor suppressors, but as well metabolic stress, such as lack of oxygen (hypoxia), low acidic pH and lack of nutrients, mechanical stress and immune/inflammatory response [157,158]. How these genetic and environmental signals play together to induce the angiogenic switch still remains unclear. Afterward, as a result of the angiogenic engagement, there is a reduction of anti-angiogenic factors parallel to a vigorous expression and release into the TME of several pro-angiogenic factors, such as VEGF and FGF (considered as the strongest angiogenic molecules), platelet-derived growth factor (PDGF), epidermal growth factor (EGF); transforming growth factor α-β (TGF-α-β), interleukin-8 (IL-8), metalloproteases (MMPs) and heparanase [159]. Once the pro-angiogenic factors are released, they contribute directly and indirectly to ECs activation and initiate the angiogenesis cascade.

1.4.2 Vascular endothelial growth factor (VEGF)

One of the most known and studied cytokines, given its crucial rule in angiogenesis, is the factor VEGF, known as VEGF-A, discovered and cloned in 1989 by Napoleone Ferrara [160]. VEGF-A was first identified for its capacity to increase vascular permeability and therefore also called vascular permeability factor (VPF). The first insights highlighting the importance of VEGF in angiogenesis came from genetic targeting experiments in mice in 1996. These experiments showed that in case of elimination of both VEGF alleles, almost complete absence of vasculature structure was observed and the mice underwent earlier embryonic death in comparison to the disruption of one allele [161,162].

At today, VEGF-A is the most potent known angiogenic factor, involved not only to increase vessel leakage but also in stimulating ECs proliferation, survival, and migration. VEGF-A is one of the six cytokines members of the VEGF/ placental growth factor (P1GF) family. Notably, VEGF-A is mostly involved in angiogenesis, whether others mostly regulate lymphangiogenesis [152]. VEGF-A is expressed as a homodimeric protein of 45 kDa molecular weight in four spliced isoforms ($VEGF_{121}$, $VEGF_{165}$, $VEGF_{189,}$ and $VEGF_{206}$) with $VEGF_{165}$ being the most predominant variant [163]. Except for $VEGF_{121}$, which is a diffusible factor, all the other factors bind to heparin and HS in the ECM and on the cell surface [164].

VEGF activates the ECs via binding to the specific receptors VEGFR-1 and VEGFR-2, which are receptor tyrosine kinases expressed exclusively on the ECs. The major angiogenic effects, however, are due to the binding of VEGF to VEGFR-2 (**Figure 6**). The binding leads to the receptor dimerization, autophosphorylation followed by activation of diverse signaling proteins, such as protein kinase C (PKC), protein kinase B (PKB/AKT) and p38 mitogen-activated protein kinases (p38/MAPK). These effectors are responsible for the activation of several downstream signaling pathways that modulate angiogenesis. Briefly, the complex VEGF-activated network includes the RAS/RAF/MEK/ERK signal cascade, known for promoting growth factor-induced ECs proliferation, PI3K-AKT signaling, which regulates cells survival, anti-apoptotic functions and permeability, p38/MAPK and FAK/paxillin pathways involved in cytoskeleton reorganization and migration of ECs. Although it might be possible to recognize specific pathways following the binding of VEGF to its receptor, the activated cascades are intricated, and many effectors represent a high level of redundancy. As a result, a complex network gets activated. The activity of VEGF and the binding to its receptor is dependent upon the binding with HSPG co-receptors like neuropilins (as Nrp-1) or other HSPGs (**Figure 6**). The binding to HSPGs regulates not only the ligand distribution and availability but also enables the formation of a ternary complex (receptor/ligand/HS) controlling ligand/receptor stability, internalization and degradation [165–167]. In 1992 and 1994, we had the first confirmations that soluble heparin and cell-associated heparin-like molecules, even though via a weak association to VEGF, are essential for the binding of VEGF to its receptor [168,169]. The authors first confirmed via a cell-based ligand/receptor binding studies that heparin and HS at the low concentrations increase the binding affinity for

VEGF to its receptors, whereas only higher concentrations lead to progressive binding inhibition [169]. Furthermore, both VEGR2 and co-receptor Nrp-1 carry an heparin-binding sequence supporting the binding [170,171]. This opens the doors to a more complex scenario for both interactions and VEGF functionality, in which HS/heparin enhances synergistically the binding of VEGF to its receptor and the co-receptor [172].

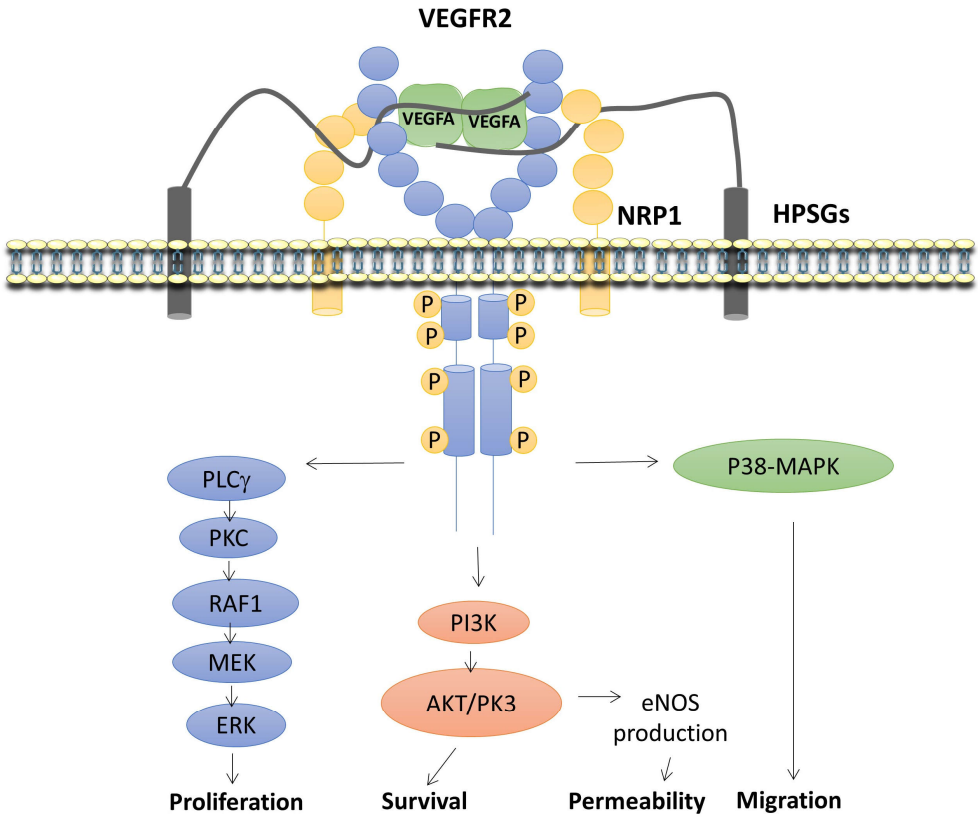

Figure 6: VEGF signaling in angiogenesis. The binding of VEGF-A to VEGFR is regulated as well by the interaction with an HSPG co-receptor like neuropilins (Nrp-1) and other HSPGs. Upon the receptor-ligand binding, the receptor undergoes dimerization and autophosphorylation of tyrosine residues on the kinase domain, which then activate several down-stream cascades. In the picture, some of the most relevant intracellular activated pathways are schematically represented.

1.4.3 Fibroblast growth factors (FGFs)

In mammals, the family of fibroblast growth factors (FGFs) is composed of 18 different proteins (FGF1-FGF10 and FGF16-FGF23) which can be further categorized into six groups with five paracrine subgroups and one endocrine subgroup, based on the similarity of their sequences [173]. FGF1 (known as acidic FGF) and FGF2 (known as

basic FGF) are paracrine factors and constitute the prototype members of this family [174,175].

The FGFs are involved in the regulation of many processes involving cell growth, migration and cell differentiation in embryonic development, as well as angiogenesis and wound healing in complex diseases, such as cancer. Both FGF1 and FGF2 factors are reported to stimulate migration and proliferation of ECs *in vivo* and to present anti-apoptotic activity [176,177].

The molecular characterization of FGFs dated 1980 when Shing and colleagues, in a search for angiogenic molecules secreted by cancer cells, identified FGFs molecules via heparin affinity chromatography [178]. The discovery led emerge another characteristic of the FGFs: besides their high angiogenic potential, they show a high affinity to heparin and HSPGs located in the ECM or at the cells surface. The binding with HSPGs serves again as a reservoir for growth factors and protects them from proteolytic degradation. In the context of HSPGs-protein binding, the interaction with FGF is the most well-studied example (**Figure 7**). Like VEGF, also for FGFs, the HSPGs act as co-receptors presenting heparin-binding domain on both receptor (tyrosine kinase receptors FGFR1-4) and ligand, enabling the formation of a ternary complex [179]. Upon the binding of FGFs, HSPGs to FGFRs, the receptor dimerizes and undergoes transphosphorylation. The phosphorylation results in the activation of effectors proteins as Grb2, SHP2, and Gab1 which enable the activation of several downstream cascades involved in angiogenesis (**Figure 7**) [173]. In brief, the pathways RAS/RAF/MEK/ERK and p38/MAPK regulate cell proliferation, differentiation, and migration; the PI3K/Akt pathway is essential for controlling cell survival and other relevant processes, whereas the activation of PLCγ, followed by IP3 recruitment, controls Ca^{2+} cellular release.

The complex interplay of FGFs with several molecules may explain the differential functionalities of FGFs, capable of eliciting different effects on the same cell line in a specific context-dependent manner [180]. In addition, FGFs differently than VEGF, are pleiotropic molecules capable of acting on a variety of cell types; a property which might reflect the capacity of FGFs to modulate angiogenesis by regulating various cell to cell interactions [181].

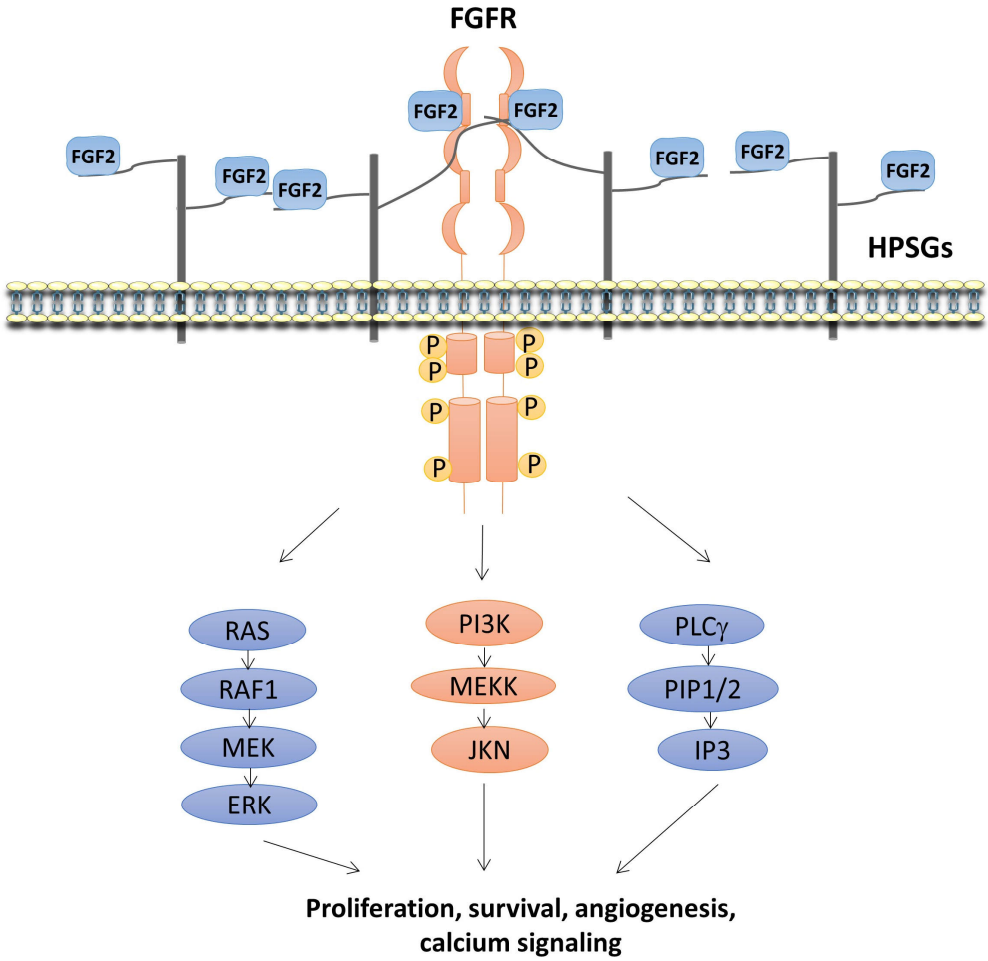

Figure 7: FGFs signaling in angiogenesis. The activation of FGF-signaling depends upon the binding of FGF ligand to FGFR and to HSPGs to both receptor and ligand (ternary complex). Activation leads to receptor dimerization and autophosphorylation of the tyrosine residues on the kinase domain. The phosphorylation controls the activation of several intracellular signals, as schematically represented in the picture.

Concerning the function of each FGFs, several genetic studies have been performed using knock-out mice, but all failed in clarifying the unique function of the growth factors. Knock-out embryo mice *Fgfr1 -/-* or *Fgfr2 -/-* die at very early stages during development, further limiting the study of FGFs contribution in developmental neovascularization [182,183]. Additionally, neither *Fgfr3 -/-* nor *Fgfr4 -/-* knockout mice showed vascular deficiencies. Furthermore, in contrast to VEGF, which is a potent inducer of vascular permeability known to cause edema and to lead the formation of hemangiomas high concentrations, FGFs overexpression does not result in these damaging effects [184].

Interestingly, FGF2 and VEGF elicit independent effects on the ECs, concerning gene expression and type of capillaries. Besides, FGF2 stimulates the expression of VEGF

in ECs and stroma cells, which is additionally required to initiate signals in response to FGF2. Contrarily, VEGF activity results independent of FGF2 [185]. In this sense, the FGFs and other growth factors simultaneously orchestrate the complex angiogenic response.

1.4.4 Heparanase

As previously mentioned, invasion and metastasis of cancer cells involve the degradation of ECM that is predominantly composed of collagens, laminins, fibronectin, vitronectin, and HSPGs. Cancer cells, via the combined activity of metalloproteases (MMPs), endoglycosidases as heparanase, serine, and cysteine proteases, enable the degradation and remodeling of the ECM. Heparanase is a mammalian enzyme (endo-β-glucuronidase) that degrades HS of proteoglycans, thereby enabling cell migration and egress from blood vessels. Thus, heparanase plays a key role in supporting cancer metastasis, angiogenesis, and inflammation [186–189].

The direct role of heparanase in angiogenesis, similarly to its metastatic function, is linked to the degradation of the HS chains of the subendothelial capillary basement membrane, which enables the ECs invasion and movement toward the angiogenic stimuli during tumor growth. Besides the direct role of heparanase in angiogenesis, the enzyme also regulates indirectly the angiogenic signaling cascade by releasing HS-bound angiogenic growth factors as FGFs, VEGF and by generating HS fragments which promote FGFs/VEGF-receptor binding, dimerization, and signaling [190].

At first, the activity of mammalian heparanase enzyme, initially purified from human placenta and platelets [191,192], was primarily associated with a group of proteins commonly described as endoglycosidic enzymes capable of degrading HS, named heparanases. Up to now, only one single genetic sequence codifying for human heparanase (heparanase-1, HPA1) is recognized, thanks to the cloning studies carried out in 1999 independently by several groups, which resulted in the same cDNA sequence [193–196].

The genetic sequence of heparanase encodes for a 61.2 kDa not-active protein precursor, which is sequentially post-translationally cleaved into an 8 and 50 kDa subunit

that non-covalently associate into a hetero-dimeric form, constituting the active heparanase. Notably, the heparanase sequence has a high degree of homology between species. This reflects a preferential expression of heparanase as dominant endoglucoronidase and unique enzyme used by the cells for degradation of HS chains of HSPGs, in contrast to the many proteins required in biosynthesis and modification of HS.

Heparanase localizes in the cells primarily within the endocytic vesicles, both late endosomes and lysosomes, assuming a perinuclear localization [197]. In these vesicles, the latent heparanase is converted into the active enzyme, therefore translocated to the cell surface and/or secreted to the ECM, where it elicits its pro-angiogenic and prometastatic function via HS degradation [198]. Regarding its enzymatic activity, heparanase catalyzes the hydrolytic cleavage at specific sites within the internal glycosidic bonds of GlcA, producing 5-7 kDa fragments. Several studies have been performed to define the substrate specificity for heparanase/HS recognition. It is generally accepted that heparanase cleavage occurs between a GlcA and an N-sulfoglucosamine residue presenting both a 3-O-sulfo or 6-O-sulfo group [199] and that additionally, the minimum recognition sequence is a trisaccharide (**Figure 9**).

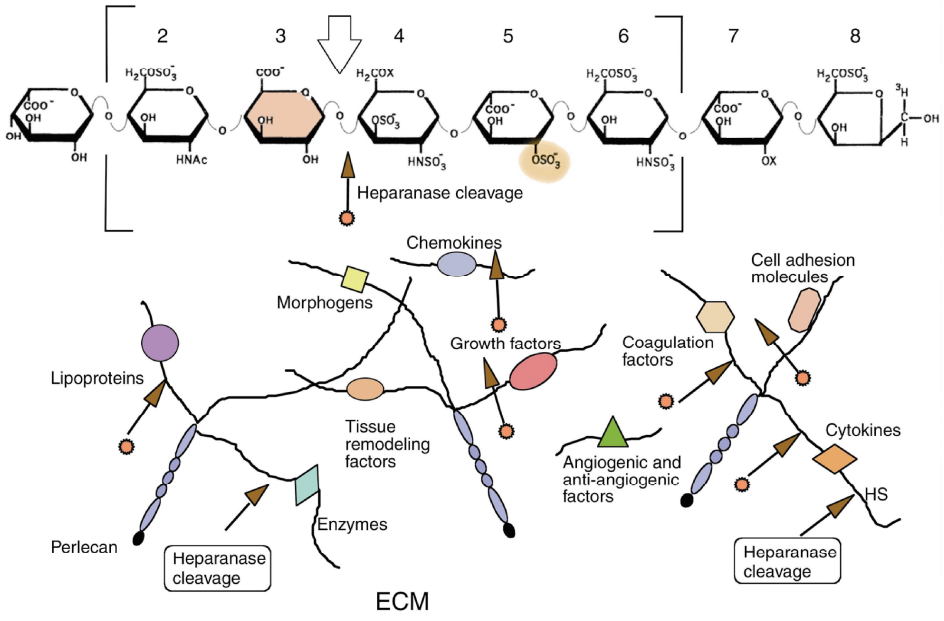

Figure 9: Cleavage of HSPGs by heparanase. Top: Heparanase cleavage site within the anti-thrombin recognition sequence of heparin (brackets). The minimal recognition sequence for substrate recognition by heparanase locates within a highly sulfated trisaccharide GlcN-GlcUA-GlcN. Cleavage takes place between GlcUA and GlcN that is 6-O-sulfated or 3, 6-O-disulfated. Bottom: Heparanase cleavage controls the availability of both HS-bound growth factors and HS-fragments, thereby regulating ligand-receptor binding and respective intracellular pathways activation. Picture reprinted under the permission of Vlodavsky I. and Friedmann Y. [189].

Overall the studies confirmed that heparanase recognizes certain sulfation patterns rather than the saccharides sequence and that the cleavage takes place at the non-reducing side of highly sulfated domains of HS [200–203].

The association of heparanase and cancer was initially observed in B16 melanoma and in T-lymphoma cells [189,204]. Since then, studies based on *in situ* hybridization and RT-PCR approaches, discovered that heparanase-1 mRNA upregulation correlates with increased heparanase activity and the metastatic potential in all cancer cells and tissues including pancreas, colon, ovary, prostate, thyroid, liver, breast, stomach, brain, salivary gland, multiple myeloma, and acute myeloma, for mentioning some [187,197,205–208]. Moreover, the high expression of heparanase associates with more aggressive tumors and reduction of post-operative survival time in cancer patients [207,208]. Studies showing increased cancer cell proliferation in case of heparanase overexpression and reduction of metastatic potential after heparanase silencing gave a more conclusive proof for the role of heparanase in cancer metastasis [209]. Besides high expression in cancer cells, heparanase expression is reduced in normal tissues, showing low-level preferential expression in the placenta, active immune cells, platelets and keratinocytes [210].

In vitro data confirming the correlation between heparanase and angiogenesis derived from immunohistochemical staining of varies human tumors. The study showed that heparanase is preferentially expressed by ECs of capillaries and small sprouting blood vessels close to the tumor, in contrast to the endothelium of mature vessels, where heparanase was not detected [211]. More consistent *in vivo* investigations, revealed that overexpression of heparanase in tumors results in increased tumor vascularization and a higher degree of microvessels maturation in several subsets of tumors [211–213]. Moreover, heparanase might elicit angiogenic responses as cell adhesion, survival, and upregulation of VEGF expression, independently of its enzymatic activity [214].

1.4.5 Angiogenesis and heparanase inhibitors: focus on heparin mimetics

VEGF and VEGF receptors are regarded as key regulators of angiogenesis. Thus, most of the relevant angiogenesis inhibitors block VEGF-mediated function in ECs.

To date, several VEGF/VEGFR inhibitors have been discovered, ranging from monoclonal antibodies, peptide inhibitors and small molecules inhibitors targeting the receptor tyrosine kinase domain on VEGFR [215].

The most famous anti-angiogenic drug is still today the monoclonal antibody Bevacizumab approved in 2004 by the FDA to treat metastatic colorectal cancer in combination with standard chemotherapy [216]. Bevacizumab binds to VEGF-A impairing the binding to its receptor. Besides its clinical efficacy, Bevacizumab treatment is often associated with several side effects, also due to the inhibition of VEGF signaling in normal endothelial cells highly expressing VEGFR [217]. Moreover, long term Bevacizumab treatment associates with the development of drug resistance [218].

As previously mentioned, angiogenesis is a multilevel complex cascade where several growth factors, and not exclusively VEGF, orchestrate the angiogenic response by cooperatively regulating multiple pathways. Furthermore, the complexity of this process additionally relies on the redundancy of function elicited by the growth factors. In this view, scientists were encouraged, to develop drugs that have multiple targets within angiogenic cascade, to achieve higher therapeutic efficacy. The capacity of HS to bind and regulate several pro-angiogenic factors like VEGF and FGFs, and to act simultaneously as a direct substrate of heparanase, made them attractive candidates for the development of anti-angiogenic molecules. In this context, an ideal HS/heparin mimetic drug would antagonize for the binding of growth factors (i.e., VEGF and FGFs) to HSPGs, thereby preventing the formation of a ternary complex of HS/growth factor/receptor. Besides, such a compound would downregulate the enzymatic activity of heparanase via competing with its natural substrate, reducing metastasis and as well interfering with the release of HS-bound growth factors.

Heparin has been logically identified as a potential anti-angiogenic compound and heparanase inhibitor. However, its high anticoagulant activity limits its use in cancer therapy [219]. In view of overcoming the limitations related to heparin, besides retaining high affinity to heparanase, several heparin mimetics and modified heparins have been designed. These low/non-anticoagulant heparins are, up to now, the most studied heparanase inhibitors. Interestingly, most of these molecules which reached various stages of clinical trials, rely on their high therapeutic potential on the additional inhibition of pro-

angiogenic growth factors, as VEGF and FGFs, via competing for their binding to HS. In **Table 3** some of the most relevant heparin-like angiogenesis inhibitors in development are reported.

Drug name	Targets	Effect	Development stage	Ref.
PI-88 (Mopafostat)	Inhibits heparanase; downregulates FGF1, FGF2, and VEGF	Preliminary efficacy in phase II	Phase III for post-operative hepatocarcinoma, discontinued (NCT01402908)	[220–226]
PG545 (Pixatimod) and PG500 series	Inhibits heparanase; downregulates FGF1, FGF2, and VEGF	Inhibition of tumor growth, metastasis, and angiogenesis *in vivo*	Phase I trial with advanced solid tumors, discontinued (NCT02042781)	[227–230]
M402 (Necuparanib)	Inhibits heparanase; downregulates ECs sprouting, HB-EGF, FGF2, and VEGF	Metastasis inhibition and prolonged survival	Phase I/II trial for pancreatic metastatic cancer in combination with gentamicin (NCT01621243)	[231]
SST0001 (Roneparstat)	Inhibits heparanase; downregulates HGF, VEGF, MMPs, and shedding of syndecan-1	Inhibition of cell invasion *in vitro* and tumor xenografts growth *in vivo*	Phase I for multiple myeloma (NCT01764880)	[232–234]

Table 3: Anti-angiogenic heparin mimetics. Synthetic heparanase inhibitors that also interfere with the activity of further pro-angiogenic factors.

When looking at the achievements in clinical trials, PI-88 (Mopafostat) (Figure 10) reached a considerable success among the anti-angiogenic heparin-like drugs, having undergone multiple phase I and II trials for the treatment of several cancer types [221–223]. In 2017, the drug progressed to phase III trials for hepatocellular carcinoma (NCT01402908). However, although the trial was discontinued, as the drug did not show sufficient efficacy, the authors claimed promising features of PI-88 in a single or combinatory therapy in future trials [220]. PI-88 is a heterogeneous mixture of highly

sulfated monophosphorylated mannose oligosaccharides, with tetra- and pentasaccharides as major components, isolated from the yeast *Pichia holstii* NRRL Y-2448 [225]. PI-88 showed a high inhibitory capacity toward heparanase (IC_{50}= 8 nM) [235]. Besides, PI-88 revealed also a high affinity for VEGF and FGFs growth factors, preventing thereby the activation of the signal [236]. Hossain and colleagues showed that PI-88 inhibits two human extracellular endoglucosamine 6-sulfatase (Sulf-1 and Sulf-2) in a concentration-dependent manner [237]. Thus, the wide target's spectrum contributes to the high anti-angiogenic and antimetastatic potential of PI-88. This heparin mimetic has however anti-coagulant properties as the drug significantly stimulates the release of tissue factor pathway inhibitor (TFPI) [238], a strong anticoagulant protein. Therefore, novel derivates of PI-88, as the series of PG500 have been designed to its anticoagulant activity [235]. PG500 are sulfated oligosaccharides linked to a lipophilic moiety (such as aglycone) and show a greater antimetastatic and antiangiogenic effect compared to PI-88 [239].

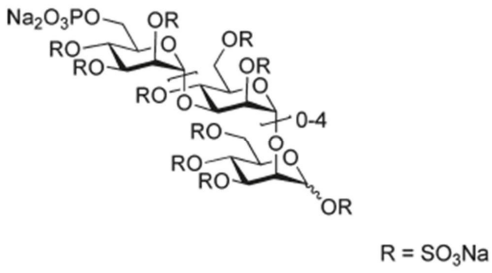

Figure 10: Chemical structure of PI-88. Reprinted under the permission of Johnstone K. D. et al. [236].

1.5 Heparin mimetic: the dendritic polyglycerol sulfate (dPGS)

Despite derivates of unfractionated heparin, as low molecular weight heparin (LMWH), have been in the last decade substituting UFH in clinics, giving their reduced heterogeneity and less variable pharmacokinetics, these drugs are not free of the disadvantages related to heparin [240]. As already mentioned, much effort has been made in order to overcome the limitations of the heparin and maximizing its therapeutic potential, via designing mimetics fully or partially synthetic with low or non-anticoagulant activity.

These compounds, which are usually anionically characterized by a high level of sulfation, resemble the structure of GAGs as heparin and/or HS, and via competition for the binding with the natural ligands or substrates, aim to interfere with the multiple cascades regulated via HS/heparin-binding proteins and enzymes. Shifaza M. and Coombe D R. offer a detailed review about heparin mimetics and their therapeutic efficacy [26]. Generally, the synthetic nature of these drugs offers several advantages over heparin, all related to an easier control over the structure, resulting in increased purity and homogeneity, scalable synthesis, reduced polydispersity, tunable functionalization and degree of sulfation; all characteristics which enable rational design of higher selective and potent anti-tumorigenic drugs.

In the context of designing a fully synthetic heparin mimetic, Türk H. et al. in 2004 synthetized highly branched polysulfated molecules based on a dendritic polyglycerol (dPG) scaffold, called dPGS [241]. Precedent studies investigating on dPG, confirmed its great potentiality in biochemical applications given its elevated biocompatibility and access to high-level functionalization, potentially enabling multivalent interactions [242–244]. Via one step-synthesis involving sulfation via sulfur trioxide-pyridine complex (SO3·py) of dPG, dPGS was produced as fully synthetic anionic highly branched polymers **(Figure 10)**.

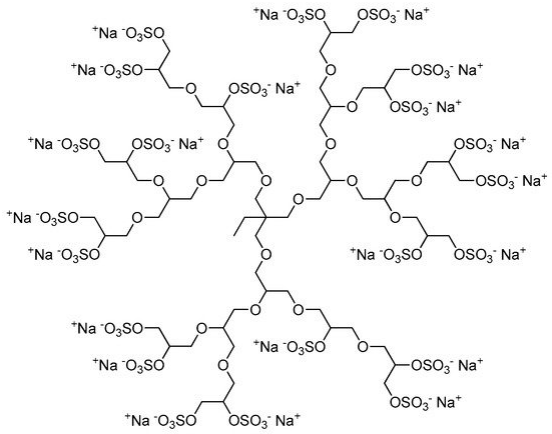

Figure 10: Representative and idealized structure of dendritic polyglycerol sulfate (dPGS). Picture reprinted from Rades N. et al. [245] licensed under a Creative Commons Attribution 4.0 International License.

1.5.1 dPGS as inhibitor of inflammation

Türk at al. used three different molecular weight dPG core structures (2.5, 5, and 10 kDa) and realized equal sulfation of ~80%. Designed as heparin analog dPGS with a core size of 5 kDa showed only an anticoagulant activity of 34% compared to heparin, but a 24-fold increase in anti-complement activity[241].

Substantial proofs of the anti-inflammatory potential of dPGS were presented by Dernedde et al., which confirmed the complement inhibition and anti-inflammatory activity of dPGS *in vivo*. [246]. In the context of inflammation, leukocytes are recruited from the bloodstream to the endothelium, followed by their extravasation toward the inflamed tissues. In this process, the adhesion molecules selectins enable the interaction between the circulating leukocytes and endothelium. Via surface plasmon resonance (SPR)-based affinity assays the authors showed that dPGS, binding to L- and P- selectins (expressed on leukocytes and endothelial cells, respectively), competitively inhibits the binding to their native ligand, the P-selectin glycoprotein ligand-1 (PSGL-1), with a binding inhibition IC_{50} value up to the picomolar range. The capacity of dPGS to interfere with selectin-binding relies on electrostatic interaction: both L- and P- selectin carry a basic binding pocket involved in the recognition of the physiological ligand PSGL-1, which binds to them via its anionic tyrosine sulfate residues. Consequently, dPGS as a highly anionic molecule would compete for the binding with the positively charged ligand recognition site on the selectins. Moreover, the high number of sulfated groups would increase the binding affinity resulting in a multivalent binding effect. The work provided *in vivo* evidence for the anti-inflammatory potential of dPGS in a skin inflammation mouse model. Moreover, based on the SPR-measured affinity of dPGS to complement factors C3 and C5, the authors confirmed *in vivo* reduced generation of anaphylatoxin C5a (as a proteolytic product of C5 factor) in a mouse model for complement activation. Silberreis et al. recently provided a detailed analysis of dPGS-mediated complement inhibition [247].The above-mentioned work and a further study verified the dependency between size and degree of sulfation; both bigger core size and a higher degree of sulfation are responsible for increasing selectins inhibitory binding [246,248]. These findings support the idea that the dPGS-dependent inhibition of L- and P-selectins operates both via electrostatic binding and by steric

shielding of the carbohydrate-binding site. In contrast, increasing the level of branching from 60 to 100% results in a 100-times lower binding affinity toward L-selectins [249].

Further studies focused on diseases result from inflammation models such as osteoarthritis and rheumatoid arthritis. Gröger et al., applied diverse anionic functionalized-dPG-dye-labeled compounds, confirmed penetration in the bone tissue and a remarkable affinity for dPGS to cartilage [250]. This aspect was further explored by Reinmann et al. which confirmed a high affinity of dye-labeled-dPGS to native and inflamed cartilage, suggesting a potential use of dPGS for cartilage targeting purposes [251]. Schneider et al. focused on dPGS treatment in an osteoarthritis model in rats [252]. Given the high affinity to selectins and complement factors, dPGS-dye-labeled structures were used to specifically target inflammation sites *in vivo*. Both a mouse model of collagen-induced rheumatoid arthritis and mice with acute allergic asthma visualized the accumulation of a dye-labeled dPGS at the inflamed site [253,254]. However, a close look at the biodistribution of radiolabeled-dPGS, demonstrated accumulation of the compound in the liver and spleen, even after 3 weeks of injection [255]. To overcome this problem Reiman et al. synthetized shell cleavable dPGS, which promised good degradation *in vitro* [256]. Remarkably, one variant, the dPG-thioglyceryl pentanoatyl sulfate (dPGTPS), containing a long, flexible and hydrophobic linker, including an ester functionality to enable enzymatic cleavage, showed fast decomposition and stronger complement inhibition capacity (**Figure 11**).

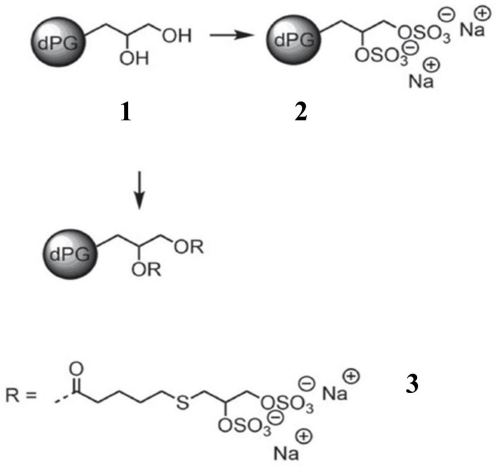

Figure 11: Schematic representation of dPGTPS structure. dPG-thioglyceryl pentanoatyl sulfate (dPGTPS) (3) synthetized as functionalized dPG (1)-based polyanion (dPG scaffold is represented as idealized fragment). Comparison to dPG functionalization leading to dPGS synthesis (2). Modified under the permission of Reimann et al. [256].

1.5.2 Potential use of dPGS in cancer therapy

Given the rapid uptake and reduced toxicity of dPGS, confirmed by several studies conducted both in non-carcinogenic and carcinogenic cell lines [250,251,257], researches have been focusing on studying the potential of dPGS as a cancer-drugs carrier. Sousa et al. showed efficient delivery of paclitaxel-dPGS conjugates and received cytotoxic effect in the lung carcinoma cell line A549 cells and squamous cancer cells A431 [258]. However, the authors observed premature drug release in plasma and in physiological solution. Ferber et al. overcame the problem by linkage of paclitaxel to dPGS via a pH cleavable hydrazone linker and successfully inhibited *in vivo* tumor growth in a mouse model of intracranial glioblastoma [259]. The glioblastoma targeting capacity of dPGS-paclitaxel relies on the affinity of the anionic compound to P-selectins, which the authors confirmed to be highly expressed in a mouse model carrying either human or mouse glioblastoma. Notably, Zhong et al. showed potent anti-tumorigenic activity *in vivo* in a human mammary xenograft mouse model, via coupling doxorubicin to biodegradable micelles of sheddable dPGS [260]. The authors claimed the tumor target capacities relate to the interconnection between tumorigenesis and inflammation, pointing to potential

dPGS-mediated binding of inflammation-related proteins as selectins, which are up-regulated at the tumor site.

1.6 Objectives

The high grade of heterogeneity within the tumor populations, the genetic instability that characterizes tumor cells, together with the elevated tumorigenic pathway redundancy, often leads to the development of drug resistance in patients in response to single-target drugs treatment [261]. Nowadays, drug resistance still represents one of the main challenges in tumor therapy, mostly responsible for the relapse after successful initial treatment [262]. In this context, multitarget drugs, which show activity on a wider spectrum of interactors, have gained high interest, and in the last decade emerged from being unattractive compounds to one of the hottest topics of the last years [263,264]. Previously have been reported the multi-target affinity of HSPGs and their functionality in regulating relevant cellular processes as tumorigenesis; characteristics which made HSPGs promising candidates for the development of multi-target drugs.

In this context, the main objective of this thesis was to evaluate the capacity of the dendritic polyglycerol sulfates, to pleiotropically interfere with multiple mechanisms essential for cancer progression. With the aim to interfere and counteract with HSPGs for the binding to proteins and enzymes regulating tumor progression, this study focused on the two relevant tumorigenic mechanisms known to functionally depend on HS binding: the Shh-signaling pathway and angiogenesis.

With this perspective, in regard to the Shh-signaling pathway, two potential inhibitors will be evaluated: dPGS and a shell cleavable variant dPGTPS. The latter variant has been chosen in view of the degradable capacities, which makes it more suitable for future *in vivo* applications. In this context, the following sub-goals were defined:

- the Shh ligand, as the initiator of Shh-signaling cascade, will be first recombinantly expressed, purified and subsequentially evaluated in binding affinity measurements

- Reporter cell lines will be used to evaluate pathway inhibition

- Further, the ability of the dendritic polyglycerol sulfates to reduce the proliferation of cancer cells, potentially Shh pathway-regulated, will be evaluated in both 2D and 3D cell culture model systems.

To assess the anti-angiogenic capacity of the polysulfates, the following points will be addressed:

- Determination of binding affinity of dPGS to the enzyme heparanase and the angiogenic growth factors VEGF, FGF1, and FGF2

- Subsequentially, *in vitro* cellular and non-cellular based assays, will be applied to study the features characterizing the interaction between angiogenic factors and dPGS, intending to assess its potential as angiogenic inhibitor.

2 Materials and methods

2.1 Materials

2.1.1 Instruments and devices

2.1.1.1 Cell culture

- Heraeus HERA safe Safety Cabinet (Thermo Fisher Scientific, Germany)
- Heraeus BB16 Function line CO_2 Incubator (Thermo Fisher Scientific, Germany)
- Shaking Waterbath 1086 (GFL-Gesellschaft für Labortechnik, Germany)
- Luna FL-Automated cell counter (Logos Biosystems, USA)
- Axiovert 25 phase-contrast microscope (Carl Zeiss, Germany)
- Inverted microscope Axio Observer Z1 (Carl Zeiss, Germany)
- Luminoskan Ascent Luminometer (Thermo Fisher Scientific, Germany)
- IncuCyte S3 (Sartorius, Germany)

2.1.1.2 Electrophoresis

- Thermo Block Grant QBT1 (Grant Instruments, UK)
- PowerPac 300 Power Supply (Bio-Rad, Germany)
- Mini Protean II electrophoresis cell system (Bio-Rad, Germany)
- Mini Sub Cell GT System (Bio-Rad, Germany)
- Safe Imager 2.0 Blue Light Transilluminator (Thermo Fisher Scientific, Germany)

2.1.1.3 Spectrophotometer

- Nanodrop ND-1000 Spectrophotometer (Peqlab, Germany)
- SpectraMax 340PC Absorbance Microplate Reader (Molecular Devices, Germany)
- Infinite M200 microplate reader (Tecan Trading, Switzerland)

2.1.1.4 Western blot

- Trans-Blot Cell (Bio-Rad, Germany)
- Siemens 13 × 18 Cassette (Siemens, Germany)

- Optimax X-Ray Film Processor (Protec Medizintechnik, Germany)

2.1.1.5 Centrifuges

- Eppendorf centrifuge 5417C (Eppendorf, Germany)
- Eppendorf centrifuge 5417R (Eppendorf, Germany)
- Heraus Varifuge 3.0 (Thermo Fisher Scientific, Germany)
- Heraus Megafuge 2.0 R (Thermo Fisher Scientific, Germany)

2.1.1.6 Other devices

- BIAcore X100 instrument (GE Healthcare, Sweden)
- Heraeus B6 Incubator (Thermo Fisher Scientific, Germany)
- Orbital Shaker 3016 (GFL-Gesellschaft für Labortechnik, Germany)
- C25KC incubator shaker (New Brunswick Scientific, Germany)
- Thermal Cycler 2720 (Thermo Fisher Scientific, Germany)
- Mini-Shaking Oven OV3 (Biometra, Germany)
- Wesbart IS89 Multi Shelf Shaker Incubator (Wesbart, UK)
- IKA MS2 Minishaker Vortex mixer (Ika, Germany)
- IKA Microplate Shaker MTS 4 (Ika, Germany)
- Rotation vacuum concentrator Rvc 2-25 (Martin Christ, Germany)
- Light plate 41x26 cm, 220 V (Rex, Germany)
- Polymax 1040 platform shaker (Heidolph, Germany)
- ABI PRISM 310 Genetic Analyser (Advance Biolabs Service, Germany)
- Gel dryer model 583 (Bio-Rad, Germany)

2.1.2 Consumables

2.1.2.1 Western blot

- Photographic paper Amersham Hyperfilm ECL (GE Healthcare, Sweden)
- Nitrocellulose membrane Hybond-C Extra (GE Healthcare, Sweden)
- Whatman cellulose chromatography (GE Healthcare, Sweden)

2.1.2.2 Chromatography

- Poly-Prep Chromatography Columns (Bio-Rad, Germany)

- Sephadex G-25 PD10 desalting column (GE Healthcare, Sweden)
- Amicon ultra-4 centrifugal filter-3 kDa MWCO (Merck, Germany)
- NucleoSEQ chromatography columns (Macherey-Nagel, Germany)

2.1.2.3 Cell culture

- Culture dish 100x20 mm (Corning, USA)
- T25, T75, T175 tissue culture flasks (Corning, USA)
- Tissue Culture Plate 96 Well Standard (Sarstedt, Germany)
- Nunc F96 MicroWell white plates (Thermo Fisher Scientific, Germany)
- Cellcarrier spheroids ULA 96-well microplates (PerkinElmer, Germany)
- µ-Slide Angiogenesis ibiTreat, 10 µl volume (Ibidi, USA)
- 50, 15 ml Centrifuge tubes High Clarity (Falcon, USA)
- 1, 2, 5, 10, 25 ml Serological pipettes (Falcon, USA)
- Millex-GP Syringe Filters 0.22 µm (Merk, Germany)

2.1.2.4 Other consumables

- Streptavidin precoated SA-sensor chip (GE Healthcare, Sweden)
- Nunc-Immuno Module 8 well-strips (Thermo Fisher Scientific, Germany)

2.1.3 Chemicals

2.1.3.1 Plasmids

- Human Shh cDNA clone (Sinobiological, China)
- pcDNA6/V5-His A plasmid (Thermo Fisher Scientific, Germany)

2.1.3.2 Primers

- The primers were synthetized and HPLC purified by Metabion International GmbH (Germany). For the sequence of Shh-N primers in bold are reported the base pairs (bps) complementary to target plasmid vector (pcDNA6/V5-His A), highlighted in grey the Kozak sequence, underlined the sequence of homology for the target gene Shh-N.
- Shh forward: 5´-**GGG AGA CCC AAG CTG GCT AGC** GCC ACC ATG CTG CTG GCG GCG AGA TGT CTG-3´
- Shh reverse: 5´-**TCA ATG GTG ATG GTG ATG ATG** ACC GGT GCC TCC CGA TTT GGC CGC CAC-3´.

- Forward primer binding at the T7 promoter: 5'-TAA TAC GAC TCA CTA TAG-3'
- Reverse primer binding at the BGH site: 5´-TAG AAG GCA CAG TCG AGG-3'

2.1.3.3 Antibodies

- Human Shh-N terminus polyclonal antibody goat IgG (R&D Systems, Germany)
- Polyclonal rabbit anti-goat immunoglobulins/HRP (Dako, Germany)

2.1.3.4 Proteins and enzymes

- Albumin fraction V biotin-free (Carl Roth, Germany)
- Bovine serum albumin (BSA) (Albumin Standard, Thermo Fisher Scientific, Germany)
- Recombinant human Heparanase/HSPE (R&D Systems, Germany)
- Human acidic fibroblast growth factor FGF1 (PeproTech, Germany)
- Human basic fibroblast growth factor FGF2 (PeproTech, Germany)
- Human vascular endothelial growth factor $VEGF_{165}$ (PeproTech, Germany)
- Restriction enzymes *Nhe*I and *Age*I (Thermo Fisher Scientific, Germany)
- Phusion hot start II High-Fidelity DNA Polymerase (Thermo Fisher Scientific, Germany)

2.1.3.5 Electrophoresis reagents

- DNA gel stain SYBR (Thermo Fisher Scientific, Germany)
- Coomassie Brillant blue G-250 (AppliChem, Germany)
- PageRuler Prestained Protein Marker (Thermo Fisher Scientific, Germany)
- Kb Plus DNA Ladder (Thermo Fisher Scientific, Germany)

2.1.3.6 Sequencing reagents

- BigDye Terminator 5× Sequencing Buffer (Thermo Fisher Scientific, Germany)
- BigDye Terminator Mix (Thermo Fisher Scientific, Germany)
- Hi-Di formamide (Thermo Fisher Scientific, Germany)

2.1.3.7 Kits

- Human Shh-N Quantikine ELISA kit (R&D Systems, Germany)
- Pierce BCA Protein Assay (Thermo Fisher Scientific, Germany)
- Zymoclean Gel DNA Recovery Kit (Zymo Research, Germany)
- Plasmid purification: NucleoBond-Xtra Midi (Macherey-Nagel, Germany)
- NucleoSpin plasmid Mini-prep kit (Macherey-Nagel, Germany)

- LDH cytotoxicity detection kit (Takara Bio, France)
- Celltiter-Glo luminescence cell viability assay (Promega, Germany)
- Celltiter-Glo3D cell viability assay (Promega, Germany)

2.1.3.8 Cell culture

- Dulbecco´s phosphate buffered saline (PBS)-$CaCl^2$, -$MgCl^2$ (Thermo Fisher Scientific, Germany)
- Dulbecco´s Modified Eagle Medium-DMEM (Gibco-Thermo Fisher Scientific, Germany)
- EGM2-Endothelial growth medium -2 Bulletkit (Lonza, Switzerland)
- 0.25% Trypsin-ethylenediaminetetraacetic acid- EDTA (Gibco-Thermo Fisher Scientific, Germany)
- Trypsin/EDTA 0.04%/0.03% (Promocell, Germany)
- Trypan blue stain 0,4% (Invitrogen-Thermo Fisher Scientific, Germany)
- Penicillin/Streptomycin (Pen/Strep) (Gibco-Thermo Fisher Scientific, Germany)
- Sodium pyruvate (Gibco- Thermo Fisher Scientific, Germany)
- Zeocin (Invitrogen- Thermo Fisher Scientific, Germany)
- Geneticin G-418 (Biochrom, Germany)
- Fetal Bovine Serum-FBS (Gibco- Thermo Fisher Scientific, Germany)
- Horse serum (Gibco, Thermo Fisher Scientific, Germany)
- Cultrex reduced growth factor basement membrane extract (BME) (Trevigen, UK)
- Beetle Juice luciferase firefly (PJK Biotech, Germany)
- Lysis juice for luciferase assay (PJK Biotech, Germany)
- Lipofectamine 3000 reagent (Thermo Fisher Scientific, Germany)

2.1.3.9 Other chemicals

- Cell proliferation reagent water-soluble tetrazolium salt (WST-1) (Merck, Germany)
- Suramin sodium salt (Sigma Aldrich, Germany)
- HBS-EP running buffer (GE Healthcare, Sweden)
- pNPP (para-nitrophenyl phosphate) alkaline phoshate substrate (Sigma Aldrich, Germany)
- HisPur Ni-NTA resin (Thermo Fisher Scientific, Germany)
- cOmplete (EDTA)-free Protease Inhibitor Cocktail (Roche, Germany)
- Imidazole (Carl Roth, Germany)
- EDTA (Carl Roth, Germany)

- Tween 20 (Bio-Rad, Germany)
- Triton X-100 (Bio-Rad, Germany)
- Tris (hydroxymethyl) aminomethane (Tris)-Base (Santa Cruz Biotechnologies, Germany)
- Tris-HCl (Serva, Germany)
- Potassium chloride (Merck, Germany)
- Heparin, sodium salt, porcine intestinal mucosa (Merck, Germany)
- Silver nitrate (Sigma Aldrich, Germany)
- Formaldehyde solution 37% wt in H_20 (Sigma Aldrich, Germany)
- Ethanol, denatured (Carl Roth, Germany)
- Tango buffer 10X (Thermo Fisher Scientific, Germany)
- Ampicillin (Amp) sodium salt (Carl Roth, Germany)
- Dimethylsulfoxide (DMSO) (Carl Roth, Germany)
- GANT61 (Sigma Aldrich, Germany)

2.1.4 Bacterial strains

- *Escherichia coli* competent bacteria DH5α

2.1.5 Cell lines

- A549, human non-small cell lung cancer cells (ATCC, Germany)
- HEK293, human embryonic kidney cells (ATCC, Germany)
- MIA-PaCa-2, human pancreatic cancer cell line (ATCC, Germany)
- MCF-7, human breast cancer cells (ATCC, Germany)
- PANC-1, human pancreatic ductal carcinoma (Leibniz-Institut DSMZ, Germany)
- Sonic hedgehog light 2 (ShhL2) cells, mouse fibroblasts NIH3T3 co-transfected with 8XGLI-luciferase reporter and renilla control gene (from James K. Chen, Stanford University, USA)
- C3H10T1/2 Clone 8, mouse embryonic fibroblasts (ATCC, Germany)
- HUVECs pooled donors human endothelial umbilical vein cells (Lonza, Switzerland)

2.1.6 Computer Software

- AnaSP, spheroids open-source analysis program [265]
- BIAevaluation software 4.1.1. (GE Healthcare, Sweden)
- IncuCyte analysis program (v2019B) (Sartorius, Germany)
- Angiogenesis analyzer ImageJ macro (https://biii.eu/angiogenesis-analyzer-imagej)
- GraphPad Prism 5 (GraphPad Software, USA)
- ApE, open-source DNA editor program (http://jorgensen.biology.utah.edu/wayned/ape/)

2.2 Molecular biology methods

2.2.1 Transformation

Plasmid transformation was performed in *E. coli* strain DH5α competent cells to enable plasmid replication and cloning. Briefly, 1 µl plasmid DNA (10 µl for cloning) was added to 50 µl stock of competent DH5α cells on ice. The transformation was carried out by heat shock (1 min on ice, 1 min at 42°C, 10-30 min on ice). Following, the bacteria suspension was added to 300 µl Luria Bertani (LB) medium (10 g/l pepton, 5 g/l yeast extract, 10 g/l NaCl, pH 7.0) in the absence of selective antibiotic. The mixture was incubated for 45 minutes at 37°C under shaking (200 rpm). A 37°C pre-warmed LB-agar plate (LB medium with 15g/l agar), containing 100 µg/ml ampicillin antibiotic, was inoculated with the 50 µl or rest volume of bacterial suspension and incubated at 37°C for the following 17 hours.

2.2.2 Exonuclease and ligation-independent cloning (ELIC)

The Exonuclease and Ligation Independent Cloning (ELIC) molecular cloning method was used for the expression of recombinant Shh-N. This cloning technique, originally described by Koskela et al. [266], requires few base pairs (bps) of homology between the ends of both PCR amplified fragment and enzymatically digested host-vector

to enable ligation-exonucleases independent. In the specific, the primers for PCR amplification of Shh-N carry 21 bps homology with the target vector (pcDNA6/V5-His A), 16 bps complementarity with Shh-N target gene and are additionally implemented with 6 bps of Kozak sequence (5´-GCC ACC-3`), which helps the initiation of eukaryotic translation (2.1.3.2). PCR amplification mixture was set up as described in **Table 4,** on ice.

Components	**Concentrations (µl)**
Template DNA (1 µg/µl)	1 µl
Primers Forward and Reverse (10 µM)	1 µl each
Phusion hot start II polymerase (HF)	1 µl
5X Phu fusion buffer	10 µl
dNTPs mix (10 mM)	2 µl
Milli Q-water	34 µl

Table 4: PCR reaction mixture

Thereafter the mixture was transferred to a Thermal Cycler 2720 (Applied Biosystems) where, following the PCR program displayed in **Table 5**, the DNA products of interest were amplified.

Step	**Temperature**	**Time**
Initial denaturation	96° C	2 min
	94° C	10 sec
35 cycles	50°C	30 sec
	72°C	30 sec
Final elongation	72°C	5 min

Table 5: Thermocycling condition for PCR

The identity of the amplified PCR product was confirmed by agar gel electrophoresis (2.2.3). In parallel, the plasmid vector was linearized via enzymatic digestion with *Nhe*I and *Age*I restriction enzymes. The digestion mixture was prepared according to **Table 6** and performed at 37°C overnight. After restriction, agar electrophoresis for the digested product was performed and the DNA bands corresponding to the linearized plasmid were extracted from the gel and cleaned with Zymoclean Gel DNA recovery kit (Zymo Research), following the manufacturer´s instructions.

The concentration of the extracted DNA and purity was determined with Nanodrop ND-1000 Spectrophotometer (Peqlab).

Component	**Volume in 10 µl**
*Age*I	0,8 µl
*Nhe*I	0,2 µl
Tango buffer 10X	1 µL
DNA 330 ng/µl	3 µl (1 µg)
Milli-Q water	5 µl

Table 6: Enzymatic restriction mixture

Shh-N PCR amplified fragments and linearized plasmid were mixed at optimal 1:3 vector: insert (v/v) ratio in water at 10 µl final volume and incubated for 5 minutes at room temperature. Thereafter, the mixture was directly used to transform DH5a competent bacteria (2.2.1). Six colonies were randomly chosen, and their plasmid DNA content was extracted and purified with NucleoSpin Plasmid kit (Macherey-Nagel) (2.2.4). As initial control for successful cloning, the DNA extracted from the clones and original vector plasmids were digested overnight with *Nhe*I and *Age*I restriction enzymes, followed by agar gel electrophoresis (2.2.3). The construct containing the insert were thereafter analyzed by sequencing (2.2.5). The plasmid result of successful cloning was further purified via midi-preparation (2.2.4) with NucleoBond Xtra Midi kit (Macherey-Nagel). The cloning products were immediately stored at -20°C and -80°C for longer storage.

2.2.3 Agarose gel electrophoresis

Agarose gel electrophoresis was used for the separation of DNA. For the electrophoresis, a 1% (w/v) agarose gel was produced in Tris-acetate EDTA (TAE) buffer (40 mM Tris, 5 mM sodium acetate and 1 mM EDTA, pH 7.2). For enabling DNA visualization 1XSYBR gel stain (Invitrogen) was included. DNA samples were mixed with 6XDNA loading buffer, loaded on the agarose gel and electrophoresis was carried out in a Mini Sub Cell GT (Bio-Rad) at 90 V constant for 30 minutes. DNA ladder 1 Kb (Invitrogen) was loaded to estimate the molecular weight migration of the DNA samples. The DNA

migration was visualized under light transilluminator Safe imager 2.0 (Invitrogen) and photographically documented.

2.2.4 Plasmids DNA extraction

NucleoSpin Plasmid kit was used for miniprep isolation of plasmid DNA from bacteria clones. For this purpose, a single bacterial colony was picked from an agar plate containing transformants with the help of a 100 µl pipette tip, and further inoculated in 4 ml LB medium (100 µg/ml Amp). The bacterial culture was incubated for 17 hours at 37°C shaking (200 rpm). The isolation was carried out following the manufacturer´s instructions.

For purifying larger and higher purity plasmid DNA, midi-prep DNA isolation via NucleoBond Xtra Midi isolation kit (Macherey-Nagel) was performed. In this case, a colony was picked from a freshly streaked agar plate and initially incubated in 4 ml LB medium (100 µg/ml Amp) for 8 hours at 37°C shaking (200 rpm). This starter culture was further diluted 1:1000 in 100 ml LB medium (100 µg/ml Amp) and incubated at 37°C for 17 hours under shaking conditions (200 rpm). The plasmid extraction followed the manufacturer's instructions. The final isolated plasmid was diluted in de-ionized water and the concentration measured via Nanodrop ND-1000 Spectrophotometer (Peqlab).

2.2.5 DNA sequencing

To confirm the successful cloning of Shh-N fragment into pcDNA6/V5-His A plasmid and to check the accuracy of inserted sequence, DNA sequencing using BigDye Terminator sequencing method (Applied Biosystems) was performed. The mixture used for PCR amplification of the samples for sequencing is displayed in **Table 7**.

Components	Concentrations (µl)
Template DNA (100-300 ng/µl)	1 µl
Primers Forward T7 binding (10 µM)	1 µl
BGH Reverse primer (10 µM)	1 µl
5XBigDye Terminator Seq. buffer	1 µl
BigDye terminator mix	1.5 µl
Milli Q-water	4.5 µl

Table 7: PCR mixture for sequencing

The PCR amplification of the products for sequencing followed the program displayed in **Table 8**.

Step	Temperature	Time
Initial denaturation	96	1 min
	96° C	10 sec
25 cycles	55°C	5 sec
	60°C	4 min

Table 8: PCR program for DNA sequencing

After the PCR reaction, the unincorporated dye-terminators were removed by NucleoSEQ chromatography columns (Macherey Nagel). Following, the samples were centrifuged under vacuum with Rotation-Vacuum-Concentrator (Martin Christ) for 7 minutes at room temperature and further resuspended in 25 µl 10% Hi-Di formamide and incubated at 95°C for 3 minutes. Finally, the samples were sequenced with ABI PRISM 310 Genetic Analyzer (Advanced Biolab Service).

2.3 Protein chemistry methods

2.3.1 Protein purification via Ni-NTA affinity chromatography

After protein expression in HEK293 cells (2.4.1) the collected supernatant was centrifuged 2 times at 1000 rpm for 5 minutes in a Varifuge 3.0 (Heraeus) to eliminate cell debris and further filtered sterile with Millex- 0.22 µm filters (Merck). The supernatant was

directly used for purification or stored at either 4°C or -20°C for longer storage. The supernatant containing Shh-N secreted protein was purified via Ni-nitrilotriacetic acid (NTA) agarose affinity chromatography via Ni-NTA agarose resin (Qiagen). 500 µl bed volume of Ni-NTA agarose was used for the purification of 10 ml supernatant. The supernatant was equilibrated with 20 mM Imidazole, 1% Tween 20 and 10% Tris buffer (pH 8.0) and loaded 3 times into the gravity column to ensure proper protein retention. The column was further washed once with 30-column volumes of washing buffer (PBS 1X, 40 mM imidazole pH 7.4, 1% Tween 20, 500 mL NaCl). The protein was eluted in 5 fractions of 500 µl with elution buffer (PBS 1X, 250 mM imidazole pH 7.4). A further wash of the column was performed with a 10 column volume of elution buffer and final re-equilibration with 30 column volumes equilibration buffer (PBS 1X, 20 mM imidazole pH 7.4, 1% Tween 20). The eluted fractions were analyzed by SDS-page (2.3.2), western blot (2.3.4) and silver gel staining (2.3.3). For PBS buffer exchange and imidazole salts elimination, the eluted fractions were mixed and passed through Sephadex G-25 PD10 desalting column (GE Healthcare), following manufacturer's instructions. Afterward, the protein was concentrated via Amicon ultra-4 centrifugal filter MWCO 3 kDa (Merck), usually reducing 8-times the initial volume to 500 µl final volume of concentrated sample. Determination of protein concentration was performed via BCA-protein assay kit (Pierce), following the manufacturer´s instructions. Protein was stored at 4°C and in the next days used for binding studies.

2.3.2 SDS-page gel electrophoresis

Shh-N protein samples were analyzed by sodium dodecyl sulfate-polyacrylamide gel electrophoresis (SDS-page) in a 12 % (w/v) Tris-glycine polyacrylamide vertical gel on a Mini Protean II chamber (Bio-Rad). The composition of the 12% Tris-glycine gel is reported in **Table 9**. Electrophoresis was performed at 17 mA constant until the samples reached running gel and then at 21 mA constant for the rest of the protein migration. The electrophoresis was performed in SDS-running buffer [3.8% (w/v) Glycin, 1.2% (w/v) Tris-Base, 0.4% (w/v) SDS, pH 8.0]. The samples were mixed with 4X sample buffer [0.25 mM Tris, 40% (v/v) Glycerol, 8% (w/v) SDS, 8% (v/v) 2-Mercaptoethanol, 0.004% (w/v) Bromophenol blue, pH 6.8] and boiled at 100°C in Thermo block (Grant Instruments) for

5 minutes. Page Ruler Prestained protein ladder (10–180 kDa) (Thermo Fisher Scientific) was used for the analysis of the protein molecular mass and as well applied for protein evaluation via Western blot analysis. After the SDS-PAGE, the gel was stained for about 30 minutes with a solution of 0.1% (w/v) Coomassie Blue G-250 (AppliChem) in 40% (v/v) methanol and 10% (v/v) acetic acid, and destained for further 30 minutes in a solution of 20% (v/v) ethanol and 10% (v/v) acetic acid.

Components	**12% Running gel**	**Stacking gel**
ddH20	1.64 mL	785 µl
1.5 M Tris HCL (pH 8.8)	1.25 mL	-
0.5 M Tris HCL (pH 6.8)	-	415 µl
30 % Acrilamide	2 mL	265 µl
10% SDS	50 µL	16.65 µl
10% APS	50 µl	16.65 µl
Temed	6.7 µL	3.35 µl

Table 9: Composition of dodecyl sulfate-polyacrylamide gel electrophoresis (SDS-page) gel

2.3.3 Silver gel staining of SDS-page gel

Silver gel was used to verify the purity of the Shh-N expressed protein, after the electrophoretic separation via SDS-page gel (2.3.2). In this method, after performing SDS-electrophoresis, the gel was exposed to a dual fixation: first via incubation for 20 min in 50% (v/v) Ethanol and 10% (v/v) acetic acid, second for 25 min incubation in 30 % (v/v) Ethanol and 0.5 M sodium acetate trihydrate solution, under constant slow-speed shaking on Orbital Shaker 3016 (GFL- Gesellschaft für Labortechnik) . Following a 3-times wash in ddH_20 for 10 minutes each, the gel was incubated in freshly prepared silver staining solution [0.1% (w/v) silver nitrate and 0.01% formaldehyde (37%)] for 40 minutes. Subsequentially, the gel was rinsed in ddH_20 and developed after incubation for 5 to 10 minutes in developing solution [2.5 % (w/v) sodium carbonate pH 11.2 and 0.01% formaldehyde (37%)], stopped upon addition of 0.05 M EDTA.

2.3.4 Western blot

Proteins were separated by SDS-PAGE 12% (w/v) gel and then transferred at 300 mA constant for 30 minutes to a Hybond C-extra nitrocellulose membrane (GE Healthcare) in Tris-glycine buffer [25 mM Tris, 191.8 mM glycine in 10% (v/v) methanol], placed in a Trans-Blot Cell (Bio-Rad). To avoid unspecific binding, the membrane was blocked for 30 min in blocking solution TBST [Tris-saline buffer (TBS) and 0.1% Tween 20) with 5% (w/v] skim milk powder. Afterward, the membrane was incubated with the polyclonal human Shh-N antibody (R&D Systems) overnight at 4°C under gentle shaking on a rocker. The membrane was then washed in TBST solution for 3 times of 10 min each and subsequentially incubated with polyclonal rabbit anti-goat immunoglobulins/HRP (1:5000 diluted) (Dako) for 30 min. The membrane was washed again 3 times with TBST for 10 min each washing step. The binding of the secondary antibody on the membrane was visualized via incubation with chemiluminescence reagents mixture described in the following table (**Table 10**).

Solution A	0.25 mg/ml luminol in 0.1M Tris-HCL (pH 8.6)
Solution B	1 mg/ml p-Coumaric in DMSO
Solution C	H_2O_2

Table 10: Mixture for the western blot chemiluminescence reaction

After 30 min exposure, the photographic paper Amersham Hyperfilm ECL (GE Healthcare) was developed by an Optimax X-Ray Film Processor (Protec Medizintechnik).

2.3.5 Surface plasmon resonance

Surface plasmon resonance (SPR) measurement was performed on a Biacore X100 (GE Healthcare) operated using BIAevaluation software 4.1.1. The measurements were carried out in HBS-EP buffer (GE Healthcare) with streptavidin-precoated (SA) sensor chip (GE Healthcare) coupled to dPGS-or dPGTPS-biotinylated molecules. The synthesis of

dPGS-biotin followed the procedure described somewhere else [267]. dPGTPS-biotin was kindly provided by Ph.D. candidate Suman Chowdhury (Freie Universität, Berlin). The measurements were carried out at 25°C constant temperature. Prior the immobilization of the dendritic polyglycerol sulfates-biotin, the chip was pretreated with three 5µl injections of 50 mM NaOH in 1 M NaCl at 5 µl/min to remove any unspecific bound contaminants, followed by a rinse with 40 µl of HBS-EP buffer at 30 µl/min. In the case of Shh-N and heparanase affinity measurements, dPGS/dPGTPS- biotinylated molecules were immobilized on one of the two flow cells to a level of ~400 RU, while for control the other cell flow was left empty. In the case of binding measurements for dPGS to angiogenic growth factors, dPGS-biotin was immobilized at lower ligand concentration (140~RU), whereas dPG-biotin was immobilized on the surface to rule out unspecific binding. The proteins were diluted as well in HBS-EP buffer [0.01 M HEPES pH 7.4, 0.15 M NaCl, 3 mM EDTA, 0.005% (v/v) Surfactant P20] at various reported concentrations. Affinity was determined by single-cycle kinetics (SCK) measurements. Five ascending protein concentrations were injected consecutively at a constant flow rate of 30 µl/min five for 180 s followed by dissociation time of 600 seconds and final regeneration with 4M $MgCl_2$ solution with a contact time of 120 s. For FGF2, in order to reduced unspecific bindings, the amount of NaCl in HBS-EP buffer was double to a final concentration of 0,3 M.

2.3.6 Heparanase activity assay

The assay based on the measurement of reducing disaccharide products catalyzed by heparanase cleavage of the synthetic heparin oligosaccharide fondaparinux. A method originally described by Hammond et al. [268], which was here applied with minor variations. Initially, Nunc-Immuno Module 8 well-strips (Thermofisher) were coated for 2 hours at 37°C under low speed shaking on IS89 shaker incubator (Wesbart) with a solution containing 4% (w/v) BSA in PBST (PBS with 0.05% Tween 20, pH 7.4.). Thereafter the strips were washed 3 times with PBST, dried and stored at 4°C for up to 1 week. Human heparanase (R&D Systems) was diluted in 40 mM Sodium acetate buffer (pH 5.0) at the concentration of 5 nM and incubated with 1 to 10 nmoles fondaparinux to a final volume of 100 µL per well. In the case of inhibition studies, dPGS was incubated 5 min with heparanase prior assay beginning, upon addition of 100 µM fondaparinux. The strips

were sealed with adhesive tape and incubated at 37°C for 18 hours. The reaction was measured upon the addition of 3 µL per well of WST-1 reagent (Roche) in 0.1 M NaOH at 100 µl final volume per well. The strips were then re-sealed and incubated for 1 hour at 60° C in oven OV3 (Biometra). The absorbance was measured at 595 nM with Infinite M200 microplate reader (Tecan Trading).

2.4 Cell biology methods

2.4.1 Cell culture

The cell lines used were cultured in the respective growth medium as displayed in **Table 11**. Generally, the cells were sub-cultured at 80-90% confluency, usually reached twice per week, via washing with Dulbecco's PBS-Ca^{2+} and Mg^{2+} free (PBS -/-) and short incubation (2-3 min) with 0.25% Trypsin-EDTA (Gibco), to enable cells detachment. Following incubation with Trypsin-EDTA, the cells were resuspended in fresh culture medium and the solution centrifuged at 1000 rpm for 5 min with Varifuge 3.0 (Heraeus). In the case of C3H10T1/2 mesenchymal cells, known for their high sensitivity to contact inhibition, sub-culturing at ~70% confluency was preferred, likewise the usage of cells at low passage numbers (< passage 7). The endothelial HUVECs were used only between passage 3 to 5 and sub-cultured at 80% confluency at a ratio of 2500-5000 cells/cm^2 in T-25/75 flasks (Thermo Fisher Scientific). For HUVECs detachment, PBS -/- was applied for washing steps and further incubation for 1 min with Trypsin/EDTA ratio of 0.04%/0.03%. (Promocell) to enable cell detachment. All cells were allowed to proliferate at 37 °C in a humidified 5% CO^2 incubator (Heraus).

Cell line	Medium
HEK293 MCF-7 PANC-1 C3H10T1/2	Dulbecco's Modified Eagle's medium (DMEM) + 10% FBS and 1% Pen/ Step
MIA-PaCa-2	DMEM +10% FBS, 2.5 % horse serum, 1% Pen/Strep
ShhL2	DMEM + 10% FBS, 1% Pen/ Step, 1% sodium pyruvate, 150 µg/mL zeocin and 400 µg/mL geneticine
HUVECs	Endothelial growth medium 2 Bulletkit (EGM2): 2% FBS, Hydrocortisone, hFGF2, VEGF, R3-IGF-1, Ascorbic Acid, hEGF, GA-1000, Heparin. At manufacturer´s concentrations

Table 11: Growth medium conditions for each cell line

2.4.2 Protein expression in HEK293 cells

The Shh-N plasmid construct previously cloned (2.2.2) and verified by sequencing (2.2.5) was then transiently transfected into HEK293 cells to enable expression of lipids modified Shh-N protein secreted in the culture medium. At 24 hours prior transfection, HEK293 cells were seeded at a density of $3x10^6$ cells/plate in a 100x20 mm culture dish (Corning) in DMEM culture medium supplemented with 10% FBS and 1% Pen/Strep. Afterward, the transfection was performed with Lipofectamine 3000 reagent (Invitrogen), following the manufacturer´s instructions. Transfection was performed for both Shh-N carrying vector and control pcDNA6/V5-His A empty plasmid, in order to obtain Shh-N conditioned medium (Shh-N CM) and control conditioned medium (control CM), respectively. In a first attempt, the supernatant was collected 72 hours after transfection. Next, for enabling both optimal purification and for cell-based applications, 24 hours after transfection, the culture medium was exchanged from 10% FBS to reduced serum conditions (2% FBS) and cells further cultivated for 72 hours (96 hours post-transfection). The supernatant was then collected, centrifuged 2 times at 1000 rpm and sterile filtrated (0.22 µm). Protein expression was confirmed by SDS-page gel electrophoresis (2.3.2) and immunodetection (2.3.4). The conditioned medium was stored at 4°C and -20°C in case of longer storage or either directly used for purification proposes (2.3.1).

2.4.3 Alkaline phosphatase (ALP) activity assay

For the assay, murine fibroblasts osteoblast precursors C3H10T1/2 cells were plated at the density of $2x10^4$ cells/well (c/w) in 96-well plate. Cells were cultivated for 24 hours in DMEM supplemented with 10% FBS and 1% Pen/Strep to reach over-confluency. Afterward, the medium was switched to 2% FBS. Dilutions of Shh-N CM and control CM (2% FBS) in fresh culture medium (2% FBS) were tested for pathway activation at ratios ranging from 1:2 to 1:1000 CM/fresh DMEM. For inhibition studies the compounds tested dPGS, dPGTPs, Heparin and GANT61 were added to the 1:10 CM/DMEM ratio mixture at the reported concentrations, generally ranging between 3 nM to 10 µM. Treated cells were then allowed to grow for 72 hours. Afterward, the medium was removed by gentle aspiration and 50 µl per well of lysis buffer [100 mM Tris pH 9.5, 250 mM NaCl, 25 mM $MgCl_2$, 1% Triton X-100 supplemented with cOmplete protease inhibitor (Roche)] was added. The plate was shaken with a rocker for 40 minutes and further stored overnight at -20°C to help cell lysis via one freeze and thaw cycle. 25 µl of the cell lysate from each well was transferred into a new 96-well plate, equilibrated to room temperature and further mixed with 25 µl of pNPP substrate (Sigma-Aldrich). The plate was gently shaken to homogenize the solution and then incubated for 30 min at 37°C. Absorbance was measured at 405 nm using microplate reader Infinite M200 (Tecan Trading).

2.4.4 Luciferase reporter assay

Shh light 2 (ShhL2) cells, a murine fibroblast NIH3T3 cell line stably co-transfected with GLI-responsive firefly luciferase reporter and a constitutive luficerase renilla expression vector, were applied for the reporter assay. ShhL2 cells were plated in a 96-well plate at the density of $6x10^4$ c/w in complete culture medium (2.4.1) and reached over-confluency after initial 24 hours of incubation. Dilutions of Shh-N CM and control CM (2% FBS) in fresh DMEM supplemented with 0,5% FBS were tested for pathway activation at ratios ranging from 1:2 to 1:1000 CM/fresh DMEM. Inhibitors were added to CM/DMEM 1:10 dilution ratio at the concentrations reported, which generally ranged between 3 nM to 10 µM. Cells were incubated for further 30 hours, then the medium was

carefully removed and the cells were treated with 30 µl per well of cell lysis solution 1X Lysis-Juice (PJK GmgH). The plate was shaken with a rocker for 40 minutes and further stored overnight at -20°C to help cell lysis via one freeze and thaw cycle. 20 µl aliquots of lysis solution from each well were collected and plated into a Nunc F96 MicroWell white plate (Thermo Fisher Scientific). Beetle-Juice reagent containing D-luciferin and ATP (PJK GmgH) was used to quantify the amount of firefly luciferase contained in the cell lysate upon automatic injection of the substrate at 1:2 (v/v) ratio lysate/reagent. The measurement was carried out with a Luminoskan Ascent microplate reader (Thermo Fisher Scientific) at an integration time of 5 sec and a delay of 2 sec.

2.4.5 Lactate dehydrogenase (LDH) assay

Cell cytotoxicity via lactate dehydrogenase (LDH) assay was performed in the case of the cell line C3H10T1/2 and ShhL2, used in the biological Shh-pathway reporter assays. The method based on the measurement of lactate dehydrogenase (LDH) activity present in the culture supernatant, which is released consequentially to cell death and plasma-membrane damage. The cells were seeded in DMEM culture medium (supplemented with 2% FBS for C3H10T1/2 and 0,5% FBS for ShhL2 cells) at the density of $5x10^3$ c/w in a 96-well plate and allowed to adhere after overnight incubation. Afterward, inhibitors (dPGTPs, dPGS, GANT61, and Heparin) at the reported concentrations were added to the cells, while 1% Triton-X100 was used for high control to induce cells death and complete LDH release. The LDH activity assay (Takara) was performed after 24 and 48 hours of incubation with the inhibitors and controls, following the manufacturer's instruction.

For calculation of percentage cytotoxicity, the following formula was applied:

$$\text{Cytotoxicity } (\%) = \frac{LDH\ (test\ sample) - LDH\ (negative\ control)}{LDH\ (positive\ control) - LDH\ (negative\ control)} \times 100$$

2.4.6 Detection of Shh-N protein in cells supernatant

For the quantification of Shh-N released in the cell culture medium, the pancreatic cancer cells PANC1 and Mia-PaCa-2, the breast carcinoma cells MCF-7, lung adenocarcinoma A549 cells, the human embryonic kidney cells HEK293 and murine mesenchymal cells C3H10T1/2 were cultivated to confluence in a 100x20 mm culture dish (Corning) with the appropriate medium (2.4.1). Cell supernatant was then collected, centrifuged twice (1000 rpm), sterile filtered (0.22 µm) and stored at 4°C until use. The amount of Shh-N released by each cell line was measured by human Shh-N ELISA kit (R&D system), following the manufacturer´s instructions.

2.4.7 Endpoint measurement (ATP quantification) of cells proliferation

The endpoint proliferation assay was performed with CellTiter-Glo luminescent assay (Promega). The assay bases on the measurement via luminescence reaction of cellular ATP, which corresponds to the quantity of metabolically active cells. The optimal number of cells per well to seed in order to maintain the cells in the log phase after 72 hours of treatment was determined for each specific cell line. In the specific, 2500 c/w for HEK293 cells, 1250 c/w for A549 cells and 2000 c/w for PANC-1 cells were plated in a 96-well plate with reduced serum DMEM (2%FBS) and allowed to adhere overnight. Subsequentially, the cells were treated with the compounds at the reported concentrations and incubated for a further 72 hours. Celltiter-Glo (Promega) was performed according to the manufacturer´s instructions. For HUVECs, the assay was applied to analyze the viability of the cells upon treatment with dPGS. In this case, 5000 c/w were plated in a 96 well/plate with complete EGM2 culture medium (2.4.1) and allowed to adhere for initial 6 hours of incubation. Afterward, dPGS was added at the reported concentrations and the viability of the cells was monitored after 72 hours.

2.4.8 Real-time monitoring of cells proliferation

Real-time cell monitoring was performed with IncuCyte (Sartorius). HEK293, PANC-1, and A549 cells were seeded at the same density as above reported for the endpoint assay. The cells were incubated in DMEM supplemented with 2% FBS for the initial 24 hours, time upon which the treatment with reported concentrations of dPGS and dPGTPS started. The proliferation rate was measured in terms of increment in cell confluency monitored via Incucyte v2019A software. For a better comparison and to rule out minor errors due to differential cell numbers between wells, the confluency value at the time point before compound addition (24 hours after seeding) was normalized to value 1. Real-time cell monitoring was performed for a total of 100 hours (76 hours after treatment).

2.4.9 Cellular spheroids formation

Spheroids were obtained via plating cells into Cellcarrier spheroids ultra-low attachment (ULA) 96-well microplates (PerkinElmer) in DMEM (2% FBS). To enable cell aggregation the plates were centrifuged at 1000 rpm for 10 min in a Megafuge 2.0 (Heraeus) directly after cells seeding. The plates were then immediately incubated. Following the protocol described by Friedrich et al. [269] spheroids were formed that reached after 4 days of incubation a diameter of around 400 µm. The spheroid's morphology was monitored via microscopic observation with Inverted microscope Axio Observer Z1 (Carl Zeiss). Bright-field pictures (4x magnification) were collected for the spheroids at each time point. The bright-field images were then analyzed via AnaSP [265], an open-source program that enables automatic extraction of the main morphological parameters (such as diameter, volume, area, and sphericity) from the bright-field images of the spheroids. The method of evaluation for the different parameters finds comprehensive explanations in the related article [265]. After optimization of initial cells seeding number, 500 c/w for PANC-1, 1000 c/w for A549 and 125-250 c/w for HEK293 cells were seeded in order to obtain macro-spheroids that reached by day 4^{th} of incubation a diameter of ~400 µm. On day 4^{th} of incubation, the treatment with dPGS and dPGTPS started. The medium was refreshed every 2-3 days via carefully exchanging 50% of the volume (=100µl) with the use of a

multichannel (8 channels) pipette. For monitoring the effect of the treatment, the differential volume growth of control untreated compared to treatment at different time points were evaluated. Following the protocol of Friedrich et al. [269] the spheroid's growth was monitored up to 5-times increase of the initial volume. This condition was applicable in case of HEK293 and PANC-1 cells. For A549, the cells showed a slow growth rate and were monitored for 15 days upon seeding without reaching 5-times initial volume. For calculation of percentage volume decrease, the growth rate of spheroids was firstly calculated via subtracting the spheroids volume measured at day 4 (V_{day4}) to the time point of the observation (V_{dayx}). Following, the growth rate of treated spheroids was divided by the growth rate of untreated ones and multiplied to 100, which gave the percentage growth rate normalized to control untreated (100%). The percentage growth reduction was then calculated subtracting 100 to the percentage normalized growth rate.

2.4.10 Spheroids cytotoxicity analysis

Spheroids were formed and treated as previously described (2.4.9). After 72 hours of incubation upon treatment, each spheroid in 100 µl volume was transferred with the help of 1 mL tip (ends cut) to a Nunc white 96-well plate (Thermofisher). Cytotoxicity test was performed via Celltiter-Glo3D kit (Promega), following the manufacturer´s instructions.

2.4.11 HUVECs angiogenic growth-factors-dependent proliferation

HUVECs, cultured between passage 3 to 6, were seeded at a density of $2x10^3$ c/w in a 96-well plate in EBM-2 endothelial basal medium supplemented only with 2% FBS and GA-1000, at the manufacturer´s concentrations. Cells were let adhere for initial 6 hours of incubation. Afterward, VEGF, FGF1, and FGF2 diluted in EBM-2 (2% FBS, GA-1000) at increasing concentrations ranging between 0.01 to 1000 ng/ml were added to the cells at 200 µl final volume. For dPGS/heparin inhibition studies, fixed concentrations of cytokines (3 ng/ml of FGF2 and 50 ng/ml of either FGF1 and VEGF) were mixed with increasing concentrations of inhibitor ranging between 5 to 50 µM in 200 µl final volume and initially incubated for 5 min prior adding it to the cells. After 72 hours of incubation, the

proliferation was measured following the addition of 20 µl per well of Celltiter AQueous one solution MTS proliferation assay (Promega) directly to the cell culture medium. The reagent contains a tetrazolium salt [3-(4,5-dimethylthiazol-2-yl)-5-(3-carboxymethoxyphenyl)-2-(4-sulfophenyl)-2H-tetrazolium, MTS] combined with an electron coupling phenazine ethosulfate (PES), and enables to estimate the number of metabolically active cells proportionally to the mitochondrial conversion of MTS to formazan. Cells were incubated in the presence of MTS reagent for further 2 hours. The absorbance was recorded at 490 nm with Infinite M200 microplate reader (Tecan Trading).

2.4.12HUVECs tubes formation assay

For tubes formation assay, HUVECs cultured always between passage 3 to 6, were sub-cultured one day before the experiment in a T25 flask (Corning) at a density of $1x10^4$ cells/cm^2, in order to reach 70% confluency after 24 hours incubation. Cultrex reduced growth factor basement membrane (BME) matrix (Trevigen) was allowed to thaw overnight in an ice bucket at 4 °C, further aliquoted on ice and stored at -20°C. Prior to the experiments, to prevent matrix jellification, which rapidly takes place above 8°C, all consumables required, such as tips and µ-slides Ibitreat (Ibidi), were let cool down to -20°C for minimum 30 min. 100 µl frozen BME matrix was rapidly thawed on ice and 10 µl was carefully added to each well of a µ-slide, also located on ice. The slide was gently tapped at the sides to ensure uniform distribution. The BME was let polymerize at 37°C for 40 min. HUVECs were diluted to a final volume of 70 µl per well at the optimal density of $9x10^3$ c/w (µ-slide) in EGM-2 containing all supplements excluded heparin in presence or absence of dPGS (5, 10 and 50 µM). The mixture of cells and inhibitors were added to each well of a BME-coated-µ-slide and incubated at 37°C. After 5-, 8- and 20-hours a phase-contrast picture (4x magnification) was collected for each well with inverted microscope Zeiss Axio Observer z-1 (Zeiss). Picture analysis was performed via ImageJ tool Angiogenesis analyzer. Tube formation efficiency was evaluated considering three parameters: total tube lengths (pixel), number of nodes and total meshes area (pixel) per field.

2.5 Statistical analysis

The Kruskal-Wallis non-parametric test followed by Dunn´s post-test was applied to compare differential treatments to control untreated, in case of data that did not follow a normal distribution. Confidence interval percentage was set to 95% and p-value ≤ 0.05 considered significant. Normally distributed data were validated by the quantile-quantile (Q-Q) plot and by the D'Agostino Pearson normality test. Assuming normal distribution, one-way ANOVA followed by Dunnett's post hoc test was applied.

3 Results

3.1 Dendritic polyglycerol sulfates as potential Shh pathway inhibitors

3.1.1 Shh-N protein expression and purification

The active fragment of Shh protein coding for Shh-N terminus was cloned into a plasmid vector pcDNA6/V5 His-A enabling eukaryotic expression. Furthermore, the DNA was fused in-frame to a poly-histidine tag for further purification purposes. The eukaryotic expression system was chosen as it enabled to express the dually lipidated (cholesterol and palmitoyl modified) active Shh-N protein. The transient transfection of HEK293 cells was achieved by lipofection. Given the lipid modifications, Shh anchors and multimerizes at the cell membrane level and, from there, it is released into the extracellular space. Therefore, it was expected to detect the protein in the cell culture medium of the transfected HEK293 cells, also called Shh-N conditioned medium (Shh CM). As a control, a parallel expression of the plasmid vector without insert was performed and the respective supernatant named control conditioned medium (Control CM). Transfection was initially performed in the presence of 10% (FBS) and 2% FBS, collected after 72 hours and 96 hours post-transfection, respectively (see 2.4.2 for details). The secretion of recombinant Shh-N was monitored via Coomassie protein staining (**Figure 12a**) and immunodetection using a polyclonal antibody against Shh-N protein (**Figure 12b**). As predicted, the Shh-N protein was released in the culture medium and migrated in a three bands pattern with a molecular mass of about 19 kDa, which agrees with the expected molecular mass of the mature Shh-N. The absence of protein was confirmed for the control supernatant derived from transfection with empty vector, carried out under the same transfection condition.

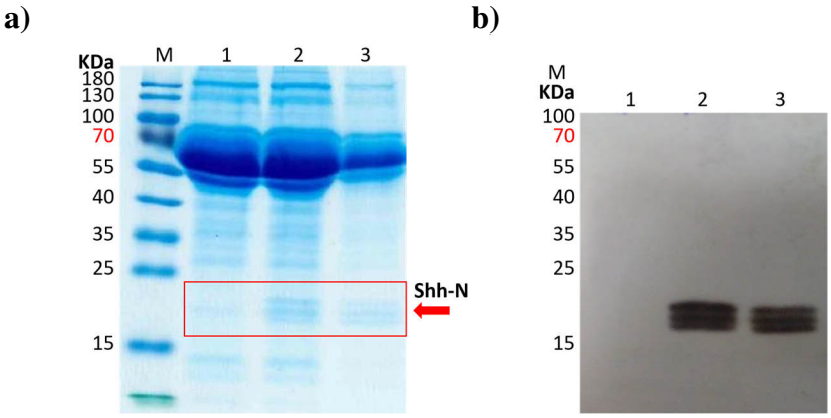

Figure 12: Shh-N protein expression in HEK293 cells. Detection via **a)** Coomassie protein staining and **b)** Western blot immunodetection. Transient expression of Shh-N protein and control empty vector in 10% FBS containing cell medium collected at 72 hours after transfection and expression of Shh-N protein in 2% FBS containing culture medium collected after 72 hours from medium switch (96 hours post-transfection).

3.1.1.1 Shh-N protein purification

The presence of the polyhistidine-tag allowed for the purification of the recombinant protein via Ni-NTA affinity chromatography (**Figure 13**). Furthermore, a reduction of FBS content from 10 (**Figure 13a**) to 2% (**Figure 13c**) during expression resulted in increased purity of the protein after purification. The silver gel staining in **Figure 13c** supports the purity of the eluted and concentrated sample (lane 8) with predominant bands corresponding to 19 kDa-migrating Shh-N, whereas only a faint band could be detected corresponding to the molecular mass of FBS (~65 kDa).

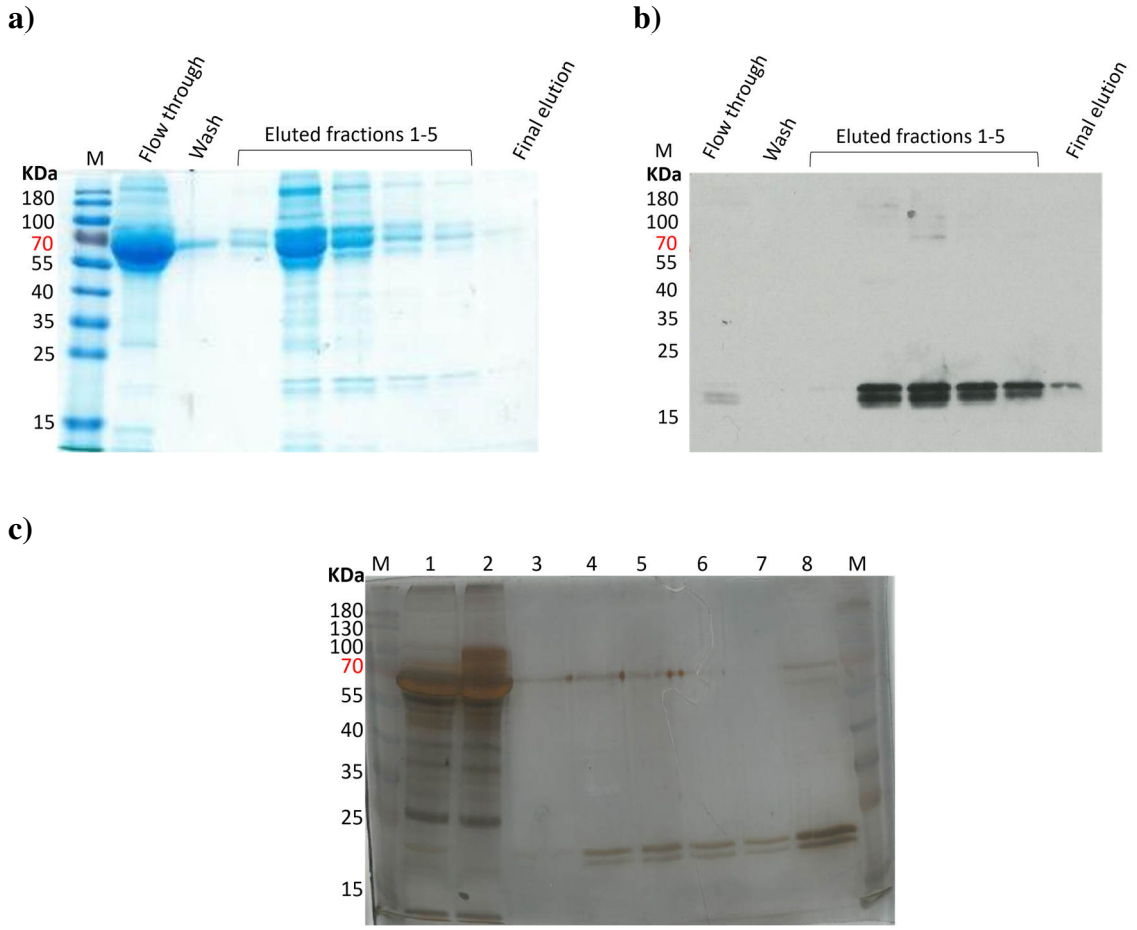

Figure 13: Shh-N protein detection and purification. a) Coomassie protein staining and **b)** Western blot immunodetection for Ni-NTA purification of Shh CM (10% FBS). M, marker; Flow-through; Wash; Eluted fractions (1-5); Final elution (column wash). **c)** Silver gel protein staining for Shh-N purification from Shh CM (2 % FBS) via Ni-NTA chromatography. 1, Shh-N CM input; 2, Flow-through; 3-7, Elution fractions; 8, Eluted fractions after PD10 column desalting and concentrated via Amicon-filter.

3.1.2 Surface Plasmon Resonance (SPR) affinity measurement for Shh-N to dendritic polyglycerol sulfates

The binding affinity of the Shh-N protein towards both dendritic polyglycerol sulfate structures dPGS and the shell cleavable variant dPGTPS was studied via surface plasmon resonance (SPR). For the binding assay, the sulfated compounds were synthetized as biotinylated ligands and further immobilized on a streptavidin (SA) precoated SPR-sensor chip. Increasing concentrations of Shh-N were injected and the interaction recorded via single-cycle kinetics experiments (SCK). The SPR sensorgrams describing Shh-N binding are shown in **Figure 14**. Binding constants are given as association constant (k_a),

dissociation constant (k_d) and equilibrium dissociation constant (K_D) and derive from the fit assuming the 1:1 Langmuir interaction model. For both macromolecules, a similar binding behavior was observed, with K_D values in nM range. Specifically, the polymer dPGS gave a K_D value of 88.7 nM, whereas a K_D value of 37.6 nM was calculated for dPGTPS.

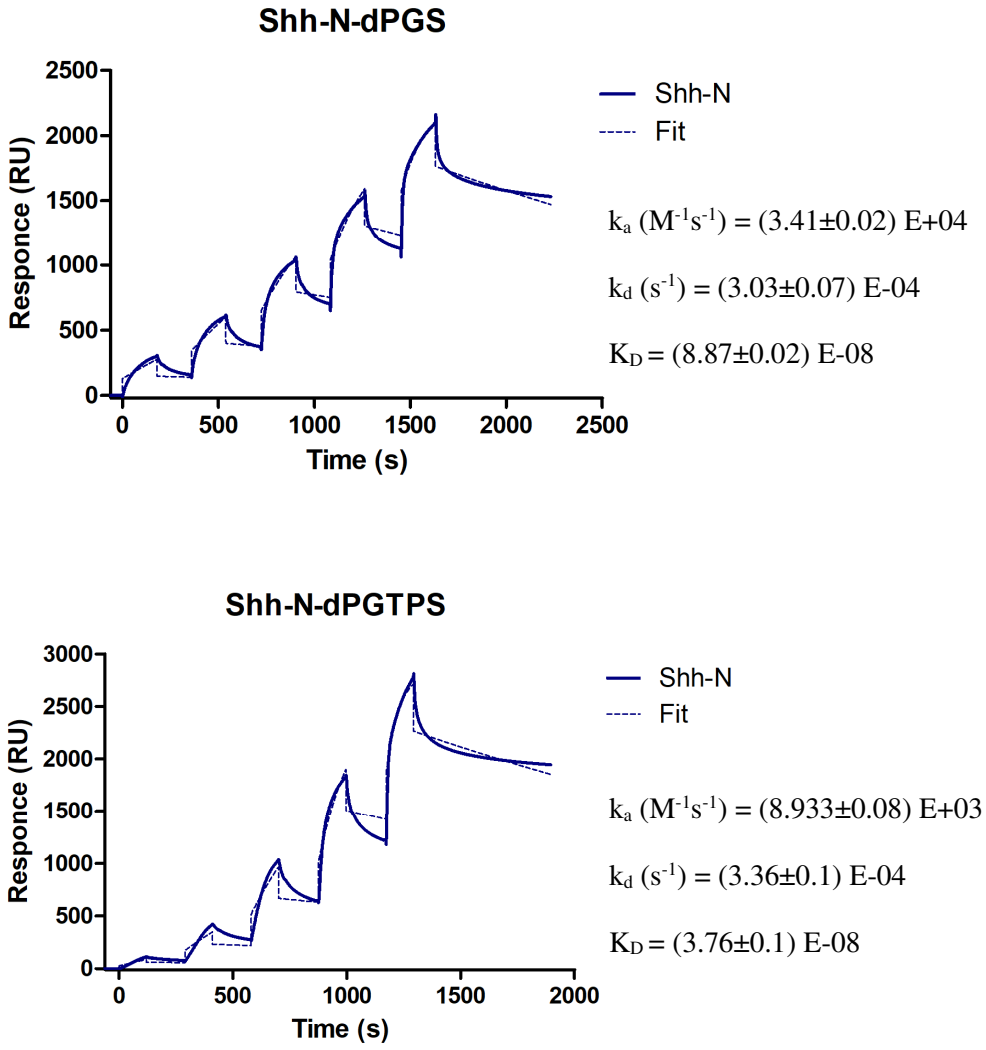

Figure 14: Single-cycle kinetics (SCK) evaluation of Shh-N-dPGS/dPGTPS interaction. Representative sensorgram of the Resonance Units (RU) response against time during SCK experiment performed via injecting five increasing concentrations of Shh-N over either dPGS (top) or dPGTPS (bottom) functionalized SPR sensor chip. The fitting was obtained by using a 1:1 Langmuir binding model. The kinetic constants (k_a, k_d, K_D ±SE) are reported beside the sensorgram. For dPGS interaction evaluation, Shh-N was injected at concentrations of 125, 250, 500, 1000 and 2000 nM, whereas for dPGTPS was injected at concentrations of 25, 74, 222, 667 and 2000 nM.

3.1.3 *In vitro* quantitative analysis of Shh-signaling pathway activation in cell-based assays

To study the Shh-signaling pathway, investigations were performed in two distinct reporter cell lines. In the first place, experiments were carried out with the C3H10T1/2 cell line, a fibroblast pre-osteoblast cell line that expresses as osteogenesis marker, the alkaline phosphatase (ALP) enzyme, upon Shh-pathway activation. Second, an NIH-3T3 reporter cell line stably transfected with a GLI-dependent firefly luciferase reporter, named Shh Light2 (ShhL2) cells, was applied. In this cell-based assay, the luciferase expression is specifically led by the activation of GLI-transcription factors as a result of Shh-pathway activation. GLI translocation to the nucleus and subsequent binding to an 8xGLI binding factor cassette activates the promoter controlling luciferase expression. The luciferase is ultimately measured, upon reaction with a specific substrate, as light signal emission.

3.1.3.1 Conditions optimization for Shh-signaling pathway activation

The activation of the Shh-pathway was first tested and optimized for both cell-based assays (**Figure 15**).

a)

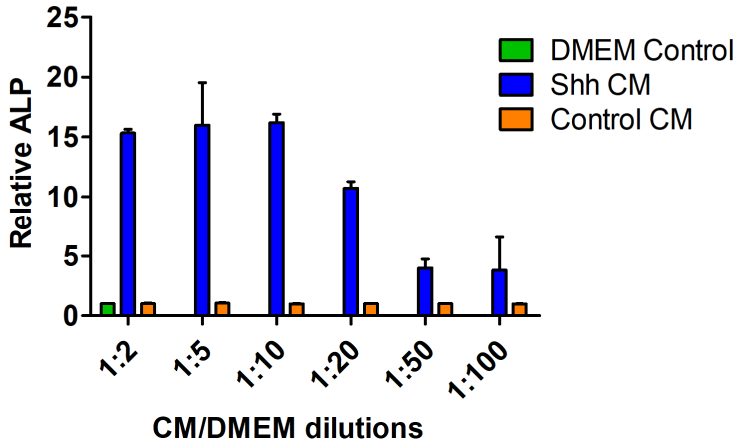

b)

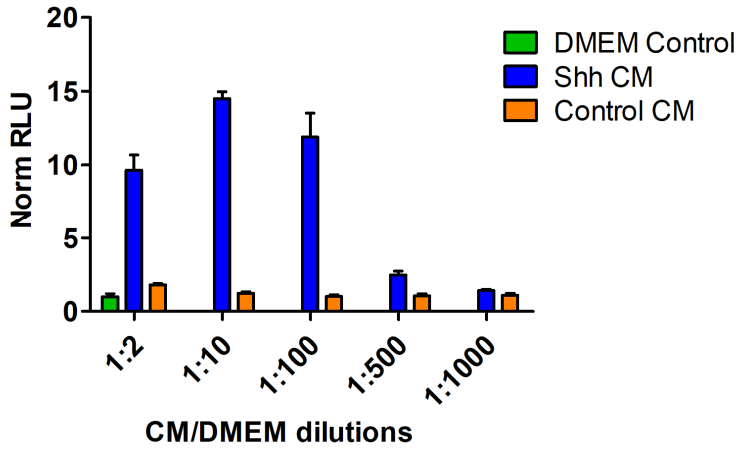

Figure 15: Activation of Shh-pathway in luciferase and ALP reporter cell-based assays. a) Activation of Shh-pathway in the C3H10T1/2-ALP reporter cell line. Reported dilution ratios of either Shh CM or control CM in fresh DMEM cell culture medium were added to the cells and incubate for 72 hours. ALP was measured via colorimetric reaction read at 405 nm absorbance. **b)** Shh-pathway activation in ShhL2 luciferase reporter cell line. Reported dilution ratios of either Shh CM or control CM in cell culture medium were added to the cells and incubated for 30 hours. Luciferase activity was measured after reaction with firefly luciferase and expressed as normalized RLU emitted. For both assays, the results are expressed as normalized to untreated control (DMEM control). Bars represent the mean of *n=4* independent experiments each performed in quadruplicates ± SEM.

Shh-pathway was stimulated by treating the cells with dilutions of either Shh CM or control CM in fresh culture medium. For further studies and for both assays the 1:10 dilution ratio of Shh-N conditioned medium was chosen as enabled a reasonable pathway activation. The absence of unspecific activation was observed in the case of treatment with control CM and with DMEM growth medium.

3.1.3.2 Inhibition of Shh-pathway in ALP- reporter cell line

At first, the capability of dPGS and dPGTPS to down-regulate Shh-pathway was tested in the ALP-reporter cell-based assay. The inhibitory activity of the dendritic polyglycerol sulfates was compared to heparin and the specific inhibitor of GLI transcription factor GANT61 (**Figure 16**).

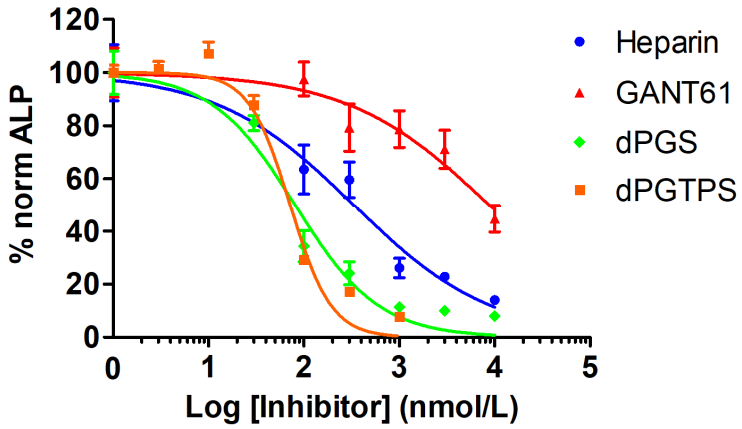

Figure 16: Inhibition of Shh-pathway in C3H10T1/2-ALP reporter cell line by dPGS, dPGTPS and controls heparin and GANT61. The pathway was stimulated with Shh CM: DMEM at a 1:10 ratio. Increasing concentrations of dPGS, heparin, GANT61 (ranging between 30 nM to 10 µM) and dPGTPS (ranging between 3 nM to 1 µM) were mixed with the stimulation medium and added to the cells. ALP production was measured after 72 hours of incubation. Both dPGS and dPGTPS showed high inhibitory potential, slightly higher than heparin and 100-fold stronger when compared to GANT61. The results are expressed as percentage normalized to Shh-pathway activation treatment set to 100% activity. Bars represent the mean of $n>4$ independent experiments each performed in quadruplicates ± SEM.

In this case, both dPGS and dPGTPS showed a comparable strong pathway inhibitory capacity with IC_{50} values of 81 and 72 nM, respectively. The natural polysulfate heparin showed indeed an IC_{50} of 330 nM and GANT61 a higher IC_{50} value of 8.8 µM.

In **Figure 17** are reported the controls experiments showing the absence of unspecific effects potentially derived from control CM in combination with the inhibitors.

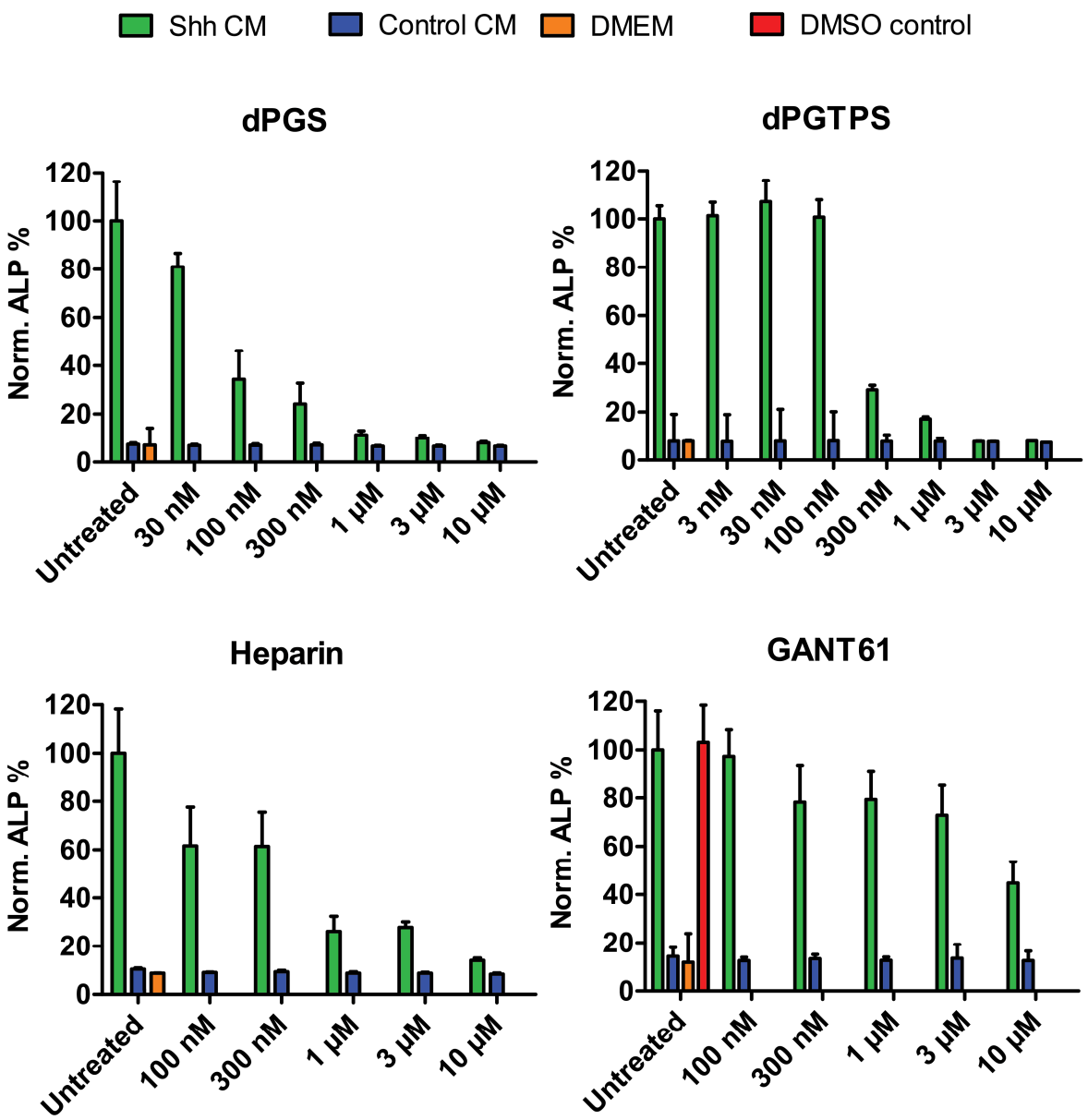

Figure 17: Control experiments: inhibition of Shh-pathway in C3H10T1/2-ALP reporter cell line by dPGS, dPGTPS and controls heparin and GANT61. The pathway was stimulated with either control CM or Shh CM diluted at a 1:10 ratio in fresh DMEM culture medium. Increasing concentrations of dPGS, heparin, GANT61 (ranging between 30 nM to 10 µM) and dPGTPS (ranging between 3 nM to 1 µM) were mixed with the stimulation medium and added to the cells. For GANT61 a control with DMSO (0,2 %) was performed. ALP production was measured after 72 hours of incubation. The results are expressed as percentage normalized to Shh-pathway activation treatment, set to 100% activity. Bars represent the mean of $n>4$ independent experiments each performed in quadruplicates ± SEM.

To confirm that the inhibition of Shh-pathway did not correspond to a side effect of the compound cytotoxicity, cell viability studies were performed by measuring the amount of the released cellular cytosolic enzyme lactate dehydrogenases (LDH) (**Figure 18**) in response to concentration-dependent treatments. For comparisons and calculations, in the

positive control, the cells are treated with 1% Triton-X for the whole duration of the experiment, in order to ensure complete cell death. The cytotoxicity assays were performed after 24 and 48 hours. The results confirmed the absence of cytotoxic effects, with only a reduction of the viability below 10% detected after 48 hours incubation.

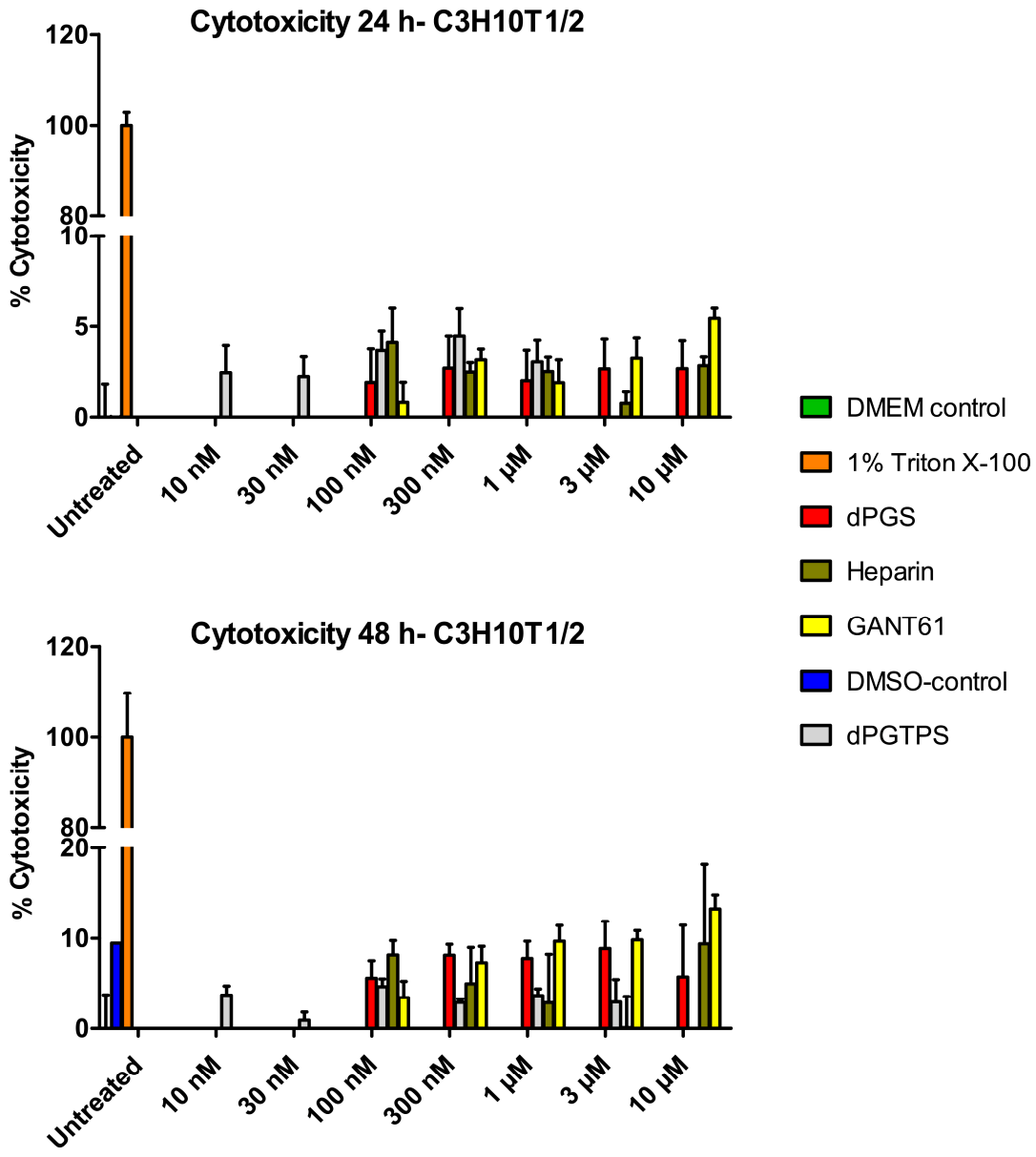

Figure 18: LDH-based cytotoxicity assay for C3H10T1/2 cells after 24- and 48-hours treatment with dPGS, dPGTPS and controls heparin and GANT61. Cells were seeded in a 96-well plate at the density of 5.000 c/w and treated after 24 hours incubation with reported concentrations of dPGS, dPGTPS, heparin, and GANT61. For the positive control, 1% Triton-X was used to ensure complete cell death. Negative control corresponds to untreated cells. For all treatments, no cytotoxicity was observed. Cytotoxicity is expressed in percentage and calculated as reported in the material and method section 2.4.5. Bars represent the mean of $n>3$ independent experiments each performed in triplicate ± SD.

3.1.3.3 Inhibition of Shh-pathway in luciferase-reporter cell line

Afterward, the inhibitory efficiency of the compounds was evaluated in the luciferase reporter cell line ShhL2 (**Figure 19**). In agreement with the ALP measurement, dPGTPS and GANT61 showed activities with respective IC_{50} values of 111 nM and 1.2 µM. However, surprisingly, the treatment with dPGS resulted in a remarkably reduced inhibition in comparison to the ALP measurements, with a measured IC_{50} of 6.5 µM, 80-fold higher than the value measured in the ALP-based assay. An even more evident reduction was noticed in the case of heparin, where apparently a slight dose-dependent inhibition can be observed, which however led only to a 15% pathway inhibition at the highest concentration tested (10 µM), impeding thus IC_{50} determination.

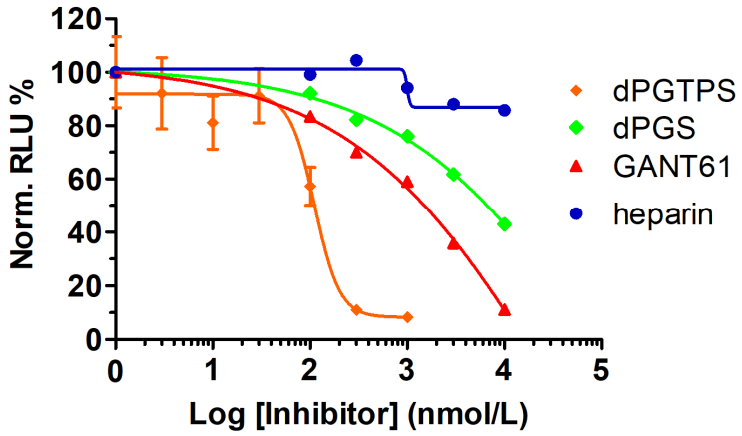

Figure 19: Inhibition of Shh-pathway in ShhL2 luciferase reporter cell line by dPGS, dPGTPS and controls heparin and GANT61. The pathway was stimulated with Shh CM: DMEM at a 1:10 ratio. Increasing concentrations of dPGS, heparin, GANT61 (ranging between 30 nM to 10 µM) and dPGTPS (ranging between 3 nM to 1 µM) were mixed with the stimulation medium and added to the cells. Luciferase expression was measured after 30 hours of incubation. dPGTPS and GANT61 inhibit Shh-pathway, in agreement with ALP assay. Contrary, dPGS, and heparin showed remarkably reduced inhibitory capacity. The results are expressed as percentage normalized to Shh-pathway activation treatment set to 100% activity. Bars represent the mean of $n>4$ independent experiments each performed in quadruplicates ± SEM.

In **Figure 20** are reported the control experiments showing the absence of unspecific pathway inhibition.

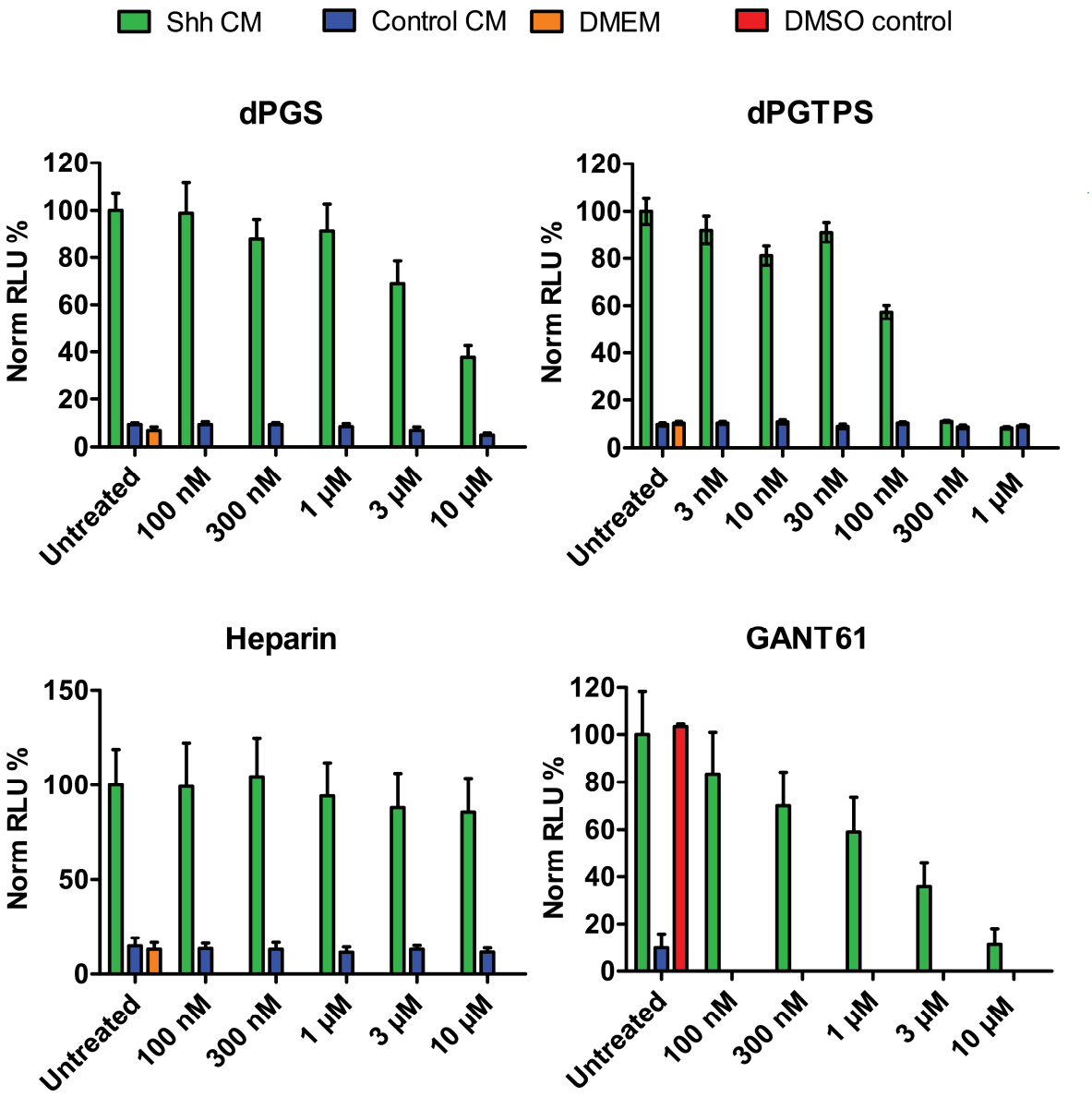

Figure 20: Control experiments: inhibition of Shh-pathway in ShhL2 luciferase reporter cell line by dPGS, dPGTPS and controls heparin and GANT61. The pathway was stimulated with either control CM or Shh CM diluted at a 1:10 ratio in fresh DMEM culture medium. Increasing concentrations of dPGS, heparin, GANT61 (ranging between 30 nM to 10 µM) and dPGTPS (ranging between 3 nM to 1 µM) were mixed with the stimulation medium and added to the cells. For GANT61 a control with DMSO (0,2 %) was performed. Luciferase expression was measured after 30 hours of incubation. The results are expressed as percentage normalized to Shh-pathway activation treatment, set to 100% activity. Bars represent the mean of *n>4* independent experiments each performed in quadruplicates ± SEM.

To evaluate the cytotoxicity of the compounds, cell viability studies via LDH cytotoxicity assay were performed for ShhL2 cells **(Figure 21).**

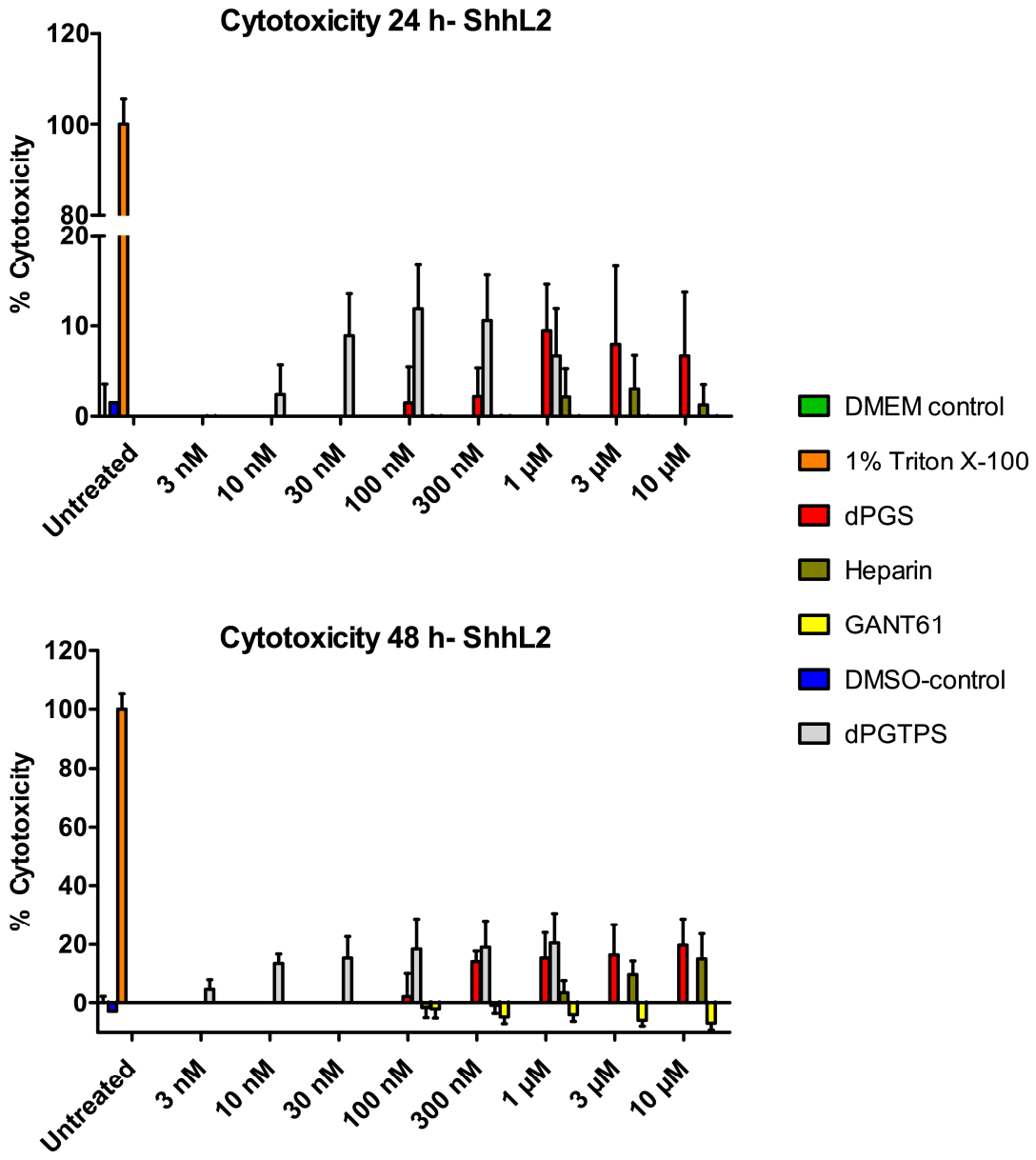

Figure 21: LDH-based cytotoxicity assay for ShhL2 cells after 24- and 48-hours treatment with dPGS, dPGTPS and controls heparin and GANT61. 24 hours after seeding the cells in a 96 well/plate at the density of 5.000 c/w and treated with reported concentrations of dPGS, dPGTPS, heparin, and GANT61 in DMEM 0,5% FBS. For the positive control, cells were treated with 1% Triton X, to ensure complete cell death. Negative control corresponds to untreated cells. For all treatments, no cytotoxicity was observed. Cytotoxicity is expressed in percentage and calculated as reported in material and method (2.4.5). Bars represent the mean of $n>3$ independent experiments each performed in triplicate ± SD.

Measurements were carried out at 24 and 48 hours of cell incubation with the tested compounds and controls. The results confirmed the absence of cytotoxic effects at 24 hours incubation with ≤10% viability reduction at the highest concentrations. However, at 48 hours an increase in cytotoxicity was observed for dPGS and dPGTPS with ≤ 20% viability reduction at concentrations above 300 nM. Despite the viability measurements were carried

out at 24- 48-hours of incubation, luciferase assay was performed always after 30 hours incubation with the compounds. Therefore, a reduced influence of the compound's toxicity on the reduction of Shh pathway activation is expected.

3.1.4 dPGS and dPGTPS effect on autocrine Shh-pathway- mediated proliferation

Shh-signaling pathway in cancer operates via diverse models of activation (1.3.3). Autocrine pathway activation depends on tumoral cells up-regulation of ligand expression, which supports the cancer cells self-operating signaling loop activation and perpetuation. Thus, cancer cells that are secreting Shh protein, are expected to possibly respond to the produced ligand and activate Shh-autocrine signaling to support their proliferation and metastasis.

3.1.4.1 Shh-N expression and release in cancer and non-malignant cells

At first was performed a screening of cells expressing Shh protein and secreting it in the cell culture medium, as an earliest indication for potential Shh-pathway activation. In addition, the selection of the specific cancer cell lines based on literature information that confirms the expression of the Shh-pathway ligand and cascade components for the cell lines included in the study. To quantify the ligand expression and secretion capacity of each cell line, cells were cultivated to confluence and the culture supernatant analyzed via a sandwich ELISA (2.4.6). The results are reported in **Figure 22.** The assay confirmed that the cancer cells included in the screening as pancreatic cancer cells PANC1 and MiaPaCa-2, breast carcinoma cells MCF-7 and lung adenocarcinoma A549 cells, differentially express and secrete Shh-N in the cell culture medium. Moreover, a significantly reduced release of Shh-N was confirmed for the control cell lines, as visible for the human embryonic kidney cells HEK293 and murine mesenchymal stem cells C3H10T1/2. Those, as non-tumorigenic cells, are expected to show reduced or absent expression of Shh

ligand, although they are known to present the signaling machinery to respond to Shh-ligand dependent signal activation.

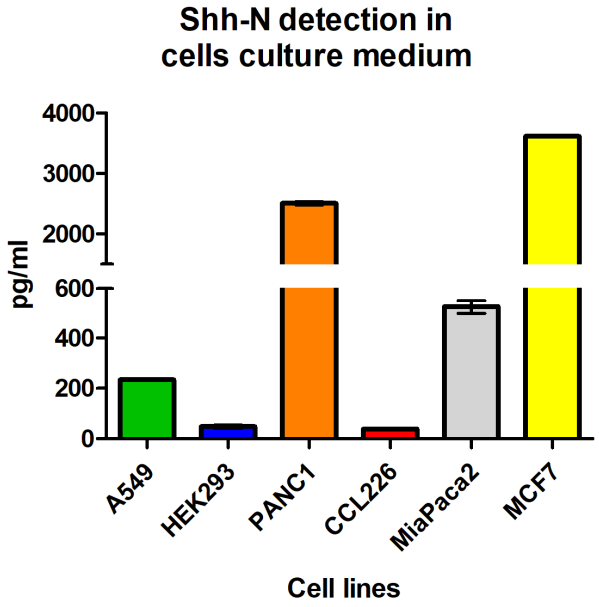

Figure 22: ELISA quantification of Shh-N secretion in cell culture medium in carcinogenic and non-carcinogenic cell lines. Cells were cultivated to confluence and cells supernatant was used for Shh-N amount quantification via sandwich ELISA. Differential Shh-N expression and secretion was confirmed by tumorigenic cell lines, whereas a significantly reduced amount of ligand was detected in control non-tumorigenic cells. Bars represent the mean of *n=2* independent experiments each performed in triplicate ± SD.

3.1.4.2 dPGTPS and dPGS-dependent anti-proliferative activity in 2D cell culture-based assays

The proliferation of A549 and PANC1 cells is known to be affected by Shh-signaling pathway. Furthermore, the above described ELISA assay confirmed the production and release of the ligand in both cell lines. Given the differential amount of Shh expressed by the individual cell lines, low-level (A549, CCL226, HEK293) and high-level (PANC-1, MCF-7) ligand producers cells could be discriminated. To assess if a differential Shh ligand-concentration might influence the anti-proliferative effect of potential Shh-pathway inhibitor, the cell lines A549 and PANC-1 were selected, whereas the HEK293 cells were included as a control cell line. A proliferation/viability endpoint method was compared to a real-time live-cell analysis method. **Figure 23** displays the influence of dPGS and dPGTPS on the proliferation of lung adenocarcinoma A549 cells.

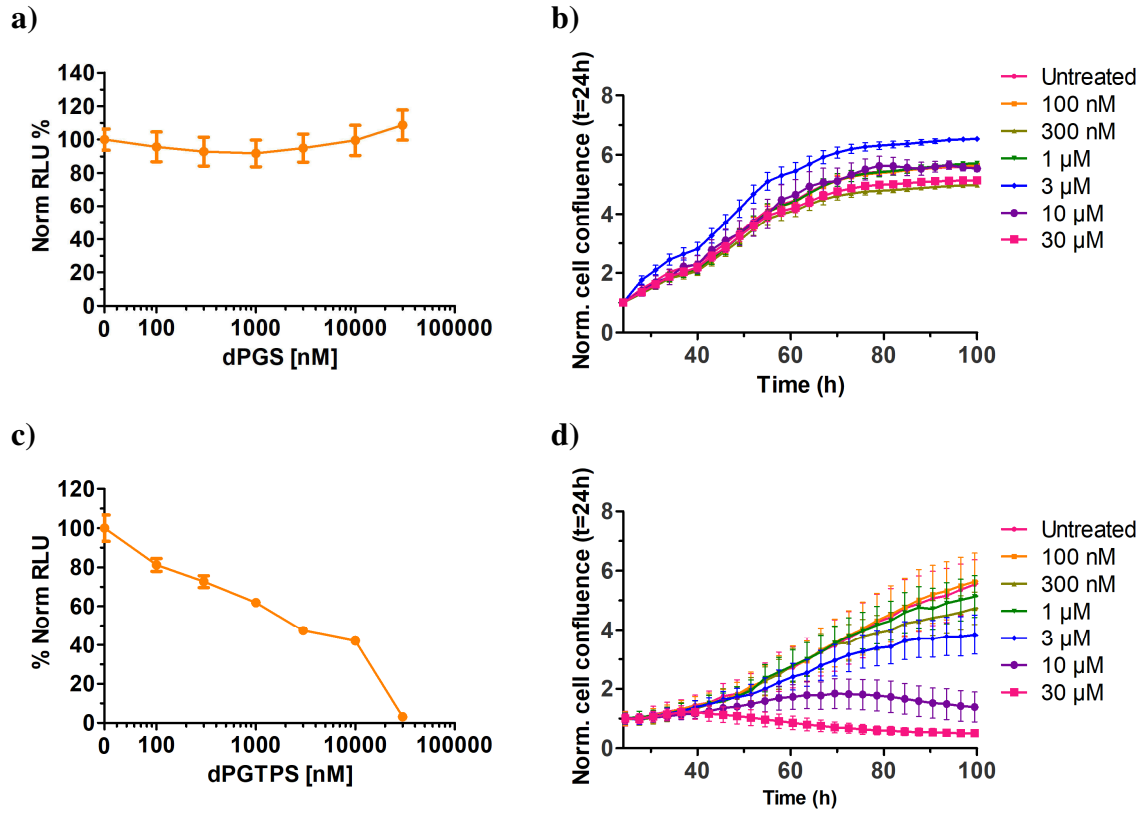

Figure 23: A549 cell proliferation studies via endpoint and real-time measurements. a-c): Endpoint evaluation of dPGS (**a**) and dPGTPS (**c**) influence on A549 cells proliferation. Results are normalized to untreated control set to 100%. Points represent the mean of $n \geq 2$ independent experiments each performed in quadruplicate ± SEM. **b-d)**: live-cells analysis of the proliferation of A549 cells upon treatment with dPGS (**b**) and dPGTPS (**d**). Results show the change in cell confluence over time upon treatment at 24 hours after cells seeding (t=24h). Results are expressed as normalized to t=24h set to 1. Points represent the mean for each condition performed in quadruplicates ±SD.

A549 cells, are low-level Shh ligand producers but known to depend also on Shh-signaling for their proliferation. Surprisingly, dPGS had no effect in terms of reduction of cell proliferation both in endpoint measurement (**Figure 23a**) and in the real-time analysis (**Figure 23b**); not even at the highest concentration (30 µM). In contrast, the sulfated compound dPGTPS showed a concentration-dependent reduction of proliferation, with an IC_{50} of 2.27 µM, when quantified via endpoint measurements (**Figure 23c**). The result obtained from the endpoint measurement additionally corresponds to the real-time proliferation analysis via Incucyte (**Figure 23d**), where at 100 hours after seeding, corresponding to 76 hours of treatment, dPGTPS treatment resulted in IC_{50} value of 3.6 µM.

Based on high Shh ligand expression, the pancreatic carcinoma PANC-1 cells were further tested (**Figure 24**).

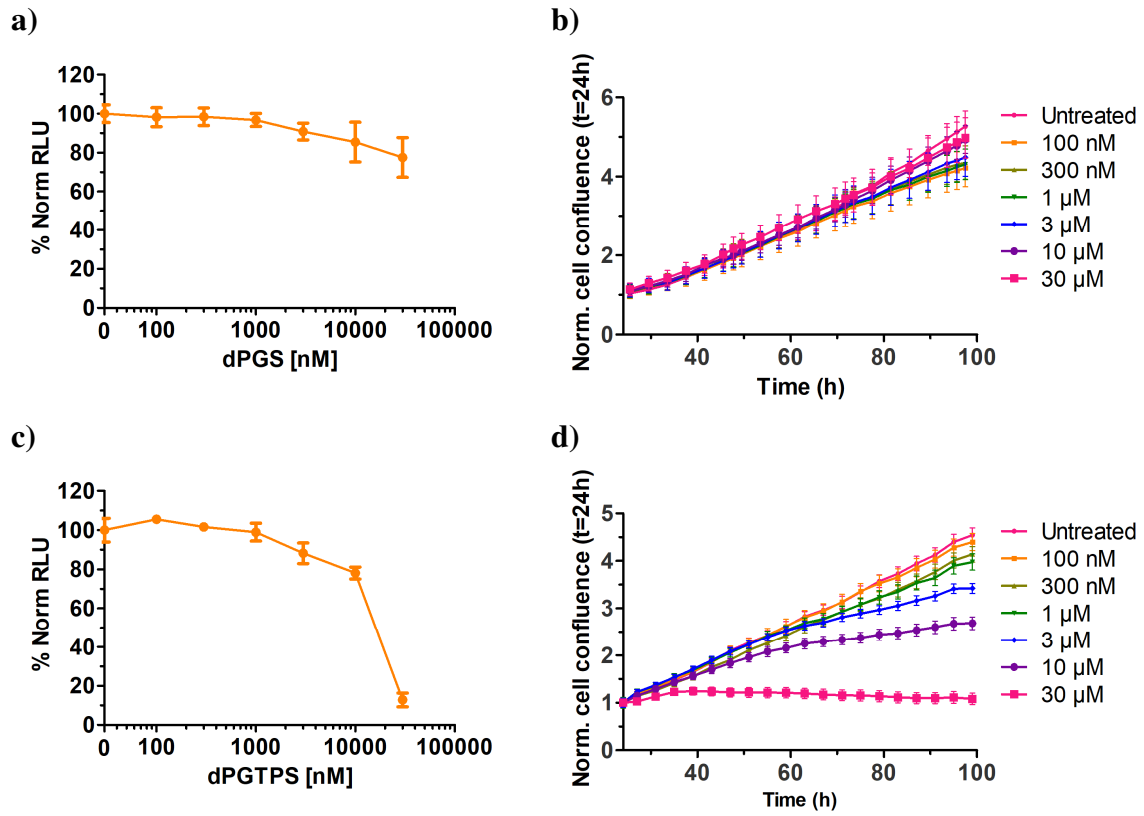

Figure 24: PANC1-1 cell proliferation studies via endpoint and real-time measurements. a-c): Endpoint evaluation of dPGS **(a)** and dPGTPS **(c)** influence on PANC-1 cells proliferation. Results are normalized to untreated control set to 100%. Points represent the mean of *n=3* independent experiments each performed in quadruplicate ± SEM. **b-d)**: live-cells analysis of the proliferation of PANC-1 cells upon treatment with dPGS (**b**) and dPGTPS (**d**). Results show the change in cell confluence over time upon treatment at 24 hours after cells seeding (t=24h). Results are expressed as normalized to t=24h set to 1. Points represent the mean for each condition performed in quadruplicates ±SD.

In the case of dPGS, despite the endpoint measurement (**Figure 24a**) showed a slight concentration-dependent decrease of proliferation, with ≤20% reduction of proliferation at 30 µM, the real-time monitoring (**Figure 24b**) exhibited an absence of substantial effect dPGS-dependent. In contrast, dPGTPS showed again a decrease in cells proliferation. Interestingly, for PANC-1 cells the anti-proliferative effect of dPGTPS was lower than in comparison to the effect observed for A549 cells. For the endpoint measurement (**Figure 24b**), dPGTPS, in a dose-dependent manner, affected cell proliferation resulting in a 20% reduction at 10 µM concentration, a value which drastically dropped to baseline for the highest concentration of 30 µM. In this case, an IC_{50} value of

15 µM was calculated. Comparable values were obtained for real-time monitoring assays (**Figure 24b**), for which an IC_{50} of 11 µM was calculated.

The results showed the absence of an anti-proliferative effect for dPGS in both cancer cell lines under study. In contrast, dPGTPS displayed a dose-dependent inhibiting effect on cancer cell proliferation. The result at this point might suggest a potential anti-tumorigenic capacity for the dPGTPS. To test this hypothesis, the effect of the polysulfates was evaluated on non-carcinogenic cell line HEK293 cells (**Figure 25**).

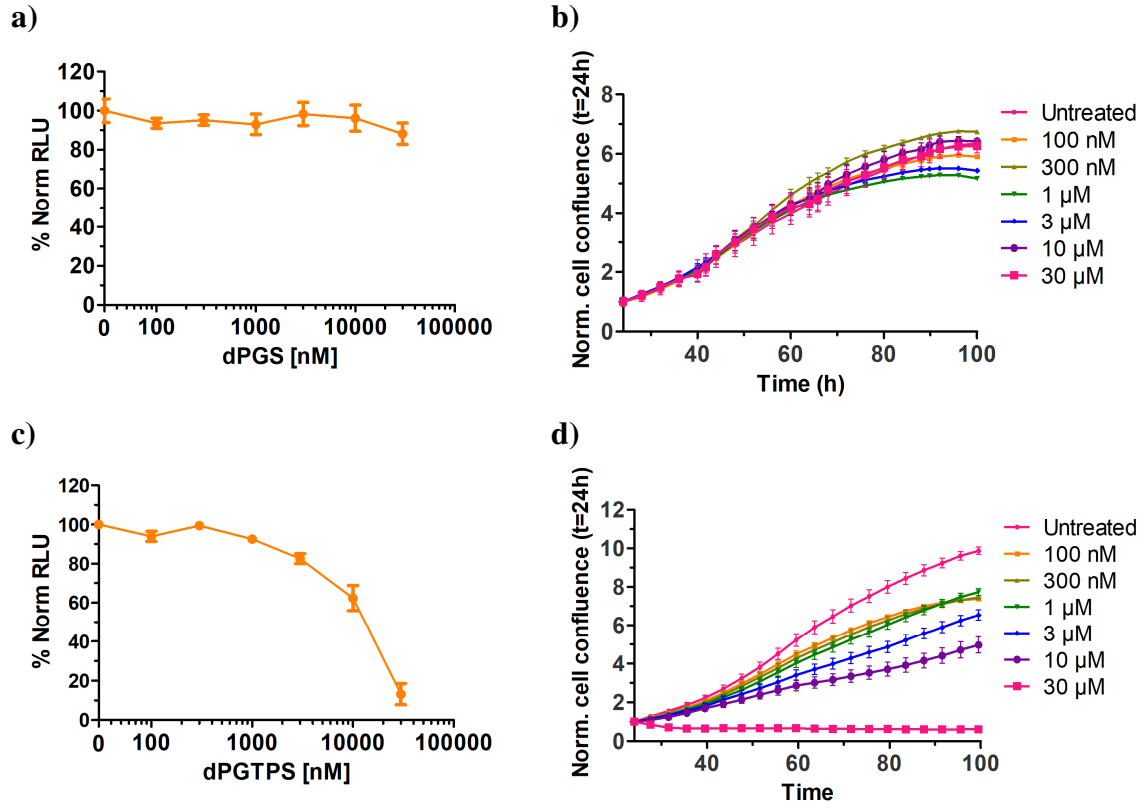

Figure 25: HEK293 cell proliferation studies via endpoint and real-time measurements. **a-c**: Endpoint evaluation of dPGS (**a**) and dPGTPS (**c**) influence on HEK293 cells proliferation. Results are normalized to untreated control set to 100%. Points represent the mean of n=3 independent experiments each performed in quadruplicate ± SEM. **b-d**: live-cells analysis of the proliferation of HEK293 cells upon treatment with dPGS (**b**) and dPGTPS (**d**). Results show the change in cell confluence over time upon treatment at 24 hours after cells seeding (t=24h). Results are expressed as normalized to the value at t=24h set to 1. Points represent the mean for each condition performed in quadruplicates ±SD.

Despite the fact that for dPGS neither in the endpoint measurement (**Figure 25a**) nor in the real-time analysis system (**Figure 25b**) an anti-proliferative effect was observed, dPGTPS induced indeed a decrease of the cells proliferation in a concentration-dependent manner. For the non-carcinogenic cells, dPGTPS treatment resulted in an IC_{50} of 11 µM in

the endpoint method (**Figure 25c**) and an IC_{50} of 10.7 µM in the live-cell analysis (**Figure 25d**).

3.1.4.3 Dendritic polyglycerol sulfates affect cellular growth in 3D-spheroids model

2D cell culture systems are able to generally represent the cells physiological conditions, but lack in recreating the real cellular environment, where ECM deposition by the cells, higher cell-to-cell, and cells-to-ECM contacts contribute in maintaining cell homeostasis, as well regulating cells response to drugs. Therefore, to better understand the effect of dPGS and the variant dPGTPS in a more physiological context, cell culture studies were performed in a 3D-cell system via the formation of cellular spheroids. Here, the cultivation of the cells occurs on an Ultra-Low Adherent (ULA)-coated surface to stimulate the formation of a single cellular aggregate, called spheroid. Given their compact assembly, the spheroids of ~400 µm diameter are considered to mimic more closely the *in vivo* microarchitecture of human solid tumors, as they develop a particular structural organization where three main cells layers can be distinguished: a proliferative external cells layer, a middle quiescent and an internal necrotic layer. Going from the external to the internal layer, hypoxia and catabolites accumulation increase, while the reduction of nutrients and metabolites takes place.

In this study, the evaluation of the spheroids proliferation was assessed via monitoring changes in volume growth after treatment, which started at day 4 after cells seeding, and ended when the spheroids reached about 5-times the initial volume or at day 15 (in case of slow-growing cells). For each cell line, the number of cells to be seeded in order to obtain medium-large spheroids of ~400 µm in diameter at day 4 was defined.

- **Lung adenocarcinoma A549 cells**

In the case of A549 cells, 1000 c/w were seeded in a 96-well plate and resulted after 4 days incubation in spheroids of approximately 400 µm diameter (**Figure 26**).

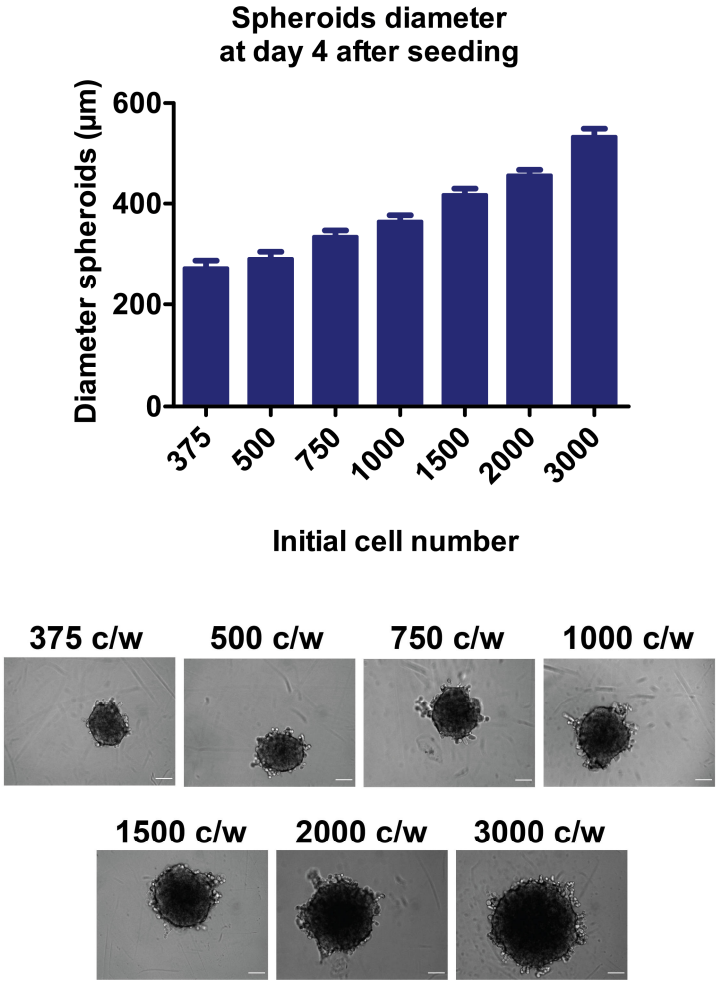

Figure 26: Cell number optimization for A549 spheroids. A549 cells were seeded in DMEM (2 % FBS) at reported cell densities per well in a ULA-96 well microplate. Images of single spheroids were collected at day 4 of incubation and the diameter (µm) analyzed via image analysis AnaSP software. For the cell number optimization study, each condition was performed in sextuplicate Representative 10x magnification phase-contrast images are shown. Scale bar = 100 µm.

Figure 27 shows the effect of the polysulfates on A549 spheroids. Surprisingly, in contrast to the lack of anti-proliferative capacity found in 2D-cells culture, a clear reduction of A549 spheroids growth was observed. The decrease in cell growth followed an apparent dose-dependent manner, and at concentrations ≥30 nM led to complete inhibition of spheroids growth. The growth was followed for 15 days (11 days of treatment) without the cells reaching 5-fold increase of the initial volume, as A549 cells, in contrast to 2D

monolayer growth, showed relatively lower growth rate when cultured as spheroids. At the end point of the observation (day 15), dPGS at the concentration of 3 nM resulted in 41% growth decrease whereas the concentrations above showed ~91% growth reduction compared to control untreated (t=15 days) set to 100%. Specifically, 30 nM induced a reduction of 91%, 300 nM of 97%, 3 µM of 83% and 30 µM of 94%. To confirm that the observed effect did not correspond to eventual compound cytotoxicity a spheroid cytotoxicity test was performed after 72 hours upon treatment start (days 7 after seeding) (**Figure 27b**). No significant dPGS-dependent cytotoxic effect was measured at all concentrations tested. dPGS at 3 nM concentration resulted in 100% spheroids viability whereas higher concentrations caused a slight viability reduction which ranged between 78% to 87% in comparison to the untreated control.

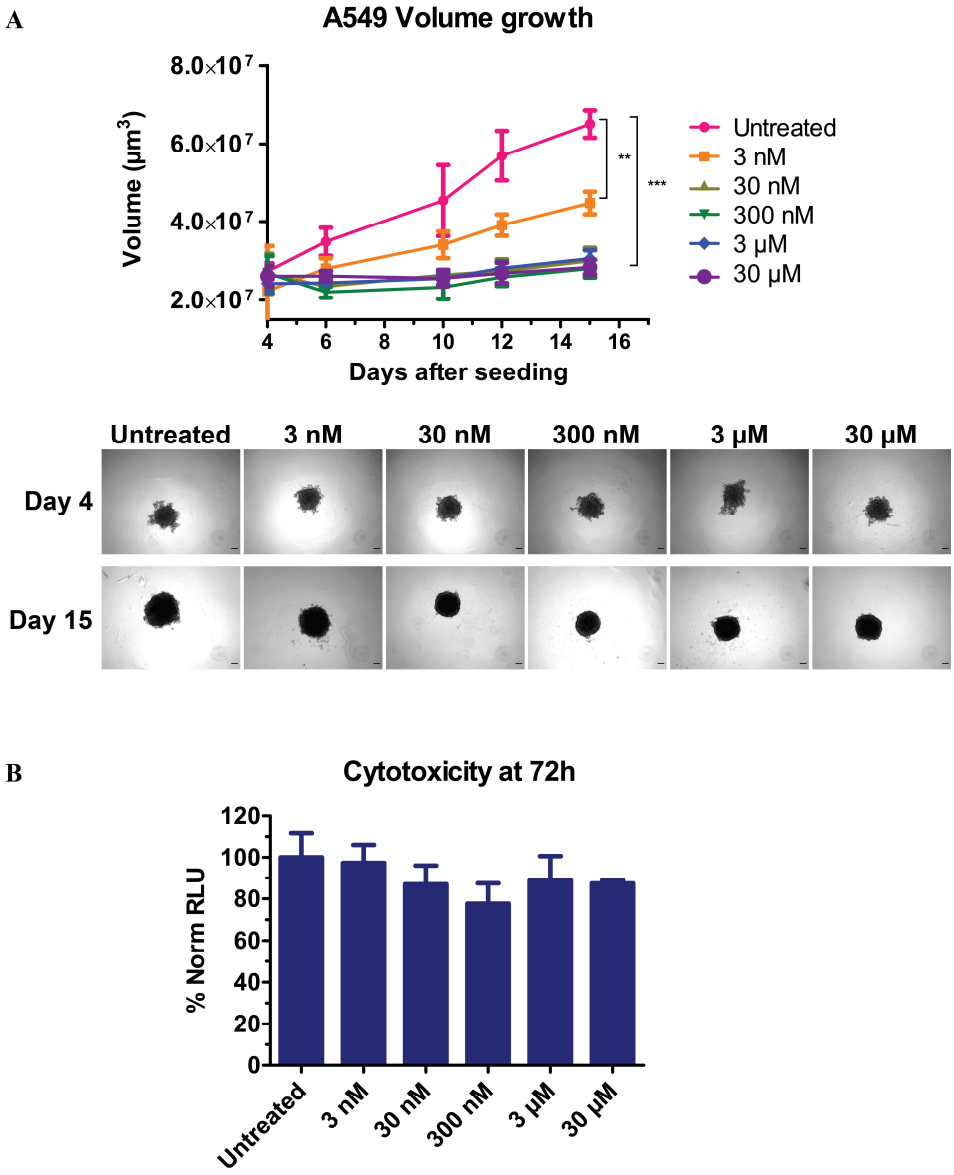

Figure 27: Growth and cytotoxicity analysis of A549 cancer cells spheroids upon dPGS treatment over a period of 15 days. A549 cells were seeded at 1000 c/w density in a ULA-96 well microplate and cultivated until day 4, time upon which dPGS treatment began. **a)** Images of single spheroids were collected at different time points over 15 days incubation. Spheroids volume of control untreated and treated with increasing dPGS concentrations was analyzed via image analysis AnaSP software. Points represent the mean of *n=3* independent experiments each performed in quadruplicate ±SEM. Statistical significance determined by Kruskal-Wallis test followed by Dunn´s post hoc test (Graphpad prism 5.03). *P<0.05, **P<0,01, *** P<0,001 vs untreated control. Some representative images (4x magnification bright field) of each condition at day 4 and at day 15 are shown. Scale bar= 100 µm. **b)** Cytotoxicity was measured at 72 hours of treatment via Cell-titer Glo 3D viability assay. Bars represent the mean *n=2* independent experiments each performed in quadruplicate ± SD. dPGS did not affect the viability of A549 spheroids.

dPGTPS displayed the same trend but with reduced anti-proliferative activity on A549 spheroids (**Figure 28a**). After 3 days of treatment, no substantial difference in growth

volume upon dPGTPS treatment was measured. Additionally, during the whole observation, 3 nM did not influence the growth of the spheroids. For higher concentrations, a reduction in spheroids volume growth was detected, especially visible at day 12 of spheroids culture. However, the highest dPGTPS concentration used (30 µM) did not show constant correspondence to this trend and additionally resulted at day 15 in spheroids damage with evident cell loss; a condition that might reflect a toxic effect in case of longer drug exposure. At the end of the observation (day 15) the concentrations above 3 nM reduced the growth of spheroids of ~58%, compared to control untreated set to 100%. Specifically, 30 nM induced a reduction of 52%, 300 nM of 68%, 3 µM of 64% and 30 µM of 49%. The cytotoxicity analysis performed at 72 hours after treatment begin did not show any substantial toxic effect (**Figure 28b**). dPGTPS at all the concentrations tested resulted in ≥80% cells viability

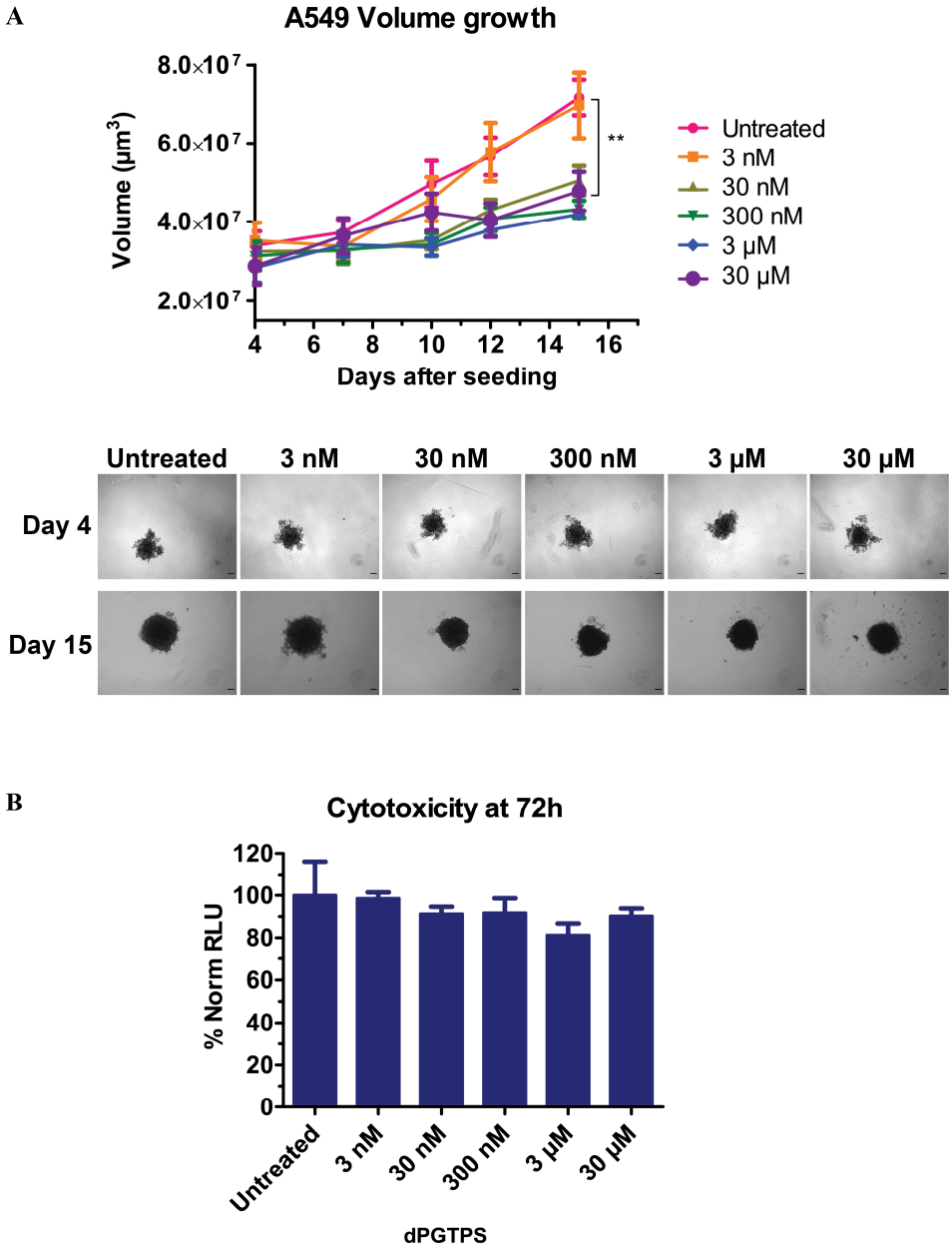

Figure 28: Growth and cytotoxicity analysis of A549 cancer cells spheroids upon dPGTPS treatment over a period of 15 days. A549 cells were seeded at 1000 c/w density in a ULA-96 well microplate and incubated for 4 days before dPGTPS treatment. **a**) Images of single spheroids were collected at different time points over 15 days incubation. Spheroids volume of control untreated and treated with increasing dPGS concentrations was analyzed via image analysis AnaSP software. Points represent the mean of *n=3* independent experiments each performed in quadruplicate ±SEM. Statistical significance was determined by Kruskal-Wallis test followed by Dunn´s post hoc test (Graphpad prism 5.03). **P<0,01 vs untreated control. Some representative images (4x magnification bright field) of each condition at day 4 and at day 15 are shown. Scale bar = 100 µm. **b)** Cytotoxicity was measured at 72 hours of treatment via Cell-titer Glo 3D viability assay. Bars represent the mean *n=2* independent experiments each performed in quadruplicate ± SD. dPGTPS did not affect the viability of A549 spheroids.

- **Pancreatic cancer PANC-1 cells**

The optimized number of PANC-1 cells to be seeded in order to obtain cellular spheroids of approximatively 400 µm diameter at day 4 was found to be 500 c/w (**Figure 29**).

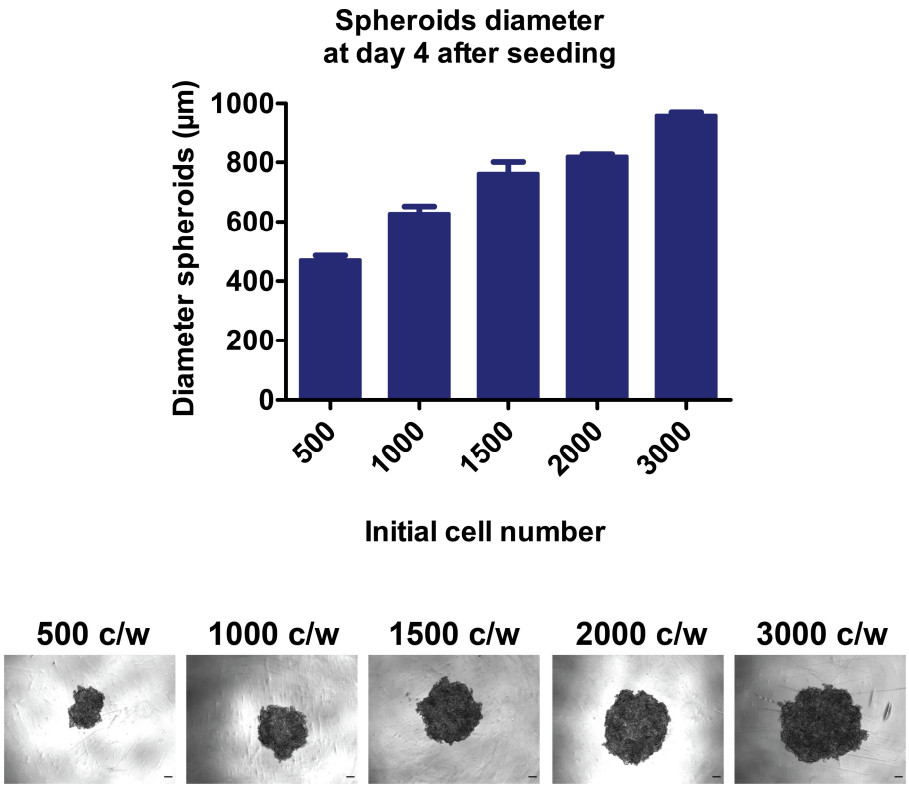

Figure 29: Cell number optimization for PANC-1 spheroids. PANC-1 cells were seeded in DMEM (2 % FBS) at reported cell densities per well in a ULA-96 well microplate. Images of single spheroids were collected at day 4 of incubation and the diameter (µm) was analyzed via image analysis AnaSP software. For the cell number optimization study, each condition was performed in sextuplicate. Representative 5x magnification phase-contrast images are shown. Scale bar= 100 µm

As observed for A549 cells, as well for the pancreatic cancer cells PANC-1, dPGS significantly reduce spheroids volume growth in a dose-dependent fashion (**Figure 30a**); even though in a reduced manner when compared to the lung adenocarcinoma cells spheroids.

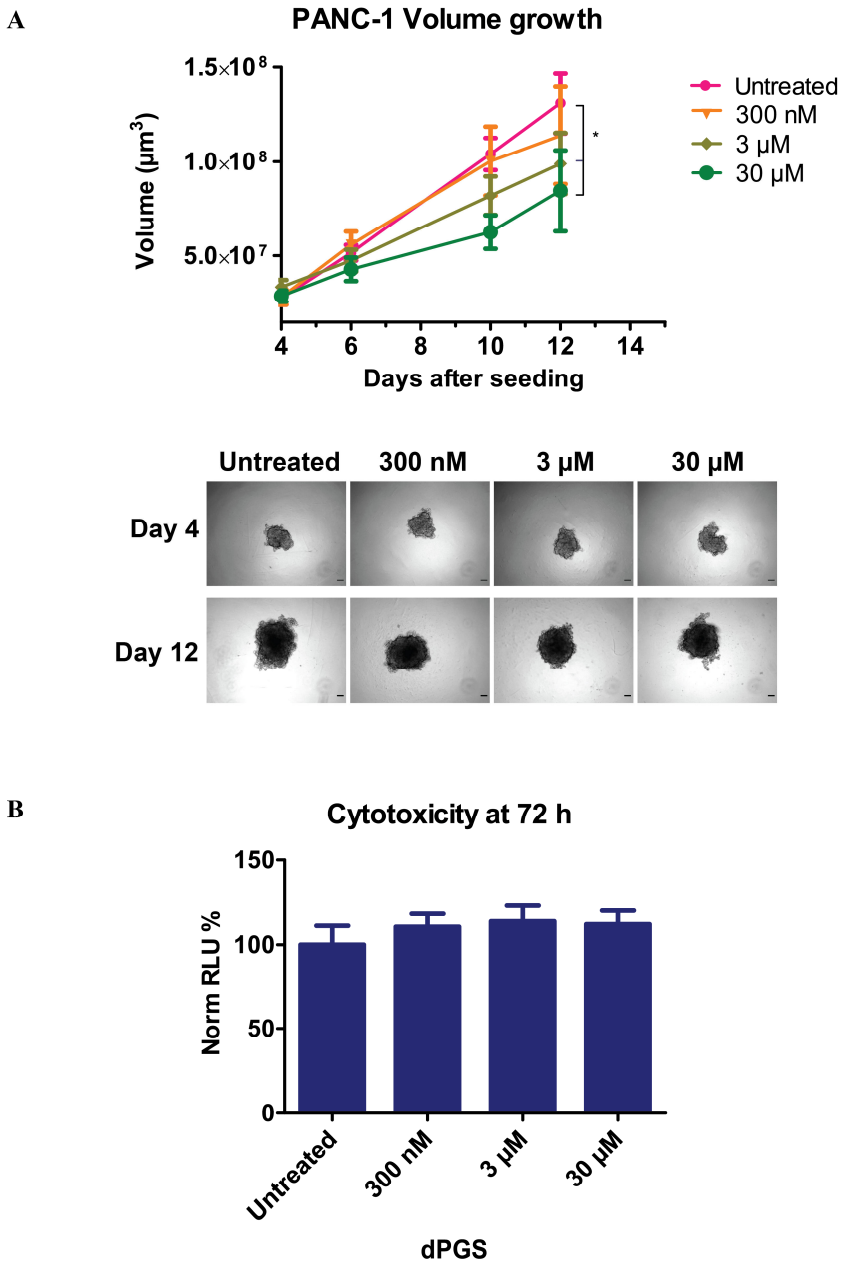

Figure 30: Growth and cytotoxicity analysis of PANC-1 spheroids upon dPGS treatment over a period of 12 days. PANC-1 cells were seeded at a density of 500 c/w in a ULA-96 well microplate and incubated 4 days before dPGS treatment. **a)** Images of single spheroids were collected at different time points over 12 days incubation. Spheroids volume of control untreated and treated with increasing concentrations of dPGS was analyzed via image analysis AnaSP software. Points represent the mean of *n=3* independent experiments each performed in quadruplicate ±SEM. Statistical significance determined by Kruskal-Wallis test followed by Dunn´s post hoc test (Graphpad Prism 5.03) *P<0,05 vs untreated control. Some representative images (4x magnification bright field) of each condition at day 4 and at day 12 are shown. Scale bar = 100 µm. **b)** Cytotoxicity was measured after 72 hours of treatment via Cell-titer Glo 3D viability assay. Bars represent the mean *n=2* independent experiments each performed in quadruplicate ± SD. dPGS did not affect the viability of PANC-1 spheroids

dPGS at the concentration of 300 nM did not influence spheroids growth, however, at the concentrations of 3 and 30 µM a clear reduction of the spheroids growth could be detected, starting already after 6 days of treatment (day 10), and remarkably after 8 days (day 12, end of the observation). On day 12, when the spheroids reached 5-fold of the initial volume and formed a visible necrotic core, a dPGS concentration-dependent volume reduction was measured. Specifically, upon the treatment with 300 nM, 3 and 30 µM dPGS, the spheroids displayed respectively 17, 37 and 46% volume reduction, compared to untreated control (t=day 12) set to 100%. Moreover, dPGS did not result toxic for PANC-1 cells, as shown by the spheroid cytotoxicity test in **Figure 30b.**

dPGTPS treatment showed indeed to not influence the growth of PANC-1 spheroids up to 3 µM, whereas 30 µM treatment resulted in visible spheroids disaggregation and cell loss, leading to 75% volume growth reduction compared to control untreated (t=day 12) set to 100% (**Figure 31a**). Moreover, a cytotoxic effect was confirmed by a toxicity test, where 34% reduction viability was observed already after 72 treatment with 30 µM dPGTPS (untreated control set to 100%). The growth inhibitory effect of 30 µM might, therefore, correspond to a cytotoxic effect rather than an anti-proliferative functionality.

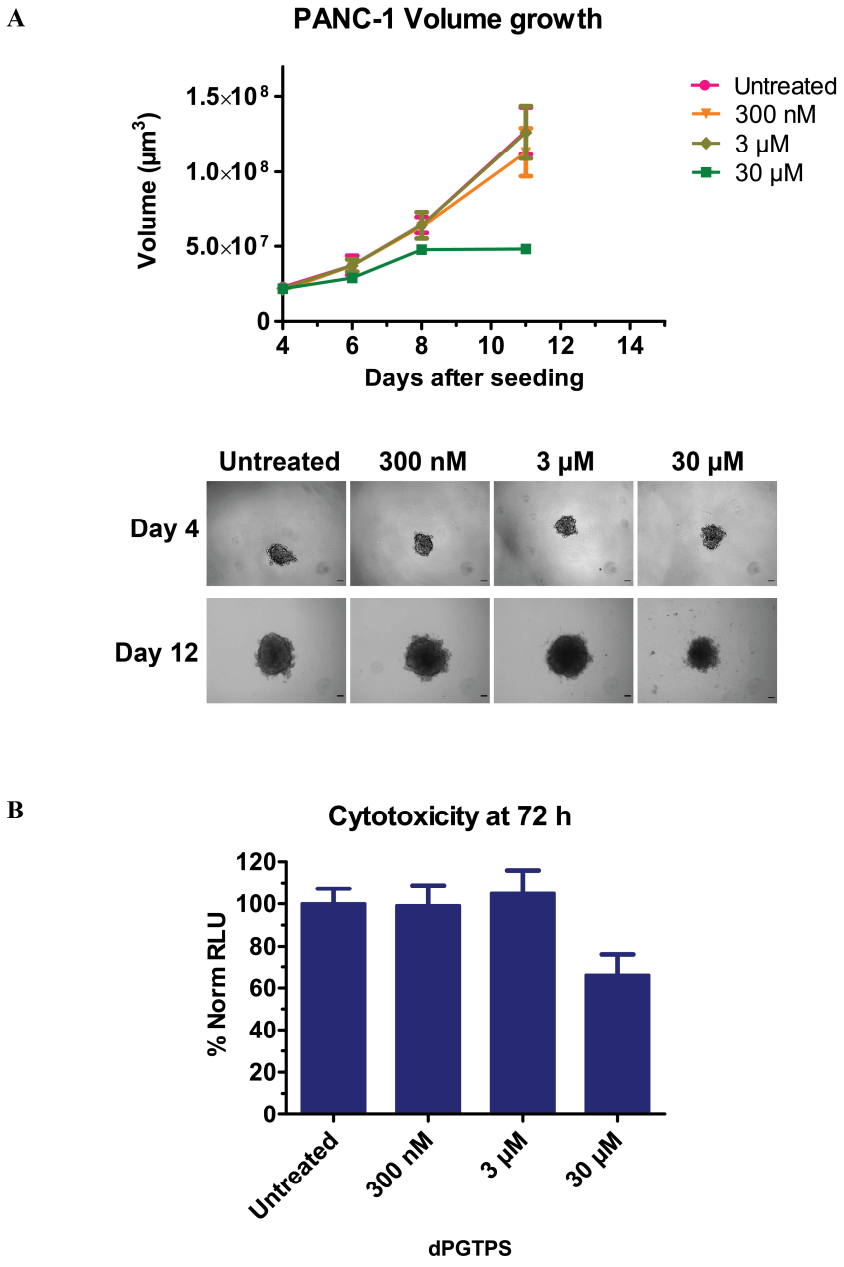

Figure 31: Growth and cytotoxicity analysis of PANC-1 spheroids upon dPGTPS treatment over a period of 12 days. PANC-1 cells seeded at a density of 500 c/w in a ULA-96 well microplate are cultivated until day 4, time upon which dPGTPS treatment began. **a)** Images of single spheroids were collected at different time points over 12 days incubation. Spheroids volume of control untreated and treated with increasing dPGTPS concentrations was analyzed via image analysis AnaSP software. Points represent the mean of *n=2* independent experiments each performed in quadruplicate ±SEM. Some representative 4x magnification bright-field images for each condition at day 4 and at day 12 are shown. Scale bar = 100 µm. **b)** Cytotoxicity was measured after 72 hours of treatment via Cell-titer Glo 3D viability assay. Bars represent the mean n=2 independent experiments each performed in quadruplicate ± SD. dPGTPS at 30 µM concentration induces PANC-1 spheroids toxicity.

- **Human embryonic kidney HEK293 cells**

The optimized initial number of HEK293 cells to be seeded in order to obtain spheroids of approximatively 400 µm diameter at day 4 was found to be 250 c/w (**Figure 32**).

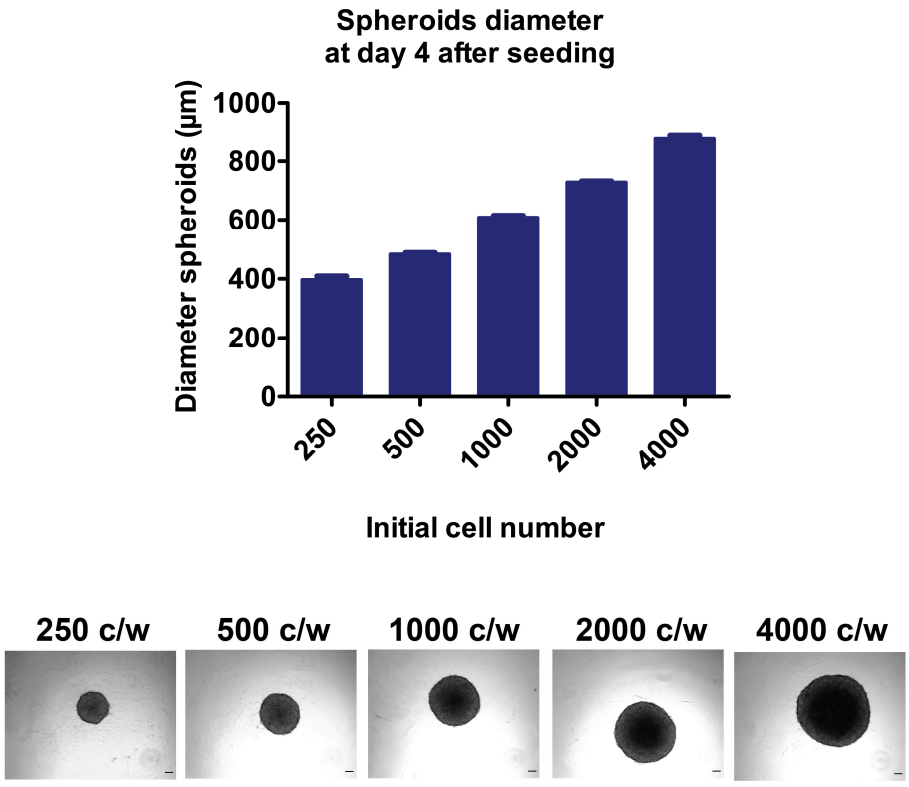

Figure 32: Cell number optimization for HEK293 spheroids. HEK293 cells were seeded in DMEM (2 % FBS) at reported cell densities per well in a ULA-96 well microplate. Images of single spheroids were collected at day 4 of incubation and the diameter (µm) was analyzed via image analysis AnaSP software. For the cell number optimization study, each condition was performed in sextuplicate. Representative 5x magnification phase-contrast images are shown. Scale bar = 100 µm

When HEK293 spheroids, which reached at day 4 a diameter of about 400 µm, were treated with dPGS at concentrations of 300 nM, 3 and 30 µM, a controversial effect was observed (**Figure 33**). At days 7, when a 3.7-fold increase of the initial volume was achieved and the spheroids reached 570 µm diameter, the treatment with dPGS caused apparent increase in volume, with the highest pick observed upon treatment with 3 µM dPGS, which visibly resulted in partial loss of integrity (**Figure 33**, day 7-dPGS 3 µM). Additionally, also 30 µM caused a modification of the shape of the spheroid, tending to a more ellipsoidal form. No effect was detected for control untreated cells.

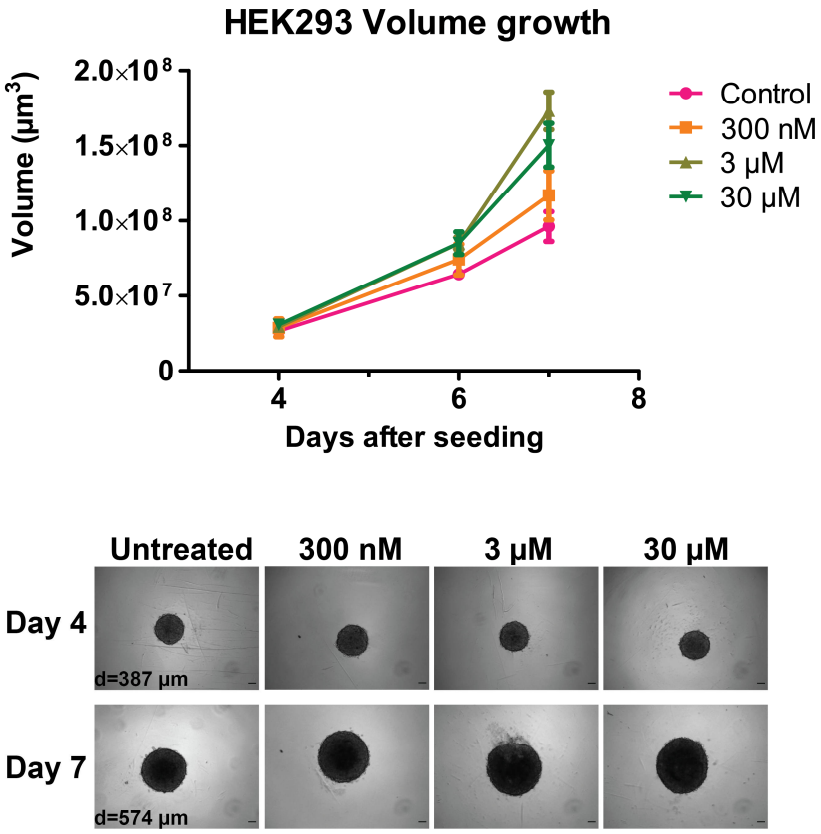

Figure 33: Growth analysis of HEK293 spheroids upon dPGS treatment over a period of 7 days. HEK293 cells seeded at a density of 250 c/w in a ULA-96 wells microplate are cultivated until day 4, upon which dPGS treatment began. Images of single spheroids were collected at different time points over 7 days incubation. Spheroids volume of control untreated and treated with increasing dPGTPS concentrations was examined via image analysis AnaSP software. Points represent the mean of *n=2* independent experiments each performed in quadruplicate ± SEM. Some representative 4x magnification bright-field images for each condition at day 4 and at day 7 are shown. Diameter (µm) of control spheroids at day 4 and 7 is reported. Scale bar= 100 µm.

To test if the effect of dPGS treatment might be dependent on the diameter of the spheroids, the number of seeded cells was reduced to 150 c/w (**Figure 34**).

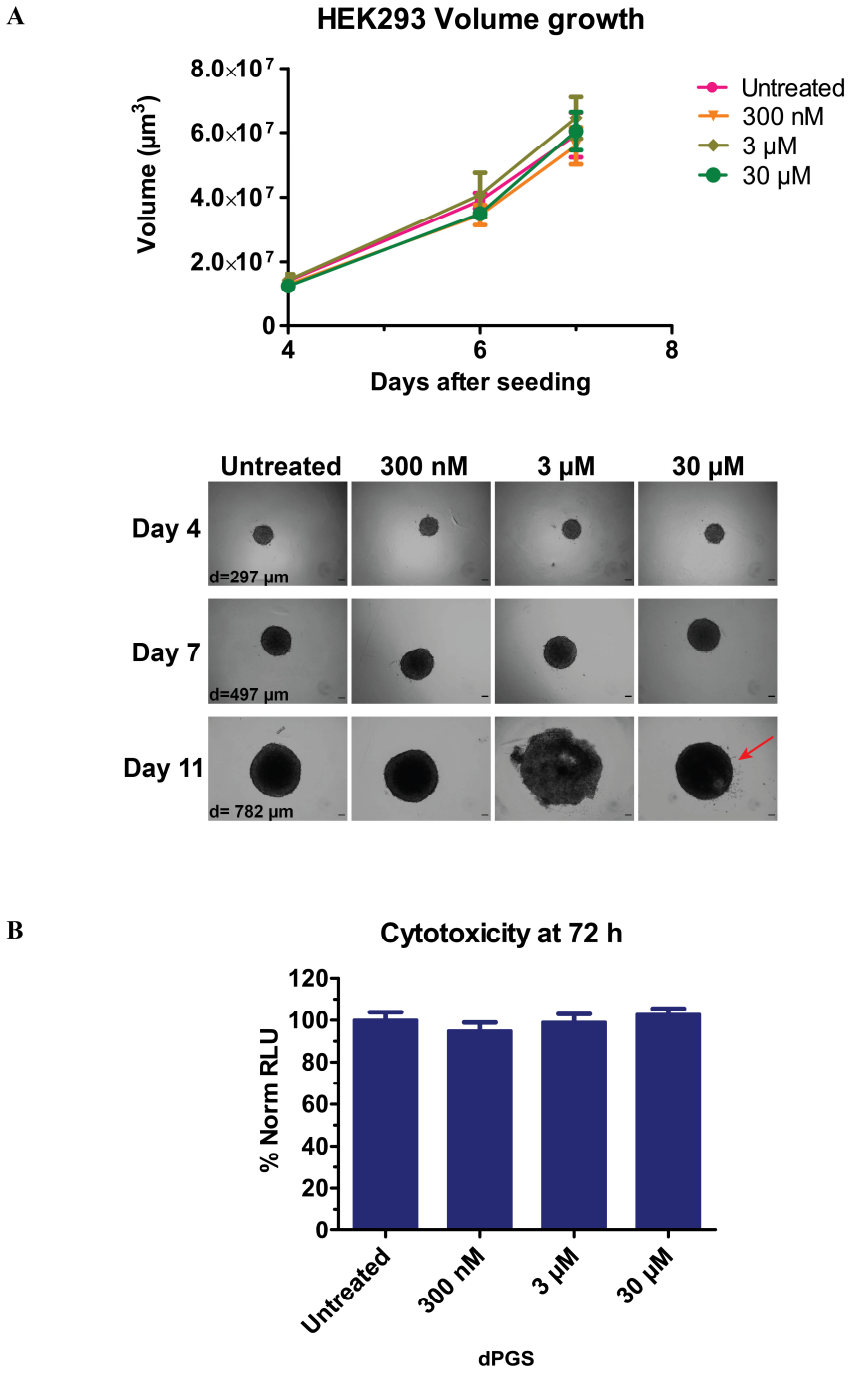

Figure 34: Growth and cytotoxicity analysis of HEK293 (150 c/w) spheroids upon dPGS treatment over a period of 7 days. HEK293 cells were seeded at a density of 150 c/w in a ULA-96 well microplate and cultivated until day 4, time upon which dPGS treatment began. **a**) Images of single spheroids were collected at different time points over 7 days incubation. Spheroids volume of control untreated and treated with increasing dPGS concentrations was examined via image analysis AnaSP software. Points represent the mean of *n=2* independent experiments each performed in quadruplicate ± SEM. Some representative 4x magnification bright-field images for each condition on days 4, 7 and 11 are shown. On day 11, in the case of 30 µM treatment, the arrow indicates early signs of loss of spheroids integrity, whereas for 3 µM treatment a clear spheroid disaggregation can be observed. Diameter (µm) of the control untreated spheroids is reported. Scale bar = 100 µm. **b**) Cytotoxicity was measured after 72 hours of treatment via Cell-titer Glo 3D viability assay. Bars represent the mean *n=2* independent experiments each performed in quadruplicate ± SD.

In this case at day 4, the spheroids have grown to a diameter of <300 µm, which reached 500 µm at day 7. Additionally, after 7 days of incubation, a 4.5-fold increase in the initial volume was achieved. At this point, dPGS did not seem to affect the volume growth of the spheroids and to cause any toxic effect (**Figure 34a-b**). However, when monitored the same spheroids at a later time point (day 11), a spheroids loss of integrity upon dPGS treatment took place: spheroid disaggregation was noticed upon treatment with 3 µM, whereas initial loss of integrity was identified in 30 µM treated spheroids. The results agree with previous observations for the experiments performed at lower cell density (**Figure 33**). To notice, that in the control untreated, the cells grew without any substantial changes in architecture.

The same experiment was performed for dPGTPS (**Figure 35**). In this case, the untreated control cells at day 4 have a diameter of 250 µm and 427 µm at day 7, moreover at day 7, a 4.4-fold increase of the initial volume was achieved. Upon dPGTPS treatment at 30 µM concentrations, a 48% reduction in spheroids volume in comparison to control untreated set to 100% was measured. Additionally, the influence of dPGS on spheroids viability did not follow a concentration-dependent trend; 3 µM dPGTPS decreased 20 % the spheroids viability whereas other concentrations showed no influence. Following the treatment for a longer time, as when observing the spheroids after 10 days of incubation, hints of loss of spheroids integrity were displayed at 3 µM dPGTPS. At this time point, the spheroids reached a diameter of 650 µm.

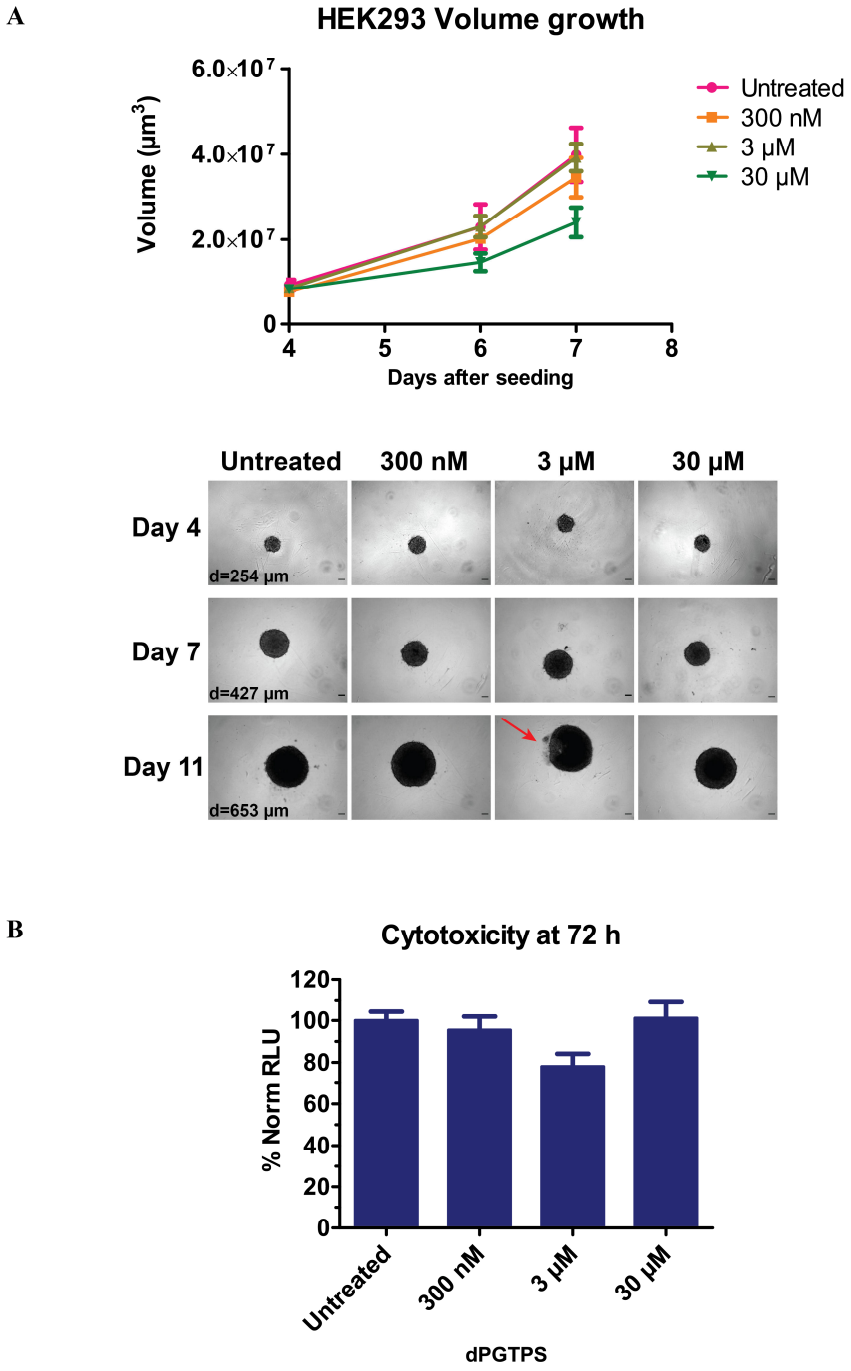

Figure 35: Growth and cytotoxicity analysis of HEK293 (150 c/w) spheroids upon dPGTPS treatment over a period of 7 days. HEK293 cells were seeded at a density of 150 c/w in a ULA-96 well microplate and cultivated until day 4, time upon which dPGS treatment began. **a**) Images of single spheroids were collected at different time points over 7 days incubation. Spheroids volume of control untreated and treated with increasing dPGTPS concentrations was examined via image analysis AnaSP software. Points represent the mean of one experiment performed in quadruplicate ± SD. Some representative 4x magnification bright-field images for each condition on days 4, 7 and 10 are shown. On day 10, in case of 3 µM treatment, the arrow indicates an early sign of loss of spheroids integrity. Diameter (µm) of the control untreated spheroids is reported. Scale bar= 100 µm. **b**) Cytotoxicity was measured after 72 hours of treatment via Cell-titer Glo 3D viability assay. Bars represent the mean one experiment performed in quadruplicate ± SD.

3.2 dPGS as a dual Heparanase and angiogenesis inhibitor

While until this point the focus has been on Shh-signaling pathway, further chapters will be aiming to evaluate the anti-angiogenic potential of dPGS in relation to its capacity to interfere with heparanase enzyme activity and to inhibit the activity of relevant angiogenic growth factors.

3.2.1 dPGS-Heparanase affinity measurement via SPR

To assess the inhibitory capacity of dPGS on heparanase activity, their binding affinity was firstly evaluated. In the assay, increasing concentrations of heparanase were injected over a SA chip during SCK experiments. The SPR sensorgram describing dPGS-heparanase binding is reported in **Figure 36**, together with the binding constants k_a, k_d and K_D derived from the fit assuming 1:1 Langmuir interaction model. dPGS and Heparanase showed a relatively strong affinity with a K_D value of 3.11 nM.

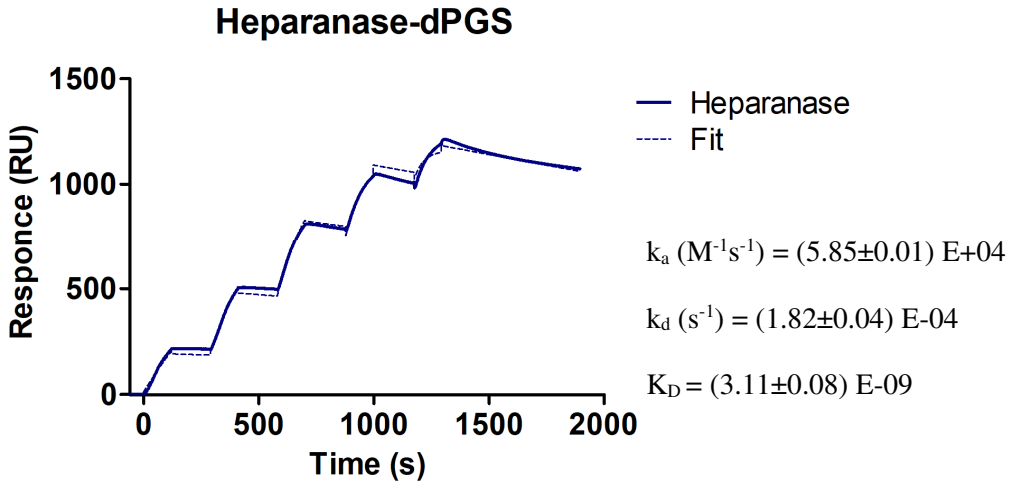

Figure 36: Single-cycle kinetics (SCK) for heparanase-dPGS interaction using SPR. Sensorgram of the Resonance Units (RU) response against time during SCK experiment upon injection of five ascending concentrations of heparanase (25, 50, 100, 200, 400 nM) on dPGS-coated sensor chip. The fit was obtained via using a 1:1 Langmuir binding model. The kinetic constants (k_a, k_d, K_D ±SE) are reported in the table beside the sensorgram.

3.2.2 Heparanase enzymatic activity assay

To evaluate whether the binding of dPGS to heparanase impacts on its catalytic activity, a heparanase activity assay was performed. The assay bases on heparanase cleavage of a homogenous substrate called fondaparinux, a fully synthetic methyl glycoside of the antithrombin III (ATIII)- activating pentasaccharide sequence of heparin. The quantification of the enzymatic activity is based on the reaction of water-soluble tetrazolium salt (WST-1) with the reducing disaccharides products of the fondaparinux cleavage by heparanase. As a first step, the assay was validated by performing complete digestion of fondaparinux via overnight incubation with 5 nM heparanase in 40 mM sodium acetate buffer (pH 5.0) at 37°C (2.3.6). The result of the digestion (**Figure 37**), which was carried out by using increasing nmoles of substrate fondaparinux, allowed for the identification of the correct amount of substrate to use for future activity experiments. In the specific, 5 nM of heparanase in the presence of 10 nmoles of fondaparinux (corresponding to 100 µM) resulted in a suitable degradation level. The experiment showed in **Figure 37** confirmed also the specificity of the detected signal, based exclusively on the reducing sugars products of enzymatic degradation; for both fondaparinux and heparanase alone a signal at the baseline level was measured.

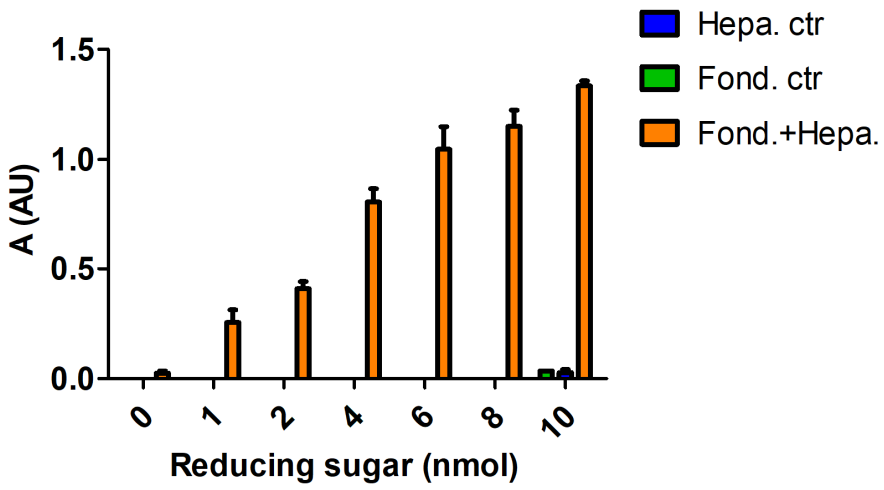

Figure 37: Heparanase activity assay validation. Response absorbance at 585 nm (Arbitary Units-AU) following overnight complete digestion of increasing nmoles of fondaparinux (1, 2, 4, 6, 8 and 10 nmoles) incubated with 5 nM heparanase at 37 °C for 24 hours in 40 mM sodium acetate buffer (pH 5.0). The specificity of the assay is validated by the absence of differential response in the case of controls where fondaparinux or heparanase alone are included. Bars represent the mean of *n=3* experiments ± SD.

3.2.2.1 Inhibition of heparanase enzymatic activity

Heparanase inhibition studies were performed for dPGS (**Figure 38a**) and as controls, for heparin and suramin (**Figure 38b**), both well-known heparanase inhibitors.

a)

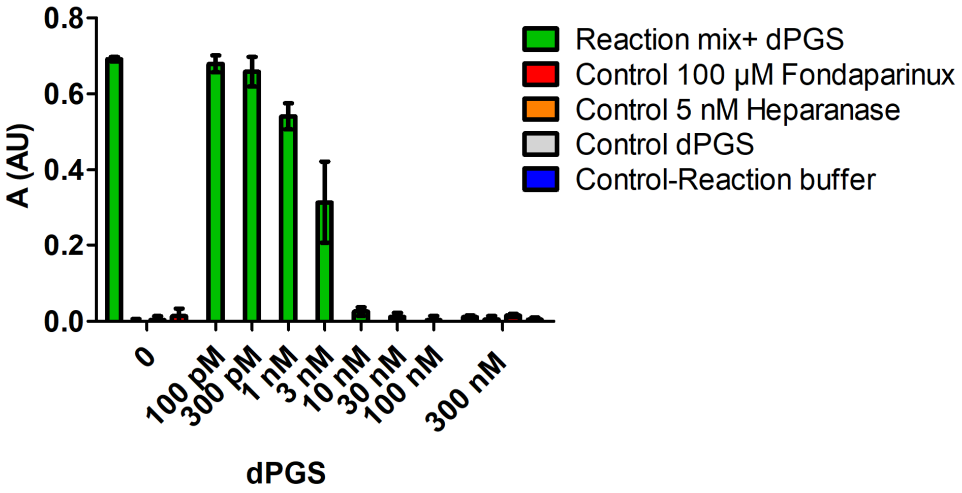

b)

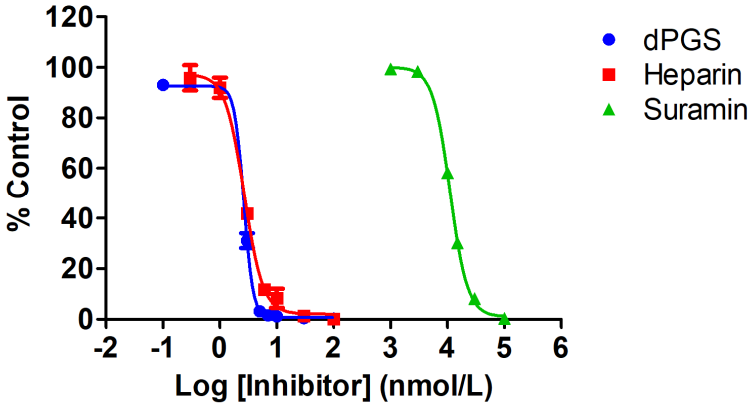

Figure 38: Inhibition of heparanase activity by dPGS, heparin, and Suramin measured by using Fondaparinux assay. **a)** dPGS-dependent inhibition of heparanase activity. Reported concentrations of dPGS ranging from 100 pM to 100 nM were mixed with 5 nM heparanase for 5 minutes prior the overnight incubation at 37°C in the presence of 100 µM fondaparinux. Controls for fondaparinux, heparanase, and dPGS are shown. Bars represent the mean of *n=3* experiments each performed in triplicates ± SD. **b)** Nonlinear regression curve showing heparanase inhibition activity for dPGS, heparin, and Suramin. For heparin concentrations ranging between 300 pM and 100 nM were used whereas for Suramin the concentrations used ranged between 1 µM and 100 µM. Points represent the mean *n=3* experiments each performed in triplicates ± S.D. Results are expressed as percentage normalized to control untreated (maximal substrate degradation) set to 100%.

The inhibitors were incubated in the presence of heparanase for 5 minutes prior to mixing with 100 µM fondaparinux and further incubation for 24 hours at 37°C.

Absence of unspecific signal derived from the degradation of inhibitors was confirmed, as shown in **Figure 38a** in the case of dPGS control. In **Figure 38b** is reported the nonlinear regression curve describing dPGS, heparin and suramin inhibition of heparanase activity. For dPGS and heparin, an almost identical IC_{50} was calculated, respectively 2.62 nM and 2.67 nM, whereas for Suramin 4000 times higher IC_{50} (11.13 μM) was measured.

3.2.3 dPGS affinity to pro-angiogenic growth factors VEGF, FGF1, and FGF2

The capacity of dPGS to bind to FGF1, FGF2, and VEGF and to potentially interfere with their activity was then investigated. Firstly, SPR binding assays were carried out via SCK experiments. The SPR sensorgram for FGF1, FGF2, and VEGF to dPGS are shown in **Figure 39**. Considering the K_D values extrapolated from the kinetic analysis assuming 1:1 Langmuir interaction model, all three growth factors displayed a good binding affinity to dPGS in the low nM range. In the specific for FGF1 a K_D of 170 nM was calculated, for VEGF a K_D of 5 nM and for FGF2 a K_D of 25 nM. Interestingly, looking at the association and dissociation constants, VEGF presents a fast k_a (10^6 $M^{-1}s^{-1}$) as well as a fast k_d (10^{-2} s^{-1}), which might describe a temporary shorter binding with consequently a reduced efficacy during treatment. For FGF1 seems indeed only dissociation to be fast (10^{-2} s^{-1}), which still could affect the target binding efficacy. Indeed, FGF2 displays a good association rate (10^4 $M^{-1}s^{-1}$) and relatively slow k_d (10^{-4} s^{-1}) suggesting that, in this case, the binding might be stable for a longer time and therapeutically more efficient.

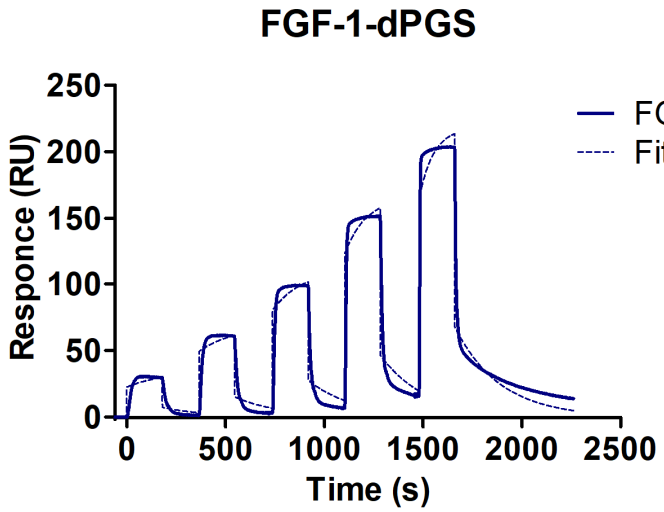

k_a ($M^{-1}s^{-1}$) = (2.6±0.15) E+04

k_d (s^{-1}) = (4.38±0.09) E-03

K_D = (1.7±0.05) E-07

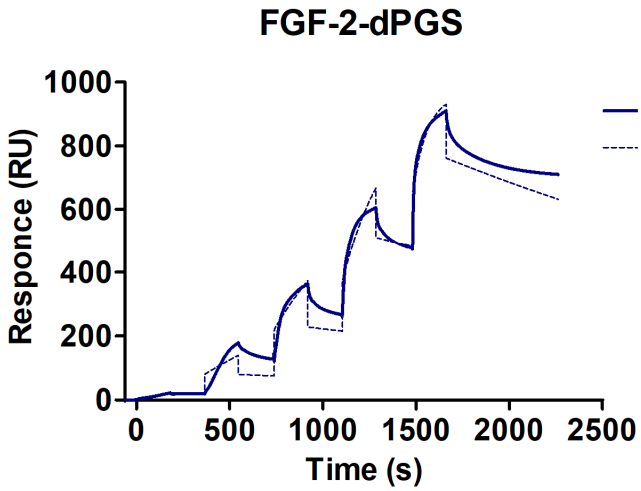

k_a ($M^{-1}s^{-1}$) = (1.2±0.02) E+04

k_d (s^{-1}) = (3.1±0.09) E-04

K_D = (2.5±0.08) E-08

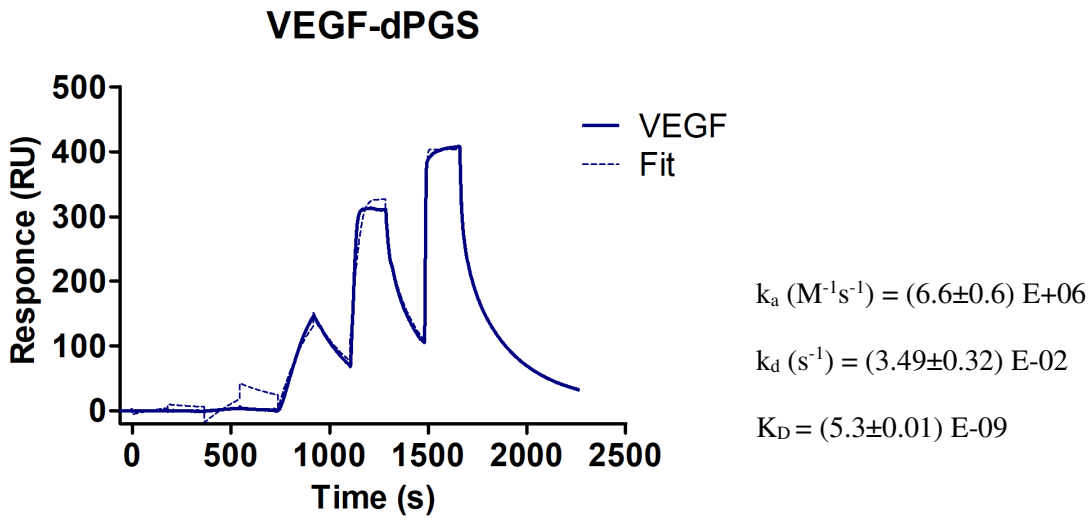

Figure 39: Single-cycle kinetics (SCK) for angiogenic growth factors-dPGS interaction using SPR. Sensorgrams of the RU response against time performed with the five increasing concentrations of growth factors injected as analytes over a dPGS-coated SA chip in SCK experiments. Concentrations applied: FGF1: 21.9, 43.8, 87.5, 175, 350 nM ; FGF2: 12.3, 37, 111, 333, 1000 nM; VEGF: 0.391, 1.56, 6.25, 25, 100 nM. The fit was obtained by using a 1:1 Langmuir binding model. The kinetic constants k_a, k_d and K_D±SE derived from the fit are reported in the tables beneath the sensorgram.

3.2.4 dPGS-inhibition of growth factors induced HUVECs proliferation

Aim of this study was to determine whether the binding of dPGS to the growth factors might also downregulate their activity, for example by impeding their binding to their receptor or, alternatively, antagonizing with HS for their storage at the ECM level. Therefore, growth factors activity assays were performed via studying the capacity of each singular factor to induce the proliferation of human umbilical vein endothelial cells (HUVECs) (**Figure 40a**). In a second step the capacity of dPGS to downregulate the growth factors-induced proliferation was investigated (**Figure 40b**).

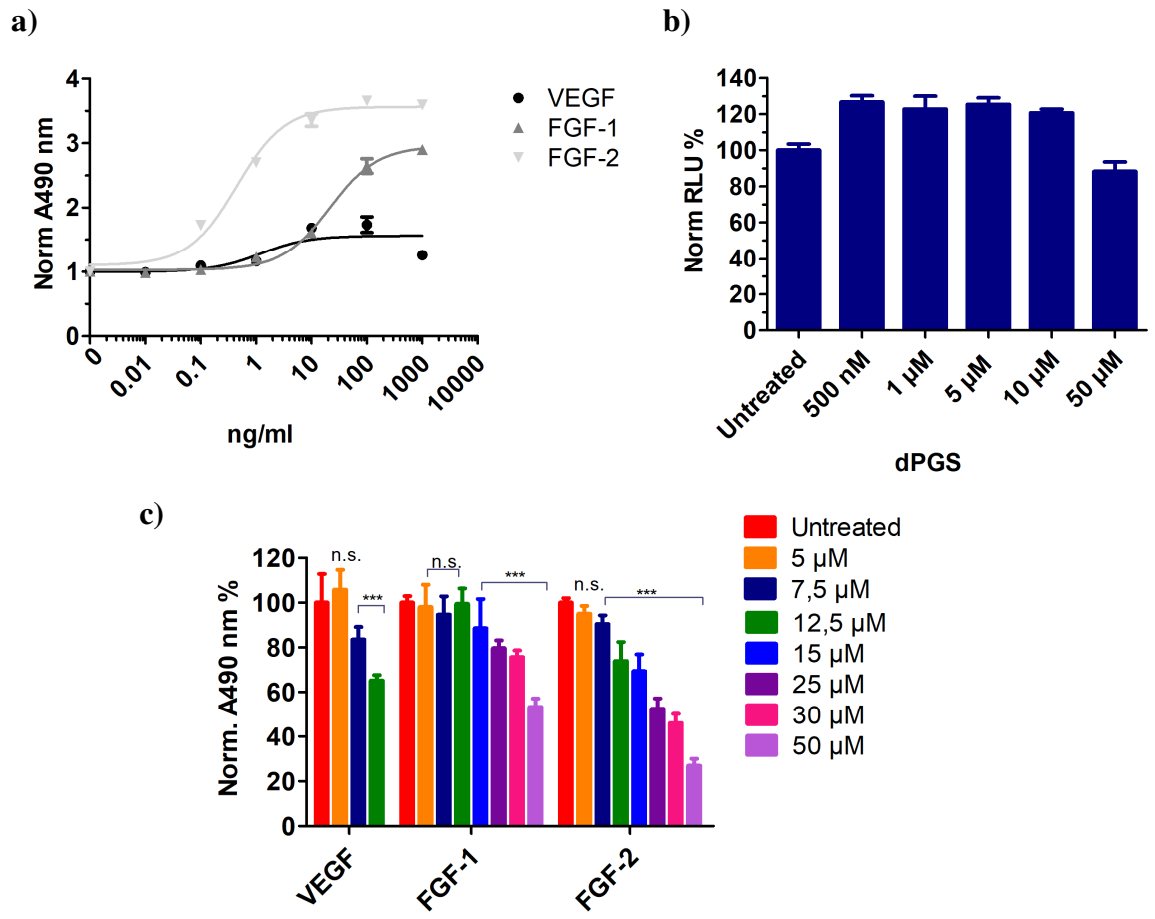

Figure 40: Angiogenic growth factors induced HUVECs proliferation and inhibition via dPGS. **a**) Growth factors-dependent stimulation of HUVECs cells proliferation. HUVEC cells were incubated for 72 hours in EBM medium supplied with either FGF1, FGF2 or VEGF growth factor at concentrations ranging between 0,1 ng/ml and 1 µg/ml. The proliferation was measured via CellTiter 96 AQueous One Solution. The values are reported as absorbance normalized to the untreated control. Points represent the mean *n=3* experiments each performed in quadruplicate ± SD. **b**) Cell viability determination for HUVECs after treatment in EGM-2 complete medium with dPGS at the reported concentrations for 72 hours. The cell viability was measured via CellTiter-Glo Luminescent Cell Viability Assay. Values are expressed in percentage of Relative Light Units (RLU) normalized to control untreated cells. Bars represent the mean *n=2* experiments each performed in quadruplicate ± SD. **c**) dPGS-dependent inhibition of growth factors-supported HUVECs proliferation. Cells were treated for 72 hours in EBM medium supplied with either 50 ng/ml FGF1, 3 ng/ml FGF2 or 50 ng/ml VEGF and increasing concentrations of dPGS ranging between 5 to 50 µM. The values are expressed in percentage as absorbance at 490 nm normalized to the untreated control. Points represents the mean *n=3* experiments each performed in quadruplicate ± S.D. *P<0.05, **P<0,01, ***P<0,001 vs vehicle control. Statistics were determined using a one-way AVOVA followed by a Dunned ´s post-test (Graphpad Prism, version 5).

The experiment reported in **Figure 40a** allowed to define the concentration of growth factors needed to stimulate HUVECs proliferation. Interestingly, the growth factor FGF2 highly supported HUVECs growth, with a 3.36-fold enhancement in comparison to control untreated cells, already at 10 ng/ml. The growth factor VEGF similarly induced a

dose-dependent proliferation increase but it reached a maximal stimulation within 10-100 ng/ml with a 1.7-fold increase, before decreasing at higher concentration. FGF1 indeed showed a good proliferative capacity, still behind FGF2 in terms of fold-enhancement, however inducing a 2.6-fold increase at 100 ng/ml. The results enabled to determine the growth factors concentration to use for further proliferation inhibition experiments. Specifically, FGF2 was applied at 3 ng/ml concentration, whereas in the case of FGF1 and VEGF 50 ng/ml were further used.

Nevertheless, before using dPGS for inhibition studies, it was necessary to verify the cytotoxicity profile of it for HUVECs. Therefore, a cell viability assay was carried out after 72 hours of incubation with increasing concentrations of dPGS (**Figure 40b**). The polysulfate did not cause significant cytotoxic effects and only a slight reduction of the viability was measured upon treatment with 50 µM (88% compared to control untreated set to 100%). Concentrations below did not result toxic and, by contrast, enhanced the proliferation up to 20% when compared to the control untreated. Accordingly, no substantial toxic effect of dPGS for the cell line used in the study was observed.

Ultimately, using the concentrations of the growth factors above mentioned and a range of concentrations of dPGS between 5 and 50 µM, the capacity of dPGS to negatively regulate the proliferation of HUVECs stimulated by FGF1, FGF2 or VEGF was examined. The inhibition of the growth factor-induced proliferation is shown in **Figure 40c**. For all three growth factors tested dPGS induced a concentration-dependent reduction of the proliferation. Notably, in the case of FGF2-stimulated proliferation, a significant dPGS-induced decrease of the proliferation was observed with a calculated IC_{50} of 21 µM. Nevertheless, given the binding evaluations for FGF1 and VEGF to dPGS (3.2.3) a less effective interaction could be assumed, which could consequentially affect the activity of the sulfated inhibitor. Considerably, for FGF1 only a hypothetical IC_{50}>50 µM was calculated. Instead, for VEGF, even though dPGS induced a concentration-dependent reduction of the growth factor-induced proliferation, the reduced VEGF-dependent stimulation of the cell proliferation limited the use of dPGS concentrations above 12.5 µM.

Moreover, in the same experimental setting, the growth factors-inhibitory activity of dPGS was compared to heparin (**Figure 41**). The growth factors studied are known to bind to heparin, but the functionality of this binding results in positive and negative stimulation of the factors activity in a concentration-dependent manner. The results confirmed a concentration-dependent inhibitory capacity of heparin especially in the case of FGF2 and VEGF, whereas no effect was observed for FGF1. Notably, dPGS in comparison to heparin always resulted in a stronger downregulation of growth factor-dependent HUVECs proliferation.

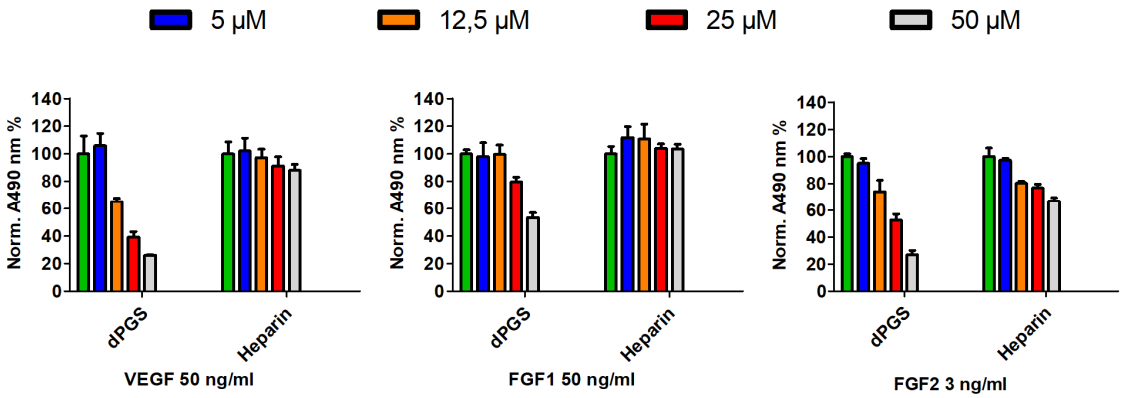

Figure 41: Comparison of growth factor-dependent HUVECs proliferation via dPGS and heparin. dPGS and heparin-dependent inhibition of growth factors-supported endothelial cell proliferation. HUVEC cells were treated for 72 hours in EBM medium supplied with either 50 ng/ml FGF1, 3 ng/ml FGF2 or 50 ng/ml VEGF and increasing concentrations of either dPGS or heparin ranging between 5 to 50 µM. The values are expressed in percentage as absorbance at 490 nm normalized to the untreated control. Points represent the mean *n=3* experiments each performed in quadruplicate ± S.D.

3.2.5 dPGS-inhibition of HUVECs tubes-like structure formation

In the context of evaluating the anti-angiogenic capacity of dPGS, the HUVECs tube formation assay was carried out (**Figure 42**). The assay bases on the capacity of HUVECs to differentiate, directionally migrate toward angiogenic stimuli, to align and branch forming three-dimensional capillary-like tubular structures, which mimic the polygonal networks of blood vessels. In the tube formation assay HUVECs adhered to a reduced growth factor basement membrane (with major protein components including laminin, collagen IV, entactin, and HSPG). For studying the inhibition of capillaries

formation via dPGS, HUVECs were seeded in EGM-2 medium containing dPGS at concentrations of 5, 10 and 50 µM. Initially, the tube formation was observed at three-time points (5, 8 and 20 hours) to estimate the timing for dPGS-endothelial tube inhibition (**Figure 42**). For easier comparisons, the assessment of total tube length per field of control untreated versus dPGS treatments is displayed. After 5 hours incubation dPGS induced a reduction of tube formation efficiency. Moreover, the effect of dPGS increased with the time resulting in a clear dose-dependent inhibition after 8- and 20-hours incubation. Especially, at 50 µM concentration dPGS induced 77% inhibition of tube-like structures formation already at 5 hours incubation, whereas after 8- and 20-hours incubation this concentration resulted in the complete absence of tubes. and induced the cells toward cluster form.

Additionally, the tube formation efficiency was assessed after 8 hours incubation via comparing three parameters: the number of nodes, total tubes length and total meshes area of dPGS treatments versus control untreated (**Figure 43**). A clear concentration-dependent inhibition of capillary-like structures was observed upon dPGS treatment for all parameters analyzed. Generally, 5 µM dPGS caused a percentage decrease in tube formation capacity which ranges between 8-21%, whereas 10 µM resulted in a 38-44% reduction, in comparison to untreated control set to 100%. Important to notice that, considering the cytotoxicity assay in **Figure 40a**, a toxic effect of dPGS can be excluded. In fact, for the tube formation assay, for example, after 8 hours incubation, dPGS reached IC_{50} at ~ 30 µM (considering all three parameters), whereas at 50 µM only a 12% reduction of the viability was observed, additionally after 72 hours incubation.

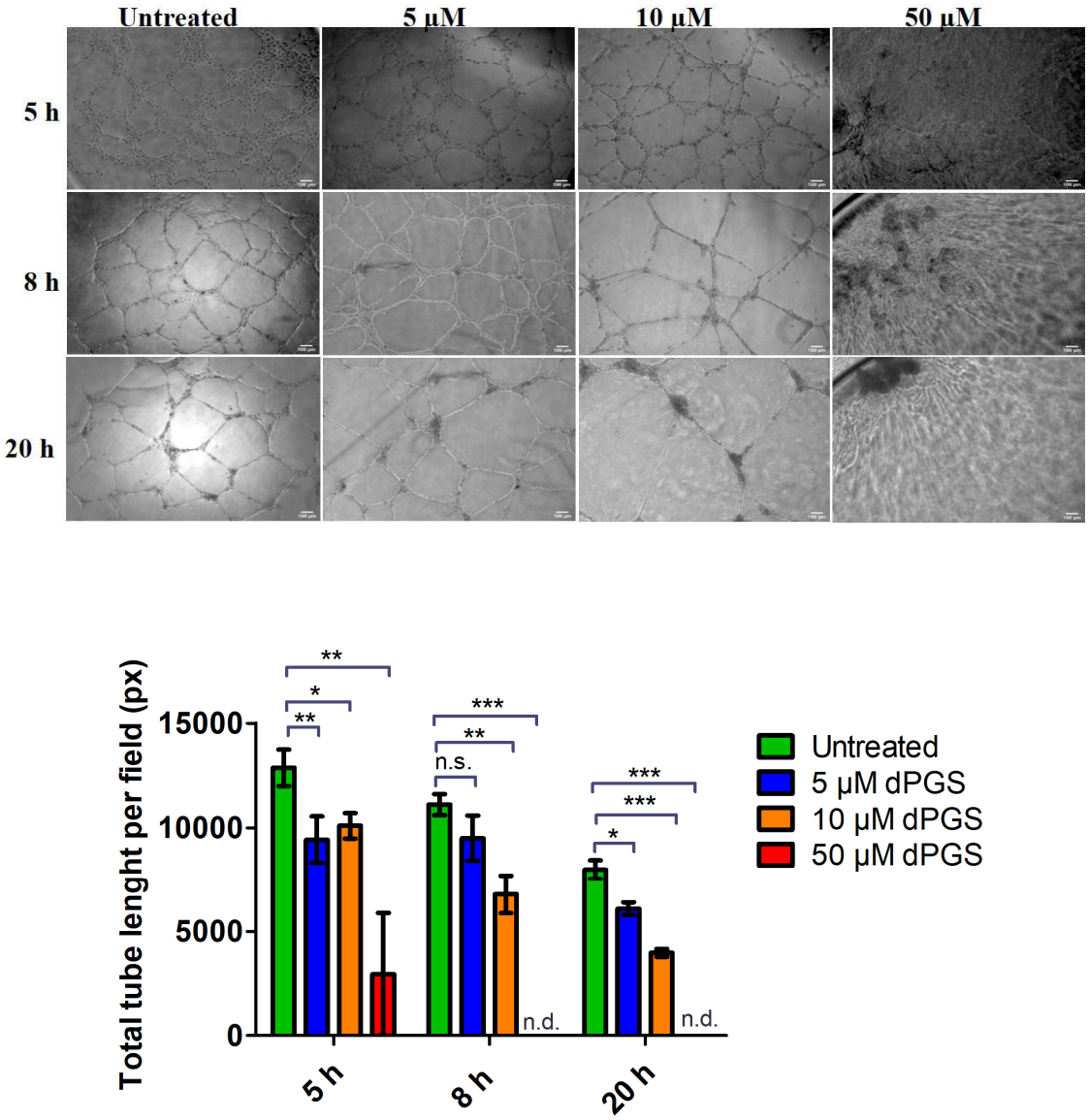

Figure 42: dPGS inhibits HUVECs-tube formation on Matrigel. Some representative images of HUVECs tube formation inhibition on a Matrigel by dPGS at 5, 10, and 50 µM after 5, 8- and 20-hours incubation. HUVEC cells were seeded in EGM-2 medium at the density of $1x10^4$ cells per well in a µ-slide plate (Ibidi) and reported dPGS concentrations. The pictures were taken with inverted phase-contrast microscope Axio Observer z.1 at 4x magnification and analyzed via ImageJ macro Angiogenesis Analyser. Parameter displayed: total tube length per field in pixels. dPGS shows a dose-dependent inhibitory effect on tube formation. When complete absence of tube formation was observed and the numerical quantification could not be performed the value was set to 0 and reported in the graph as non-determined (n.d.). Bars represent the mean *n=2* independent experiments each performed in triplicates ± S.D. *P<0.05, **P<0,01, *** P<0,001 vs untreated control. Statistical significance determined non-parametric Kruskal-Wallis test followed by Dunn´s post hoc test (Graphpad Prism 5.03).

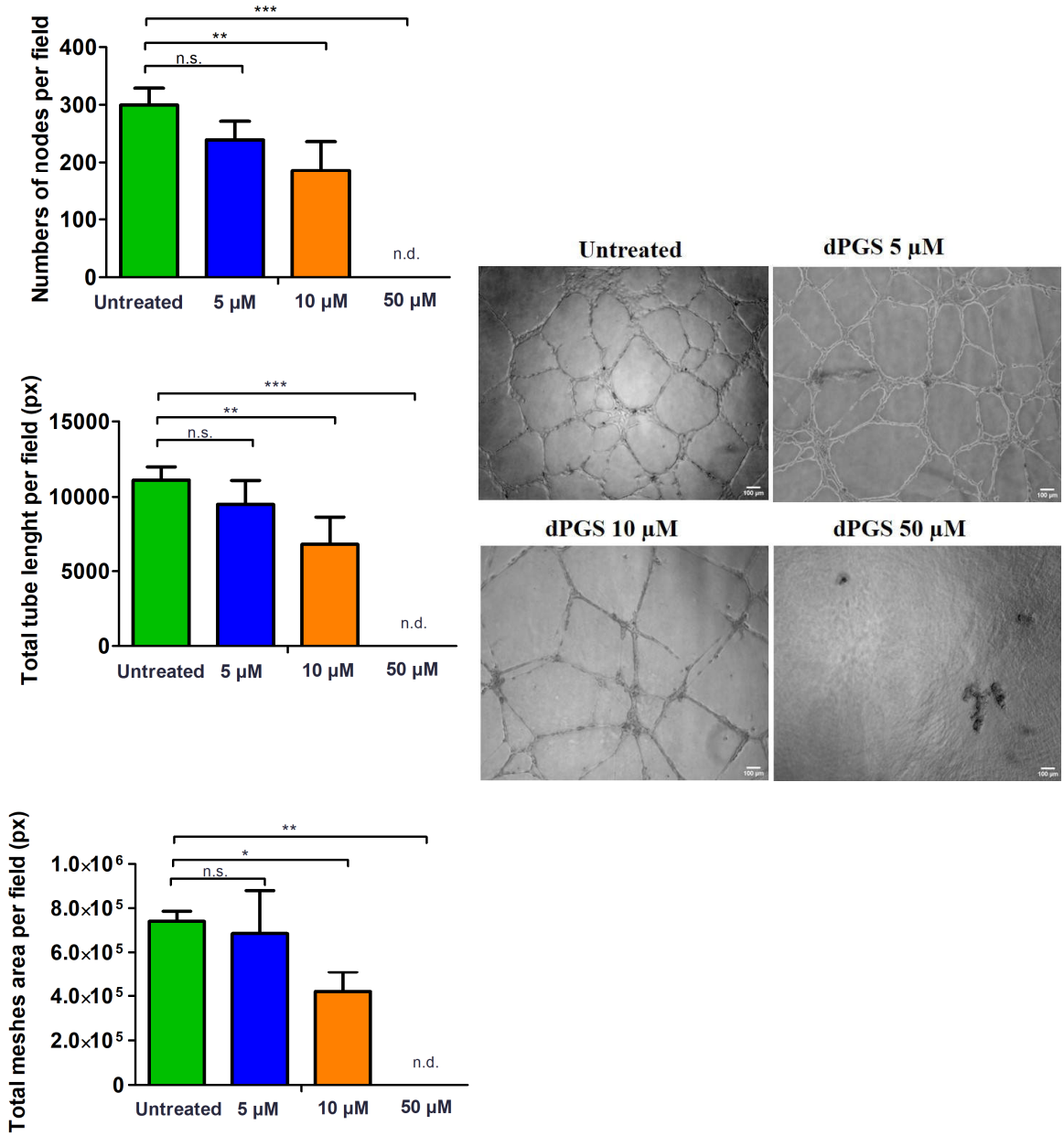

Figure 43: Quantification of dPGS- inhibition of HUVEC-tube formation after 8 hours incubation via three parameters analysis. Representative images of HUVECs tube formation inhibition on a Matrigel by dPGS at 5, 10, and 50 µM after 8 hours incubation. 4x magnification phase-contrast pictures were analyzed via ImageJ macro Angiogenesis Analyser. Parameter displayed: total number of nodes, tube length, meshes area per field (px). Bars represent the mean *n=2* independent experiments each performed in triplicates ± S.D. *P<0.05, **P<0,01, *** P<0,001 vs untreated control. Statistical significance determined by non-parametric Kruskal-Wallis test followed by Dunn´s post hoc test (Graphpad Prism 5.03).

4 Discussion

4.1 General considerations regarding the aim of the study

Cancer is a complex, multifactorial and heterogeneous disease derived from the accumulation of several adaptive genetic and epigenetic mutations, which alter multiple pathways to ultimately drive the neoplastic transformation [2,9]. Traditional therapies based on the use of cytotoxic agents, as chemotherapy, have a reduced cancer cell specificity, thereby causing diverse side effects in patients [270]. To circumvent this problem, outstanding progress has been made in the last decades to unravel the mechanisms governing tumorigenesis, leading to the design of compounds that specifically hit single tumor targets, the so-called "target drugs", with reduced off-target side effects. Although targeted therapies still represent a great promise in the treatment of several cancer types, they suffer of considerable drawbacks that limit their therapeutic efficiency. The heterogenic nature of cancer but also to its adaptive capabilities refer to this problem. A single targeted therapy often results in development of therapeutic resistance with cancer relapse as consequence of genetic modifications of the target. Besides, limited efficiency due to multiple pathways redundancy, compensatory cross-talks and alternative pathways activation occur. An example is the acquired resistance in patients in response to the first FDA approved anti-angiogenic drug, the monoclonal antibody Bevacizumab against VEGF [218,271].

Thus, for the treatment of complex pathologies such as cancer, it appears more likely to achieve a higher therapeutic efficiency via modulating multiple targets rather than a single one, though at the expense of specificity [272]. In this context, multi-target drugs gained considerable interest during the last, and from being unattractive compounds became an emerging therapeutic alternative.

The multi-target drug design is a challenging task with respect to off-target effects. In this context, HSPGs are a suitable blueprint for the development of multi-target drugs given to their affinity to a wide variety of proteins and enzymes by which they regulate pleiotropic physiological and pathophysiological functions. Interactions of HSPGs to

proteins mostly depend on electrostatic binding between HS and basic motifs located on the targets. In this context, the potential of the HS analogue heparin for the treatment of complex diseases as cancer, inflammation, and infection has been well documented [37–41]. However, the anticoagulant capacity besides its animal origin are known limitations for a therapeutic application. Consequently, attentions have been addressed towards synthetic heparin mimetics with reduced heparin derived-side effects, besides retaining a high therapeutic efficacy.

In this regard, the aim of this investigation was to evaluate the potential of a synthetic heparin mimetic, the dendritic polyglycerol sulfate (dPGS), with respect to modulating multiple tumorigenic pathways. In particular, among the long list of HS-regulated cancer signals, this work focused on two relevant tumor-promoting mechanisms: the Shh-pathway and angiogenesis. Background of this work are extensive *in vitro* and *in vivo* validations of the anti-inflammatory and anti-complement capacity of dPGS [246,247,251,254,273], which support the more recent *in vivo* studies on the tumorigenic targeting abilities of dPGS, applied as a drug carrier [259,260]. Thus, in this study for the first time, the anti-tumorigenic capacities of dPGS in relation to other relevant cancer signaling mechanisms have been investigated.

4.2 Shh-N protein expression and binding characterization to dendritic polyglycerol sulfates

Initially, the human recombinant Shh protein was successfully expressed in eukaryotic cells (HEK293 cells). The mammalian expression system is a widely used system to enable the expression of Shh protein carrying the dual lipidation necessary for the protein activity [70,274]. Only the active part of the protein, the 19 kDa Shh-N terminal fragment, was expressed as recombinant fusion protein linked to a C-terminal His-tag for further purification. This construct, lacking the autocatalytic and cholesterol transferase enabling C-terminal domain, resulted in the variant also named Shh-Nu, carrying only the N-terminal palmitoylated modification, which shows reduced membrane anchoring capacity, and thus can be easily secreted in the medium [59]. Nevertheless, Shh-Nu is known for presenting unaltered binding affinity to the PTCH receptor and analogous

activity in comparison to the ShhNp (fully lipidated) in cell-based studies [58]. On the contrary, in developmental studies, the lack of the cholesterol motif impairs protein trafficking, thereby altering long-range signaling and maximal pathway activity [60,61,63].

The presence of secreted ~19 kDa Shh-N in the conditioned medium derived from HEK293 cells transiently transfected was confirmed via Coomassie gel staining and immunodetection (**Figure 12**). Interestingly, for the expressed Shh-N three bands pattern could be detected. Several evidence report that for ShhNp (dually lipidated) two variants with a slightly differential migration pattern are secreted and correspond to the membrane-tethered fraction (cholesterol-modified and palmitoylated) and a soluble one (due to lipids removal via Disp and sheddases) [70,79,275]. Having expressed the cholesterol-deficient Shh-Nu, it can be assumed that the predominant secreted variant corresponds to the soluble form lacking cholesterol but carrying palmitoylation, which is easily released in the medium given its reduced membrane tethering. Besides, the palmitoylated Shh variant can be either secreted as membrane-anchored protein, as for the unprocessed ShhNp, or as processed soluble form lacking both cholesterol and palmitoylation due to sheddases cleavage of the palmitoyl motif. Potential cellular material as plasma membrane fragments carrying Shh-N not removed by centrifugation might also correspond to one of the observed bands.

As usual first step generally characterizing the here described experimental approach, the binding affinity between protein and sulfated compounds was assessed via SPR analysis. In the case of Shh-N, the expressed and purified protein was applied for SPR affinity measurements to dPGS and the degradable variant dPGTPS. Both variants carry the same core (dPG) and share an equal sulfation degree (~90%). In contrast to dPGS, dPGTPS contains a long, flexible and hydrophobic linker, which carries an ester functionality enabling hydrolytic and cellular enzymatic cleavage [256]. Moreover, the variant used in the present study contains azide groups, which enables further dye coupling for *in vivo* imaging. Despite the structural differences, the two variants showed the same binding behavior for Shh-N. K_D values in the nanomolar range were achieved (**Figure 14**). Interestingly, Zhang et al. studied the affinity via SPR of mouse-derived Shh to heparin and its natural ligand HS [276]. The authors report a good binding affinity for heparin with a K_D value of 67 nM and observed a weaker interaction toward HS (K_D 32 µM), which

suggests a preferential binding for Shh to highly sulfated regions. Research from Whalen and coworkers calculated an 800 nM K_D affinity for murine Shh to heparin while a K_D of 14.5 µM was measured in case of HS binding [83]. In this context, the binding studies performed in the present work support as well an enhanced binding affinity to Shh for highly sulfated compounds, which is as well analogous to its interaction to heparin. The data from dendritic polyglycerol sulfates imply an effective competitive role in a physiological context regarding the weaker affinity for Shh to its natural ligand HS.

4.3 Cell-based evaluation of dPGS/dPGTPS-dependent Shh pathway inhibition

The nature of the previously confirmed affinity was further evaluated in more psychological context via measuring the Shh pathway activity in two reporter cell-based assays: the luciferase reporter (**Figure 19**) and alkaline phosphatase (ALP) expression assay (**Figure 16**). These two methods are widely used as indicators of pathway activity and efficiently applied for evaluating the activity of agonists/antagonists of Shh pathway *in vitro* [277,278]. Briefly, ALP assay is based on the capacity of Shh pathway to induce osteoblast differentiation in a mouse mesenchymal cell line, the C3H10T1/2. Exogenous Shh ligand binds to PTCH receptor, expressed by the mouse fibroblasts, and results in increased expression of cell differentiation biomarker ALP [279–281]. Regarding the luciferase report system, a mouse embryonic fibroblast NIH-3T3 cell line was stably co-transfected with a GLI-dependent firefly luciferase reporter plasmid containing eight GLI binding sites (8xGLI-BS) and renilla luciferase (pRL-TK) as internal control plasmid [126]. The stimulation of Shh pathway results in nuclear translocation of the transcription factor GLI and binding to the 8xGLI binding sites on the luciferase promoter, stimulating the enzyme expression.

In both assays, the activation of the pathway was specifically obtained upon cell incubation with Shh CM. A control with a specific Shh-pathway inhibitor was included by using a small molecule that antagonizes the activity of GLI-transcription factors, GANT61 [143]. For both bioassays, the specific downstream pathway inhibitor GANT61 showed comparable down-regulating activity with IC_{50} in µM range (IC_{50} of 8.8 µM for

ALP-assay and 1.2 µM for luciferase reporter activity). Notably, the results are in agreement with the expected activity for GANT61 found in the literature, which reports an IC_{50} of ≥5µM for both bioassays [282]. However, while for dPGTPS an equally strong inhibitory capacity was confirmed in both methods (IC_{50} of 72 and 111 nM for ALP and luciferase assay, respectively) a conflicting behavior was observed for dPGS and heparin. Treatment with dPGS resulted in an IC_{50} for the ALP-assay of 81 nM, which reflects a strong interference potential, whereas in the luciferase reporter system the IC_{50} increased 80-fold (6.5 µM). Even more pronounced, heparin only showed a good inhibitory potential in the nM range in the ALP-assay whereas for the luciferase-based system no significative down-regulating activity was detected.

To explain the different behavior of dPGS and dPGTPS in the luciferase-based assay, several cytotoxicity studies were performed, and they ruled out any cytotoxic effect contribution. However, a possible limitation of the study, in the case of the luciferase-reporter assay, was the lack of normalization to the internal control (renilla luciferase). Moreover, the reduced amount of FBS (2% for ALP production in C3H10T1/2 cells compared to 0.5% in the luciferase-expressing cell line ShhL2) might play a role. Nevertheless, the different architecture of both sulfated polymers seems to influence the outcome.

Besides the Shh-pathway, bone morphogenic proteins (BMPs) and Wnt signals contribute to the osteoblast differentiation, via acting on the key regulatory element Runx2, essential for ALP expression [283,284]. Since it has been discovered that Shh ligand drives mesenchymal pre-osteoblasts cell differentiation and induces ALP expression, the synergism between Shh-pathway and BMPs signals found several confirmations. Although, Shh did not seem to directly affect the expression of relevant BMPs at the mRNA level [278,280,281]. Later, Zhao et al. confirmed a GLI-2-dependent upregulation of BMP-2 at the mRNA level and GLI-2-mediated Shh-BMP-2 synergistic enhancement of ALP expression and osteoblast differentiation [285]. Similarly, for Wnt proteins, several evidence suggest that Shh-Wnt crosstalk is involved in regulating ALP expression in C3H10T1/2 cells, as confirmed by the reduction of both Shh- and BMP-2-induced ALP expression upon treatment with Wnt specific inhibitors [286,287]. Interestingly, both BMP-2 and Wnt are known to bind with high affinity to heparin [288–291]. In this context, it

might be assumed that dPGS, dPGTPS, and heparin could act synergistically on other effectors that are up-regulated upon Shh-pathways activation, resulting in a decreased ALP expression. To the best of my knowledge, only Manikowski et al. studied the ability of soluble heparin and HS oligosaccharides to inhibit Shh-pathway activation, by inhibiting C3H10T1/2 cell differentiation [80]. If from one side my results find consistency in the findings of Manikowski, on the other hand, the divergence observed in the two bioassays, as in the case of heparin activity, suggests a potential shortcoming of the mentioned work concerning the lack of confirmation in alternative cell-based assays.

Still, an unsolved question is why dPGTPS showed good inhibitory activity in the luciferase-based assay. Either the compound interferes directly with the luciferase activity or its distinct architecture enables a more efficient cellular uptake and intracellular distribution compared to dPGS. Regarding the ester functionalized linker of dPGTPS, which is prone to hydrolytic cleavage [256], it can be hypothesized that the effect observed for dPGTPS could be a consequence of intracellular degradation. Degradation in lysosomes, where the Shh-dPGTPS complex potentially accumulates after entry, could result in the release of polysulfated shell fragments containing the hydrophobic linker. After the lysosomal escape, these fragments might target intracellular GLI factors or be recycled and inserted into the plasma membrane where binding of additional exogenous Shh further contributes to pathway inhibition. However, this theory would require further investigations.

4.4 Evaluation of the anti-proliferative capacity of dPGS and variant in 2D cell culture-based assays

It was investigated whether dPGS and dPGTPS, via binding to Shh-N, could interfere with pathway activation and consequentially limit cancer cell proliferation. Overexpression of key regulators of the Shh pathway, including the ligand itself has been demonstrated in the pancreatic ductal carcinoma cell lines PANC-1 and Mia-PaCa-2 [292,293] and the breast carcinoma cell line MCF-7 [294,295], whereas in the non-small cell lung cancer cells line A549 lower amount of ligand compared to high GLI-factors expression is confirmed [296].

Whether the secreted ligand activates autocrine or paracrine Shh-pathway is somehow contradictory. For A549 cells, while Singh et al. report an autocrine pathway-dependent cell proliferation [297], Bermudez et al. showed the absence of response to exogenous Shh ligand, thus supporting paracrine signaling [296]. For pancreatic cancer cells while paracrine signal finds more confirmations [119,123,124] yet Petrova et al. supported autocrine activation [147].

Thus, in this study, for each cell-line, the secretion of Shh-N was firstly verified and quantified via ELISA-based assay (**Figure 22**). A remarkable Shh-N expression and release was confirmed in the case of PANC-1 and MCF-7 cells, besides a reduced level for A549 cells, and around basal level for the control non-carcinogenic cell lines HEK293 (human embryonic kidney) and C3H10T1/2 (mouse fibroblasts).

Subsequentially, autocrine-stimulated cancer cell was studied in the low-level Shh ligand producer A549 cell line (**Figure 23**) and the high-level ligand producer PANC-1 (**Figure 24**). Cell line HEK293 (**Figure 25**) served as a control. Proliferation was quantified via endpoint measurements and in real-time. The consistency of the two methods was in agreement with already published evaluations [298]. Notably, dPGS had no influence on cell proliferation, not even at the highest concentration used (30 µM). In the context of Shh-pathway, it might be expected that dPGS would potentially inhibit the autocrine pathway activation and as a result limit cell proliferation. Nevertheless, this scenario relies on the eventuality that these cells would preferably use autocrine instead of paracrine Shh-signaling, a point that requires further studies.

Contrary, dPGTPS induced a concentration-dependent reduction of cell proliferation, which also includes the non-tumorigenic control cell line HEK293. This again points to additional effects of this compound.

4.5 Evaluation of anti-proliferative capacities of dPGS/dPGTPS in 3D spheroids model

Significantly, 3D cell culture-based systems, as cellular spheroids, are known to resemble more *in vivo* situations as the 2D monolayer culture are able to. Spheroids, as

microscale cells clusters formed by self-assembly, develop above 400 µm diameter a necrotic hypoxic internal core, a middle quiescent and an external proliferating layer, which results upon oxygen and nutrients limitation besides waste and ECM accumulation (along a gradient from extern to intern), as observed in many solid tumors [299,300]. Furthermore, in contrast to 2D cell culture system, the cells within the spheroid i) retain their genetic profile, original morphology and polarity, ii) show increased cell-cell adhesion, which regulates mechanotransduction and signaling in response to growth factors, iii) depone their own ECM with increasing cells-ECM contact, which in turn activates survival and proliferation pathways [301]. Generally, the increased cells adhesion and ECM density are limiting factors for drugs diffusion, and, along with hypoxia, are the causes of increasing therapeutic resistance observed in 3D in comparison to 2D monolayer culture, which moreover reflects the failure rate of drugs when applied *in vivo* studies [302]. Thus, 3D cell culture systems provide insights closer to *in vivo* situations not achievable by traditional 2D monolayer cell studies.

Therefore, in this study, was analyzed the effects of polysulfates on spheroids that reached after 4 days of incubation a ~400 µm diameter. As a parameter for growth evaluation, the change in spheroids volume was quantified, as one of the common feature applied in tumoral spheroid characterization [265]. The monitoring was performed over 15 days in case of low-rate growing A549 cells and, for faster-growing cells such as PANC-1 and HEK293, up to 5-times increase of the initial volume ($5xV_{day4}$), according to the protocol of Friedrich et al. [269]. Moreover, at 72 hours after treatment, viability tests were carried out, to exclude the eventuality of cytotoxic influences. Nevertheless, a more precise evaluation of the spheroids viability could be obtained by performing cytotoxicity analysis for each time point during the whole morphological observation, such as by real-time analysis.

Contrary to the 2D cell-based assays, each of the cell lines studied responded to dPGS and dPGTPS treatment in a cell line-dependent manner. In case of A549 cells, dPGS at concentrations ≥30 nM caused ~91% volume reduction after 15 days incubation. Nevertheless, this effect is observable even after 2-day treatment (**Figure 27**). A surprising result considering the monolayer measurements. For PANC-1 cells, dPGS induced a clear dose-dependent growth reduction at the end of the observation (8 days of

treatment), though to a lower extent than A549 spheroids (**Figure 30**). Additionally, after 72 hours of incubation, no significant toxic effect was observed for both cell lines.

Given the strong anti-proliferative effect observed for A549 cellular spheroids the reasons for dPGS-dependent growth reduction, in this case, might rely on:

1) Spheroid's differential characteristics compared to the 2D cell culture system. Spheroids are i) able to depose their own ECM with increased secretion of collagen, fibronectin-1, and laminin [303–305], ii) show upregulated expression of integrins (cell-ECM contacts) and E-cadherins (cell-cell interaction) [306,307], iii) additionally, the increased hypoxia, derived from the 3D cellular assembling, induces over-expression of HIF (hypoxia-induced factor), which is involved in upregulation of pro-angiogenic factors.

2) binding of dPGS to a long list of ECM, proangiogenic factors, membrane and membrane-associated proteins, including β–integrins, transferrin receptor and collagen [250,308].

3) the high rate of dPGS internalization, confirmed in the case of A549 cells [249,257,309], following possibly clathrin/caveolin-mediated endocytosis and energy independent mechanisms [308], which might positively contribute to enhancing the anti-proliferative effect.

The same trend of response was also detected for PANC-1 cells, but clear significant growth retardation was only detected at 30 µM dPGS treatment.

Thus, the results on the spheroids growth, especially for A549 cells, rather than referring to the capacity of dPGS to influence Shh-related proliferation, provides new insights on the anti-proliferative cell-dependent potential of dPGS, additionally in a context mimicking closely *in vivo* situations, whether the precise mechanism of action remains unclear.

Interestingly, MacDonald et al. showed a growth reduction of pancreatic cancer spheroids treated with the heparin mimetic necuparanib (M402) [310]. The authors observed that the spheroids of pancreatic cancer cells reduced their diameter

and increased sphericity upon compound treatment. Similarly, in my investigation, both A549 and PANC-1 cells showed a reduction of the size of the spheroids upon treatment, rather than cell loss and disaggregation, as usually caused by toxic agents. Furthermore, MacDonald et al. via proteomic analysis of the supernatant from tumor-stroma cells co-cultured spheroids identified several proteins involved in tumorigenic pathways, which undergo alteration upon treatment with necuranib. Similarly, an additional set of proteins expressed during tumor spheroids growth might explain the effect of dPGS. Notably, in a published poster, but not in the mentioned article, the authors report the necuparanib-induced reduction of proliferation also in 2D culture system, performed however over a time of seven days incubation [311]. This suggests one possible explanation for the inconsistency between the 2D and 3D proliferation assays observed in my study, which might also lie on the shorter length of the treatment in case of monolayer cell proliferation.

Indeed, in the case of HEK293 cells, a diameter dependent change in the morphology of the cells was observed upon dPGS treatment at concentrations above 300 nM. For the spheroids which reached ~400 µm diameter after 4 days of incubation and ~600 µm after 3 days treatment (7 days of culture), dPGS treatment-induced evident loss of spheroid integrity at 3 µM and slight conformational changes at 30 µM, resulting in apparent volume increase upon treatment. Reducing the initial number of cells and enabling the formation of ~300 µm diameter by day 4th of incubation, led to spheroid formation at day 7of ~500 µm diameter, unaffected by dPGS treatment both in morphology and growth rate. Additionally, at this time point, no cytotoxic effect was observed. However, a later observation of the same spheroids, when they reached diameter ~800 µm, revealed again the same trend of structural alteration. Importantly, for the control spheroids, no conformational changes were detected during the whole incubation time. Given the diameter-dependent effect, it could be assumed that factors, such as the formation of the necrotic core and hypoxia increase, which generally takes place ≥400 µm diameter, could play an important role in explaining the effect of dPGS on the morphology of HEK293 cells. A further explanation could be the increase of stress on the spheroids surface, due to the rapid HEK293 cells proliferation, which would result in increased sensitivity to dPGS. In fact, spheroids are known to undergo morphological changes during long-term growth, potentially losing the structural integrity as events that not necessary

corresponds to increased toxicity [312,313]. Given the rapid proliferation characterizing the HEK293 cells, it might be possible to rapidly reach unstable conditions within the 3D structure, resulting in unpredictable morphological changes. Thus, while HEK293 is very robust and a stable cell line in 2D monolayer, it might not be very suitable for 3D systems.

Spheroids treatment with dPGTPS resulted in reduced activity when compared to dPGS. Furthermore, dPGTPS treatment of cells monolayer and spheroids substantially differ in cytotoxicity: in the monolayer, a concentration-dependent proliferation reduction effect could be observed, whereas in the spheroids the treatment caused only a slight increase of the toxicity, additionally cells-specific. The increase of spheroids resistance in comparison to monolayer is well described [314,315].

It can be concluded that the results obtained for dPGS and dPGTPS regarding their influence on tumorigenic and non-tumorigenic cell spheroid growth provide preliminary insights concerning the anti-proliferative activity in 3D culture. Further investigations are necessary to clarify the initial observations.

4.6 dPGS as a potential inhibitor of heparanase and angiogenesis

In the context of developing anti-angiogenic compounds, given the complex mechanisms interplay and pathways redundancy involved within the angiogenic cascade, multi-target strategies might be of therapeutic advantage. As several angiogenic factors depend on the interaction with HS in order to elicit their signals, heparin shows increased anti-angiogenic capacities while regulating synergistically multiple factors along the angiogenic signaling, targeting of proangiogenic growth factors (such as FGFs, HBEGF, and VEGF) and additionally blocking the endoglucoronidase heparanase.

As previously mentioned, several heparin mimetics with low-anticoagulant capacities have been synthetized in order to overcome the therapeutic limitations related to heparin, while retaining high heparanase inhibitory capacity and moreover high affinity to the pro-angiogenic growth factors. In this context, it was investigated whether dPGS, interacts with both heparanase and the relevant pro-angiogenic growth factors. To note that

the studies concerning angiogenesis have solely been performed with dPGS, which might be the starting point to expand future investigations.

SPR binding studies showed a high affinity for dPGS to heparanase with K_D value of 3.1 nM, additionally characterized by a slow dissociation rate, which indicates stable binding (**Figure 36**). Furthermore, the pro-angiogenic growth factors present a good binding affinity to dPGS with K_D values in low nM range (**Figure 39**), in particular: 170 nM for FGF1, 5.9 nM for VEGF, and 25 nM for FGF2. The K_D values reported in literature for heparin-binding to FGF1 range between 5 to 180 nM [316,317], for FGF2 between 7.9 and 23 nM [167,318] and for VEGF from 157 to 165 nM [317]. The range of results is attributed to different experimental methodologies. Interestingly, Siska et al. performed SPR studies via using a SA-sensor chip and measured a K_D value for heparin-binding to FGF1 of 4.2 nM, FGF2 of 5.3 nM and VEGF of 42 nM [320]. In comparison to heparin, dPGS showed a 40-fold and 4.7-fold lower binding affinity to FGF1 and FGF2, respectively, while the binding to VEGF is enhanced of 4.7-fold. However, when compared to PI-88, a famous anti-angiogenic heparin mimetic (chapter 1.4.5), dPGS showed an increased affinity regarding FGF2 binding (K_D=95 nM for PI-88) and a comparable affinity to VEGF (K_D=2 nM for PI-88). In contrast PI-88 showed a 850-fold higher affinity to FGF1 (K_D=200 pM) in comparison to dPGS [235].

As the binding studies give important preliminary information, further studies in a more physiological context, are essential to better understand the relevance of the interactions. With this aim in view, *in vitro* non-cell based assays were carried out to evaluate the capacity of dPGS to inhibit the activity of human heparanase, while cell-based *in vitro* studies were performed to validate the down-regulation dPGS-dependent of angiogenic processes elicited by the proangiogenic growth factors.

To assess heparanase activity, the method described by Hammond et al. and based on the cleavage of the synthetic heparin oligosaccharide fondaparinux [268] was applied. In the assay, the capacity of dPGS to act as heparanase inhibitor was compared with its analogue heparin and the commercial heparanase inhibitor Suramin. Suramin is a polysulfonated naphthylurea-based small molecule able to inhibit heparanase with an IC_{50} of 46 µM [321], but with reduced therapeutic applicability due to high toxicity [197]. The results in **Figure 38b** confirmed that the strong binding affinity earlier measured (K_D=3.1

nM) mirrors a strong enzymatic inhibitory capacity for dPGS, with an IC_{50} of 2 nM. Likewise, heparin showed an equally strong inhibitory capacity as dPGS, with matching IC_{50} value, confirming overall the extreme potential of heparin to inhibit heparanase, in agreement previous studies [322,323], and relevantly in accordance with the IC_{50} measured by Loka et al. [324]. Moreover, a 4000-times higher IC_{50} was measured for Suramin, confirming its modest inhibitory potential, in agreement with previous studies [321]. Interestingly, the comparison of dPGS to anti-angiogenic compounds already introduced in clinical trials as PI-88 ($IC_{50\ of}$ 8 nM) and its derivative PG545 (IC_{50} of 6 nM) [235], dPGS has competitive performance. Furthermore, dPGS might possibly compete with one of the most potent heparanase inhibitor, the non-anticoagulant N-acetylated glycol-split heparin roneparstat (SST0001) with reported IC_{50} of 3 nM [233]. Future cell-based *in vitro* assays and *in vivo* models are necessary for further evaluations with respect to the high relevance of heparanase in diverse pathological settings.

The anti-angiogenic potential of dPGS was further evaluated by its ability to downregulate pro-angiogenic growth factors induced-HUVECs proliferation. Therefore, the initial growth factors dose-dependent enhancement of the HUVECs proliferation was confirmed, which allowed defining the concentrations required to reach maximal stimulation (**Figure 40a**). Interestingly in the case of VEGF, a maximum of a 1.7-fold increase was measured in comparison to the untreated control at 10-100 ng/ml, while a concentration above resulted in a signal reduction. By contrast, maximal stimulation with 3.4-fold enhancement was observed in case of treatment with 10 ng/ml of FGF2, whereas FGF1 resulted in a 2.6-fold enhancement at 100 ng/ml concentration. This differential capacity of the FGFs compared to VEGF to induce ECs proliferation, especially in the case of HUVECs, is consistent with previous findings. Bompais et al. observed in HUVECs a 1.6-fold maximal enhancement for VEGF at 8 ng/ml while 2 ng/ml of FGF2 induced a 2.7-increase [325]. Similarly was reported a ~1.3 increased activity of FGFs in comparison to VEGF [326–328]. In agreement with the inter-dependency of differential growth factors to synergistically promote the angiogenic response, the combination of the angiogenic factors would stimulate the proliferation of HUVECs to a greater extent than a single cytokine [326].

By inducing HUVECs growth factors-dependent proliferation with either 3 ng/ml FGF2 or 50 ng/ml of VEGF and FGF1, the anti-angiogenic capacity of dPGS was further studied. As shown in **Figure 40c**, dPGS reduced in a dose-dependent manner HUVECs proliferation stimulated by the growth factors. As expected from the binding studies, a stronger inhibition was observed in the case of FGF2 with a calculated IC_{50} of 21 µM. For VEGF a clear inhibition could be detected with a 40% reduction upon treatment with 12.5 µM dPGS. The proliferation of FGF1 was also reduced by dPGS but to a lower extent (IC_{50} >50 µM). It is of note that the dPGS within this range of concentrations did not induce toxicity as confirmed by the viability test performed at 72 hours after incubation (**Figure 40b**). Compound PI-88 shows in the same experimental setting IC_{50} values ranging between 40 µM, in case of FGF1-stimulation, to 10 and 20 µM, in case of FGF2 and VEGF-stimulation respectively [329]. Of note, in the mentioned work the initial stimulation values are not reported. Moreover, dPGS induced stronger inhibition in comparison to UFH (Figure 41). Heparin showed a slight dose-dependent reduction of FGF2 and VEGF-induced ECs proliferation, which reflects the anti-angiogenic feature of heparin at high concentrations, while a pro-angiogenic character is expected at lower concentrations [169].

To evaluate further the angiogenic potential of dPGS *in vitro*, the reduction of three-dimensional capillary-like tubular structures formation by HUVECs on a growth factor-reduced basement membrane matrix was assessed. In this experimental setting, the capacity of HUVECs to adhere and form branches on the matrix depends upon the stimulation of the ECs with complete growth medium that contains several growth factors such as FGF2, VEGF, insulin-like growth factor (IGF-1) and epidermal growth factors (EGF). Although dPGS is able already after 5 hours to reduce the formation of tubes like-structures, longer incubation time resulted in a clear dose-dependent inhibition. After 8 hours of incubation, dPGS decreased tube formation to 50% at a concentration of around 30 µM (**Figure 41**). The result might reflect the synergistic inhibition of FGF2 and VEGF. Nevertheless, inhibition due to the binding of dPGS to the low content of laminin or collagen that constitutes the matrix cannot be excluded. Notably, PI-88 inhibits at 18 hours HUVECs tube-formation of 29% at 10 µM concentration [329], whereas dPGS already reached around 40% reduction after 8 hours incubation. In this term, dPGS might be able to compete in terms of efficiency with other anti-angiogenic heparin mimetics relying on both on heparanase and angiogenic growth factors inhibition. Furthermore, it is

of interest that a hydrophobic moiety, as in the case of the PI-88 derivative PG-545 enhances the anti-angiogenic potential [235]. Thus, testing of the dPGS derivative dPGTPS, which contains a hydrophobic linker, could hypothetically result in an increased protein affinity and stronger anti-angiogenic potential.

4.7 Concluding remarks and future perspective

The aim of this work was to evaluate the anti-tumorigenic potential of dendritic polyglycerol sulfates, besides their well-known anti-inflammatory and anticomplement capacities. In the context of inhibiting HSPG-regulated tumorigenic processes, the capacity of dendritic polyglycerol sulfates to interfere with the sonic hedgehog signaling pathway and the process of angiogenesis was evaluated. SPR-based assays confirmed affine binding of the two synthetic polysulfates, dPGS and the degradable derivative dPGTPS to the Shh-N protein, heparanase, and pro-angiogenic growth factors (VEGF, FGF1, and FGF2).

Protein binding per se could result in either positive or negative regulation of physiological pathways. Therefore, further activity studies are necessary to unravel whether binding inhibits or supports protein function. Concerning the Shh-pathway, the polysulfates demonstrated good inhibitory capacity in the low nanomolar range in an alkaline phosphatase reporter cell line. In a second approach, activation of the sonic hedgehog pathway was evaluated via a luciferase-reporter cell-based assay. While the compound dPGTPS showed again effective inhibition, the IC_{50} of dPGS tremendously increased to 6 µM, but still, a dose-dependent inhibition was detectable. Besides shielding of the Shh protein secondary effects seem to mediate better inhibition in the case of dPGTPS.

The anti-proliferative capacities of the sulfated compounds were studied in two cancer cell lines, PANC-1 and A549, which secrete the Shh-ligand and are known to be dependent on the Shh-pathway for cell proliferation. In this regard 2D and 3D cell culture-based systems were applied. While dPGS did not show to significantly influence the cell growth in 2D monolayer assays, dPGTPS caused a concentration dependent reduction of the cell proliferation, significantly in the case of A549 cells. Interestingly, in the 3D spheroid-based system, dPGS and dPGTPS significantly reduced A549 cell growth and, to a lesser extent, also PANC-1 cell growth. The results might reflect the different properties

the cells adopt to grow within the multilayer spheroid architecture in contrast to monolayer culture. These first data highlight the relevance of the 3D culture system that closer reflects tumorigenesis under *in vivo* conditions. Future studies concerning the anti-tumorigenic capacities of polysulfates should intensify research in this area.

Concerning angiogenesis, dPGS demonstrated a high potential as a heparanase inhibitor, with an IC_{50} in the low nanomolar range. In this regard, it would be extremely interesting to further expand this study by applying dPGS in heparanase-driven endothelial cell sprouting and ECM degradation in metastatic processes, i.e., reduction of invasiveness and tumorigenesis of highly metastatic cell lines known to express a high level of endogenous heparanase. Further, dPGS also inhibited angiogenic growth factors activities, probably by competitive binding and shielding receptor recognition. Moreover, via acting on multiple targets simultaneously, dPGS potentially leads to an amplified anti-angiogenic response. Further *in vitro* studies should evaluate the reduction of EC migration and invasion likewise *in vivo* models might support more substantially the anti-angiogenic potential of dPGS.

Thus, in the context of multitarget drug development for tumor therapy, multivalent polysulfates such as dPGS and dPGTPS demonstrate promising features to target intrinsic cancer-associated pathways.

5 Summary

In the context of drug development for the treatment of complex diseases such as cancer, it might be necessary to interfere with multiple targets. Inspired by the multiple functions of heparan sulfate proteoglycans (HSPGs) several compounds have been developed in the past. Here the fully synthetic dendritic polyglycerol sulfates dPGS and dPGTPS were evaluated with respect to their overall anti-tumorigenic properties. Primarily focused on the sonic hedgehog (Shh) pathway, which is upregulated in several aggressive tumors, it was found that both compounds reduce pathway activation. Shh binding was analyzed via SPR and gave the following K_D values: 88.7 nM for dPGS and 37 nM for dPGTPS. The inhibition of the Shh-signaling pathway was further evaluated in two reporter cell-based systems: a luciferase reporter and an alkaline phosphatase (ALP) assay. While dPGTPS showed consistently strong pathway inhibitory activity (IC_{50} of 72 nM in the ALP and 111 nM in the luciferase assay), dPGS displayed a different behavior (IC_{50} of 81 nM in ALP and 6.5 µM in luciferase assay), which might be attributed to the different architecture of the polysulfates. Cancer cell line proliferation also mediated by the Shh pathway was further analyzed in 2D cultures and 3D spheroid-based assays. In monolayer 2D studies, dPGS did not show any influence, while dPGTPS at µM concentrations reduced cell proliferation. By contrast, in 3D spheroid-based cultures, both dPGS and dPGTPS, significantly arrested the growth of A549 spheroids, although the latter compound to a lower extent.

At the molecular level growth factors mediate cell proliferation. Therefore, binding of FGF1, FGF2, and $VEGF_{165}$ to the polysulfates was analyzed, again via SPR. All proteins bound tightly to the sulfated compounds (i.e., K_D of 25 nM for FGF2-dPGS interaction). Further, the capacity of dPGS to hamper angiogenic processes was confirmed in case of inhibition of HUVECs proliferation. FGF2-induced HUVECs proliferation was reduced upon dPGS treatment (IC_{50}=21 µM) and cell differentiation to initiate three-dimensional capillary-like tube formation dose-dependently blocked.

Heparanase is an essential enzyme to initiate remodeling of the extracellular matrix (ECM) during tumorigenesis. The polysulfate dPGS displayed a remarkable affinity to the protein (K_D of 3.11 nM) and blocked its enzymatic activity (IC_{50} = 2 nM).

To conclude, these findings emphasize the potential of synthetic polysulfates and should inspire future studies to explore their anti-tumorigenic efficacy.

6 Zusammenfassung

Für die Entwicklung von Medikamenten die zur Behandlung komplexer Krankheiten eingesetzt werden sollen, kann es hilfreich sein multiple Zielstrukturen zu adressieren. Inspiriert durch die zahlreichen Funktionen der Heparansulfat-Proteoglykane (HSPG) wurden in der Vergangenheit zahlreiche Verbindungen synthetisiert. In dieser Arbeit wurden die vollsynthetisch hergestellten dendritischen Polyglycerinsulfate dPGS und dPGTPS hinsichtlich ihrer antitumorgenen Wirkung untersucht. Zunächst fokussiert auf den Sonic Hedgehog (Shh)-Signalweg, der in vielen agressiven Tumoren reaktiviert wird, konnte gezeigt werden, dass beide Verbindungen die Aktivität vermindern. Bindung des Proteins Shh wurde mittels Oberflächenplasmonresonanz Spektroskopie untersucht und ergab K_D Werte von 88,7 nM für dPGS und 37 nM für dPGTPS. Die Inhibition des Shh-Signalweges wurde weiterhin in zwei zellbasierten Systemen evaluiert: einem Luciferase Reportertest und einem Alkalischer Phosphatase (ALP) Reportertest. Während dPGTPS übereinstimmend eine ausgeprägte Hemmung in beiden Reportersystemen zeigte (IC_{50} von 72 nM im ALP Test und 111 nM im Luciferase-basierten Test), ergab der Einsatz von dPGS ein anderes Bild (IC_{50} von 81 nM in ALP Test und 6.5 µM in Luciferase-basierten Test), was möglicherweise auf die unterschiedliche Architektur der beiden Polysulfate zurückzuführen ist.

Da die Proliferation von Krebszelllinien ebenfalls durch den Shh-Signalweg vermittelt werden kann, wurde dies in 2D-Zellkulturen und im 3D-Spheroid Modell untersucht. In Monolagen wachsender 2D Zellkultur zeigte dPGS keinen Einfluss, während dPGTPS in µM Konzentration eine Reduktion der Zellproliferation ergab. Ein anderes Verhalten ergab sich im 3D-Spheroid Modell. Hier zeigte sich, dass sowohl dPGS als auch dPGTPS signifikant das Wachstum von A549 Spheroiden verzögerte, wobei dPGTPS sich als weniger effektiv erwies.

Auf molekularer Ebene vermitteln Wachstumsfaktoren die Zellproliferation. Daher wurde die Bindung von FGF1, FGF2 und $VEGF_{165}$ an die Polysulfate mittels Oberflächenplasmonresonanz Spektroskopie untersucht. Hierbei zeigten alle Proteine eine hochaffine Bindung an die sulfatierten Verbindungen (z. B. K_D von 25 nM für die FGF2-dPGS Bindung). Weiterhin wurde die Fähigkeit von dPGS die Angiogenese zu beeinflussen

durch Hemmung der Proliferation am Beispiel von HUVECs bestätigt. FGF2-induzierte Proliferation von HUVECs wurde durch dPGS gehemmt (IC_{50}=21 µM) und Zelldifferenzierung, hin zu einem dreidimensionalem kapillar-ähnlichen Netzwerk, blockiert.

Heparanase ist ein essentielles Enzym, das Remodelierungsprozesse der extrazellulären Matrix (ECM) in der Tumorgenese einleitet. Das Polysulfat dPGS zeigte eine bemerkenswerte Bindungsaffinität an das Protein (K_D von 3.11 nM) und blockierte dessen enzymatische Aktivität (IC_{50}=2 nM).

Zusammenfassend weisen die Befunde auf das hohe Potential der synthetischen Polysulfate hin, die in weitere Studien zur Wirksamkeit ihrer antitumorgenen Eigenschaften untersucht werden sollte.

7 References

1. Greaves, M. Nothing in cancer makes sense except. *BMC Biol.* 2018.
2. Cooper, G.M.; Hausman, R.E. The Development and Causes of Cancer. *Cell A Mol. Approach* 2007.
3. Stratton, M.R.; Campbell, P.J.; Futreal, P.A. The cancer genome. *Nature* 2009.
4. Gariglio, P. Oncogenes and tumor suppressor genes. In *Molecular Oncology Principles and Recent Advances*; 2012 ISBN 9781608056118.
5. Howlander, N.; Noone, A.; Krapcho, M.; Miller, D.; Brest, A.; Yu, M.; Ruhl, J.; Tatalovich, Z.; Mariotto, A.; Lewis, D.; et al. SEER Cancer Statistics Review, 1975-2016. *Natl. Cancer Inst.* 2019.
6. Nowell, P.C. The clonal evolution of tumor cell populations. *Science (80-.).* 1976.
7. Hanahan, D.; Weinberg, R.A. The Hallmarks of Cancer Review Douglas. *Cell* 2000, *100*, 57–70.
8. Hanahan, D.; Weinberg, R.A. Hallmarks of cancer: The next generation. *Cell* 2011.
9. Grizzi, F.; Chiriva-Internati, M. Cancer: Looking for simplicity and finding complexity. *Cancer Cell Int.* 2006.
10. World Health Organisation Global cancer data. *Int. Agency Res. cancer* 2018, 13–15.
11. Lanzi, C.; Cassinelli, G. Heparan sulfate mimetics in cancer therapy: The challenge to define structural determinants and the relevance of targets for optimal activity. *Molecules* 2018.
12. Wang, M.; Zhao, J.; Zhang, L.; Wei, F.; Lian, Y.; Wu, Y.; Gong, Z.; Zhang, S.; Zhou, J.; Cao, K.; et al. Role of tumor microenvironment in tumorigenesis. *J. Cancer* 2017.
13. Yue, B. Biology of the extracellular matrix: An overview. *J. Glaucoma* 2014.
14. Walker, C.; Mojares, E.; Del Río Hernández, A. Role of extracellular matrix in development and cancer progression. *Int. J. Mol. Sci.* 2018.
15. Teti, A. Regulation of cellular functions by extracellular matrix. *J. Am. Soc. Nephrol.* 1992.
16. Frantz, C.; Stewart, K.M.; Weaver, V.M. The extracellular matrix at a glance. *J. Cell Sci.* 2010.
17. Lu, P.; Weaver, V.M.; Werb, Z. The extracellular matrix: A dynamic niche in cancer progression. *J. Cell Biol.* 2012.
18. Wullkopf, L.; West, A.K. V.; Leijnse, N.; Cox, T.R.; Madsen, C.D.; Oddershede, L.B.; Erler, J.T. Cancer cells' ability to mechanically adjust to extracellular matrix stiffness correlates with their invasive potential. *Mol. Biol. Cell* 2018.
19. Yanagishita, M. Function of proteoglycans in the extracellular matrix. *Pathol. Int.* 1993.
20. Parish, C.R. The role of heparan sulphate in inflammation. *Nat. Rev. Immunol.* 2006.
21. Stringer, S.E. The role of heparan sulphate proteoglycans in angiogenesis. In Proceedings of the Biochemical Society Transactions; 2006.
22. Dudas, B.; Rose, M.; Cornelli, U.; Pavlovich, A.; Hanin, I. Neuroprotective properties of glycosaminoglycans: Potential treatment for neurodegenerative disorders. In Proceedings of the Neurodegenerative Diseases; 2008.
23. Yip, G.W.; Smollich, M.; Götte, M. Therapeutic value of glycosaminoglycans in cancer. *Mol. Cancer Ther.* 2006.
24. Pérez, S.; Gautier, C.; Imherty, A. Oligosaccharide conformations by diffraction methods. In *Carbohydrates in Chemistry and Biology*; 2008 ISBN 9783527618255.
25. Naggi, A.; Casu, B.; Perez, M.; Torri, G.; Cassinelli, G.; Penco, S.; Pisano, C.; Giannini, G.; Ishai-Michaeli, R.; Vlodavsky, I. Modulation of the heparanase-inhibiting activity of heparin through

selective desulfation, graded N-acetylation, and glycol splitting. *J. Biol. Chem.* 2005.

26. Mohamed, S.; Coombe, D.R. Heparin mimetics: Their therapeutic potential. *Pharmaceuticals* 2017.
27. Knelson, E.H.; Nee, J.C.; Blobe, G.C. Heparan sulfate signaling in cancer. *Trends Biochem. Sci.* 2014.
28. Meneghetti, M.C.Z.; Hughes, A.J.; Rudd, T.R.; Nader, H.B.; Powell, A.K.; Yates, E.A.; Lima, M.A. Heparan sulfate and heparin interactions with proteins. *J. R. Soc. Interface* 2015.
29. Stevens, R.L.; Austen, K.F. Recent advances in the cellular and molecular biology of mast cells. *Immunol. Today* 1989.
30. Rabenstein, D.L. Heparin and heparan sulfate: Structure and function. *Nat. Prod. Rep.* 2002.
31. Weiss, R.J.; Esko, J.D.; Tor, Y. Targeting heparin and heparan sulfate protein interactions. *Org. Biomol. Chem.* 2017.
32. Capila, I.; Linhardt, R.J. Heparin - Protein interactions. *Angew. Chemie - Int. Ed.* 2002.
33. Cardin, A.D.; Weintraub, H.J. Molecular modeling of protein-glycosaminoglycan interactions. *Arterioscler. Thromb. Vasc. Biol.* 1989, *9*, 21–32.
34. Flonia Levy-Adam, Ghada Abboud-Jarrous, Marco Guerrini, D.B.; Israel Vlodavsky, and N.I. Identification and Characterization of Heparin/Heparan Sulfate Binding Domains of the Endoglycosidase Heparanase. *J. Biol. Chem* 2005, *280*, 20457–20466.
35. Humphries, D.E.; Wong, G.W.; Friend, D.S.; Gurish, M.F.; Qiu, W.T.; Huang, C.; Sharpe, A.H.; Stevens, R.L. Heparin is essential for the storage of specific granule proteases in mast cells. *Nature* 1999.
36. Forsberg, E.; Pejler, G.; Ringvall, M.; Lunderius, C.; Tomasini-Johansson, B.; Kusche-Gullberg, M.; Eriksson, I.; Ledin, J.; Hellman, L.; Kjellén, L. Abnormal mast cells in mice deficient in a heparin-synthesizing enzyme. *Nature* 1999.
37. Borsig, L. Heparin as an inhibitor of cancer progression. In *Progress in Molecular Biology and Translational Science*; 2010.
38. Norrby, K. Heparin and angiogenesis: A low-molecular-weight fraction inhibits and a high-molecular-weight fraction stimulates angiogenesis systemically. *Pathophysiol. Haemost. Thromb.* 1993.
39. Weiler, J.M.; Edens, R.E.; Linhardt, R.J.; Kapelanski, D.P. Heparin and modified heparin inhibit complement activation in vivo. *J. Immunol.* 1992.
40. Mousavi, S.; Moradi, M.; Khorshidahmad, T.; Motamedi, M. Anti-inflammatory effects of heparin and its derivatives: A systematic review. *Adv. Pharmacol. Sci.* 2015.
41. Ludwig, R. Therapeutic Use of Heparin beyond Anticoagulation. *Curr. Drug Discov. Technol.* 2009.
42. WuDunn, D.; Spear, P.G. Initial interaction of herpes simplex virus with cells is binding to heparan sulfate. *J. Virol.* 1989.
43. Ramsbottom, S.; Pownall, M. Regulation of Hedgehog Signalling Inside and Outside the Cell. *J. Dev. Biol.* 2016.
44. Petrova, R.; Joyner, A.L. Roles for Hedgehog signaling in adult organ homeostasis and repair. *Dev.* 2014.
45. Zhou, J.X.; Jia, L.W.; Liu, W.M.; Miao, C.L.; Liu, S.; Cao, Y.J.; Duan, E.K. Role of sonic hedgehog in maintaining a pool of proliferating stem cells in the human fetal epidermis. *Hum. Reprod.* 2006.
46. Ihrie, R.A.; Shah, J.K.; Harwell, C.C.; Levine, J.H.; Guinto, C.D.; Lezameta, M.; Kriegstein, A.R.; Alvarez-Buylla, A. Persistent Sonic Hedgehog Signaling in Adult Brain Determines Neural Stem Cell Positional Identity. *Neuron* 2011.
47. Watkins, D.N.; Berman, D.M.; Burkholder, S.G.; Wang, B.; Beachy, P.A.; Baylin, S.B. Hedgehog signalling within airway epithelial progenitors and in small-cell lung cancer. *Nature* 2003.
48. Büller, N.V.J.A.; Rosekrans, S.L.; Westerlund, J.; van den Brink, G.R. Hedgehog signaling and maintenance of homeostasis in the intestinal epithelium. *Physiology* 2012.

49. Hanna, A.; Shevde, L.A. Hedgehog signaling: Modulation of cancer properies and tumor mircroenvironment. *Mol. Cancer* 2016.

50. Hahn, H.; Wicking, C.; Zaphiropoulos, P.G.; Gailani, M.R.; Shanley, S.; Chidambaram, A.; Vorechovsky, I.; Holmberg, E.; Unden, A.B.; Gillies, S.; et al. Mutations of the human homolog of drosophila patched in the nevoid basal cell carcinoma syndrome. *Cell* 1966, *85*, 841–851.

51. Goodrich, L. V.; Milenković, L.; Higgins, K.M.; Scott, M.P. Altered neural cell fates and medulloblastoma in mouse patched mutants. *Science (80-.).* 1997.

52. Chari, N.S.; McDonnell, T.J. The sonic hedgehog signaling network in development and neoplasia. *Adv. Anat. Pathol.* 2007, *14*, 344–352.

53. Jiang, J.; Hui, C. chung Hedgehog Signaling in Development and Cancer. *Dev. Cell* 2008.

54. Girardi, D.; Barrichello, A.; Fernandes, G.; Pereira, A. Targeting the Hedgehog Pathway in Cancer: Current Evidence and Future Perspectives. *Cells* 2019.

55. Nüsslein-volhard, C.; Wieschaus, E. Mutations affecting segment number and polarity in drosophila. *Nature* 1980.

56. Dessaud, E.; McMahon, A.P.; Briscoe, J. Pattern formation in the vertebrate neural tube: A sonic hedgehog morphogen-regulated transcriptional network. *Development* 2008.

57. Porter, J.A.; Young, K.E.; Beachy, P.A. Cholesterol modification of hedgehog signaling proteins in animal development. *Science (80-.).* 1996.

58. Pepinsky, R.B.; Zeng, C.; Went, D.; Rayhorn, P.; Baker, D.P.; Williams, K.P.; Bixler, S.A.; Ambrose, C.M.; Garber, E.A.; Miatkowski, K.; et al. Identification of a palmitic acid-modified form of human Sonic hedgehog. *J. Biol. Chem.* 1998.

59. Porter, J.A.; von Kessler, D.P.; Ekker, S.C.; Young, K.E.; Lee, J.J.; Moses, K.; Beachy, P.A. The product of hedgehog autoproteolytic cleavage active in local and long-range signalling. *Nature* 1995.

60. Lewis, P.M.; Dunn, M.P.; McMahon, J.A.; Logan, M.; Martin, J.F.; St-Jacques, B.; McMahon, A.P. Cholesterol modification of sonic hedgehog is required for long-range signaling activity and effective modulation of signaling by Ptc1. *Cell* 2001.

61. Gallet, A.; Rodriguez, R.; Ruel, L.; Therond, P.P. Cholesterol modification of Hedgehog is required for trafficking and movement, revealing an asymmetric cellular response to Hedgehog. *Dev. Cell* 2003.

62. Dawber, R.J.; Hebbes, S.; Herpers, B.; Docquier, F.; Van Den Heuvel, M. Differential range and activity of various forms of the Hedgehog protein. *BMC Dev. Biol.* 2005.

63. Gallet, A.; Ruel, L.; Staccini-Lavenant, L.; Thérond, P.P. Cholesterol modification is necessary for controlled planar long-range activity of Hedgehog in Drosophila epithelia. *Development* 2006.

64. Goetz, J.A.; Singh, S.; Suber, L.M.; Kull, F.J.; Robbins, D.J. A highly conserved amino-terminal region of Sonic Hedgehog is required for the formation of its freely diffusible multimeric form. *J. Biol. Chem.* 2006.

65. Chen, M.H.; Li, Y.J.; Kawakami, T.; Xu, S.M.; Chuang, P.T. Palmitoylation is required for the production of a soluble multimeric Hedgehog protein complex and long-range signaling in vertebrates. *Genes Dev.* 2004.

66. Kohtz, J.D.; Lee, H.Y.; Gaiano, N.; Segal, J.; Ng, E.; Larson, T.; Baker, D.P.; Garber, E.A.; Williams, K.P.; Fishell, G. N-terminal fatty-acylation of sonic hedgehog enhances the induction of rodent ventral forebrain neurons. *Development* 2001.

67. Burke, R.; Nellen, D.; Bellotto, M.; Hafen, E.; Senti, K.A.; Dickson, B.J.; Basler, K. Dispatched, a novel sterol-sensing domain protein dedicated to the release of cholesterol-modified Hedgehog from signaling cells. *Cell* 1999.

68. Jakobs, P.; Schulz, P.; Ortmann, C.; Schürmann, S.; Exner, S.; Rebollido-Rios, R.; Dreier, R.; Seidler, D.G.; Grobe, K. Bridging the gap: Heparan sulfate and Scube2 assemble Sonic hedgehog release complexes at the surface of producing cells. *Sci. Rep.* 2016.

69. Tukachinsky, H.; Kuzmickas, R.P.; Jao, C.Y.; Liu, J.; Salic, A. Dispatched and Scube Mediate the Efficient Secretion of the Cholesterol-Modified Hedgehog Ligand. *Cell Rep.* 2012.

70. Ohlig, S.; Pickhinke, U.; Sirko, S.; Bandari, S.; Hoffmann, D.; Dreier, R.; Farshi, P.; Götz, M.; Grobe, K. An emerging role of Sonic hedgehog shedding as a modulator of heparan sulfate interactions. *J. Biol. Chem.* 2012.

71. Vyas, N.; Walvekar, A.; Tate, D.; Lakshmanan, V.; Bansal, D.; Cicero, A. Lo; Raposo, G.; Palakodeti, D.; Dhawan, J. Vertebrate Hedgehog is secreted on two types of extracellular vesicles with different signaling properties. *Sci. Rep.* 2014.

72. Ramsbottom, S.A.; Pownall, M.E. Regulation of hedgehog signalling inside and outside the cell. *J. Dev. Biol.* 2016.

73. Bellaiche, Y.; The, I.; Perrimon, N. Tout-velu is a Drosophila homologue of the putative tumour suppressor EXT-1 and is needed for Hh diffusion. *Nature* 1998.

74. Vyas, N.; Goswami, D.; Manonmani, A.; Sharma, P.; Ranganath, H.A.; VijayRaghavan, K.; Shashidhara, L.S.; Sowdhamini, R.; Mayor, S. Nanoscale Organization of Hedgehog Is Essential for Long-Range Signaling. *Cell* 2008.

75. Beachy, P.A.; Hymowitz, S.G.; Lazarus, R.A.; Leahy, D.J.; Siebold, C. Interactions between Hedgehog proteins and their binding partners come into view. *Genes Dev.* 2010.

76. Zhang, F.; McLellan, J.S.; Ayala, A.M.; Leahy, D.J.; Linhardt, R.J. Kinetic and structural studies on interactions between heparin or heparan sulfate and proteins of the hedgehog signaling pathway. *Biochemistry* 2007.

77. Farshi, P.; Ohlig, S.; Pickhinke, U.; Höing, S.; Jochmann, K.; Lawrence, R.; Dreier, R.; Dierker, T.; Grobe, K. Dual roles of the Cardin-Weintraub motif in multimeric sonic hedgehog. *J. Biol. Chem.* 2011.

78. Filmus, J.; Capurro, M. The role of glypicans in Hedgehog signaling. *Matrix Biol.* 2014.

79. Ortmann, C.; Pickhinke, U.; Exner, S.; Ohlig, S.; Lawrence, R.; Jboor, H.; Dreier, R.; Grobe, K. Sonic hedgehog processing and release are regulated by glypican heparan sulfate proteoglycans. *J. Cell Sci.* 2015.

80. Manikowski, D.; Jakobs, P.; Jboor, H.; Grobe, K. Soluble heparin and heparan sulfate glycosaminoglycans interfere with sonic hedgehog solubilization and receptor binding. *Molecules* 2019.

81. Chan, J.A.; Balasubramanian, S.; Witt, R.M.; Nazemi, K.J.; Choi, Y.; Pazyra-Murphy, M.F.; Walsh, C.O.; Thompson, M.; Segal, R.A. Proteoglycan interactions with Sonic Hedgehog specify mitogenic responses. *Nat. Neurosci.* 2009.

82. Chang, S.C.; Mulloy, B.; Magee, A.I.; Couchman, J.R. Two distinct sites in sonic hedgehog combine for heparan sulfate interactions and cell signaling functions. *J. Biol. Chem.* 2011.

83. Whalen, D.M.; Malinauskas, T.; Gilbert, R.J.C.; Siebold, C. Structural insights into proteoglycan-shaped Hedgehog signaling. *Proc. Natl. Acad. Sci.* 2013.

84. Amakye, D.; Jagani, Z.; Dorsch, M. Unraveling the therapeutic potential of the Hedgehog pathway in cancer. *Nat. Med.* 2013.

85. Denef, N.; Neubüser, D.; Perez, L.; Cohen, S.M. Hedgehog induces opposite changes in turnover and subcellular localization of patched and smoothened. *Cell* 2000.

86. Mastronardi, F.G.; Dimitroulakos, J.; Kamel-Reid, S.; Manoukian, A.S. Co-localization of Patched and activated sonic hedgehog to lysosomes in neurons. *Neuroreport* 2000.

87. Roth, W.; Wild-Bode, C.; Platten, M.; Grimmel, C.; Melkonyan, H.S.; Dichgans, J.; Weller, M. Secreted Frizzled-related proteins inhibit motility and promote growth of human malignant glioma cells. *Oncogene* 2000.

88. Persson, M.; Stamataki, D.; Welscher, P. Te; Andersson, E.; Böse, J.; Rüther, U.; Ericson, J.; Briscoe, J. Dorsal-ventral patterning of the spinal cord requires Gli3 transcriptional repressor activity. *Genes*

Dev. 2002.

89. Hynes, M.; Stone, D.M.; Dowd, M.; Pitts-Meek, S.; Goddard, A.; Gurney, A.; Rosenthal, A. Control of cell pattern in the neural tube by the zinc finger transcription factor and oncogene Gli-1. *Neuron* 1997.

90. Choudhry, Z.; Rikani, A.A.; Choudhry, A.M.; Tariq, S.; Zakaria, F.; Asghar, M.W.; Sarfraz, M.K.; Haider, K.; Shafiq, A.A.; Mobassarah, N.J. Sonic hedgehog signalling pathway: A complex network. *Ann. Neurosci.* 2014.

91. Bonifas, J.M.; Pennypacker, S.; Chuang, P.T.; McMahon, A.P.; Williams, M.; Rosenthal, A.; De Sauvage, F.J.; Epstein, E.H. Activation of expression of hedgehog target genes in basal cell carcinomas. *J. Invest. Dermatol.* 2001.

92. Oliver, T.G.; Grasfeder, L.L.; Carroll, A.L.; Kaiser, C.; Gillingham, C.L.; Lin, S.M.; Wickramasinghe, R.; Scott, M.P.; Wechsler-Reya, R.J. Transcriptional profiling of the Sonic hedgehog response: A critical role for N-myc in proliferation of neuronal precursors. *Proc. Natl. Acad. Sci. U. S. A.* 2003.

93. Bigelow, R.L.H.; Chari, N.S.; Undén, A.B.; Spurgers, K.B.; Lee, S.; Roop, D.R.; Toftgård, R.; McDonnell, T.J. Transcriptional Regulation of bcl-2 Mediated by the Sonic Hedgehog Signaling Pathway through gli-1. *J. Biol. Chem.* 2004.

94. Morrow, D.; Cullen, J.P.; Liu, W.; Guha, S.; Sweeney, C.; Birney, Y.A.; Collins, N.; Walls, D.; Redmond, E.M.; Cahill, P.A. Sonic hedgehog induces notch target gene expression in vascular smooth muscle cells via VEGF-A. *Arterioscler. Thromb. Vasc. Biol.* 2009.

95. Li, X.; Deng, W.; Nail, C.D.; Bailey, S.K.; Kraus, M.H.; Ruppert, J.M.; Lobo-Ruppert, S.M. Snail induction is an early response to Gli1 that determines the efficiency of epithelial transformation. *Oncogene* 2006.

96. Cochrane, C.R.; Szczepny, A.; Watkins, D.N.; Cain, J.E. Hedgehog signaling in the maintenance of cancer stem cells. *Cancers (Basel).* 2015.

97. Katoh, M.; Katoh, M. Notch ligand, JAG1, is evolutionarily conserved target of canonical WNT signaling pathway in progenitor cells. *Int. J. Mol. Med.* 2006.

98. Bouldin, C.M.; Harfe, B.D. Aberrant FGF signaling, independent of ectopic hedgehog signaling, initiates preaxial polydactyly in Dorking chickens. *Dev. Biol.* 2009.

99. Mullor, J.L.; Dahmane, N.; Sun, T.; Altaba, A.R. Wnt signals are targets and mediators of Gli function. *Curr. Biol.* 2001.

100. Shimokawa, T.; Tostar, U.; Lauth, M.; Palaniswamy, R.; Kasper, M.; Toftgård, R.; Zaphiropoulos, P.G. Novel human glioma-associated oncogene 1 (GLI1) splice variants reveal distinct mechanisms in the terminal transduction of the hedgehog signal. *J. Biol. Chem.* 2008.

101. Lo, H.W.; Zhu, H.; Cao, X.; Aldrich, A.; Ali-Osman, F. A novel splice variant of GLI1 that promotes glioblastoma cell migration and invasion. *Cancer Res.* 2009.

102. Cao, X.; Geradts, J.; Dewhirst, M.W.; Lo, H.W. Upregulation of VEGF-A and CD24 gene expression by the tGLI1 transcription factor contributes to the aggressive behavior of breast cancer cells. *Oncogene* 2012.

103. Niyaz, M.; Khan, M.S.; Mudassar, S. Hedgehog Signaling: An Achilles' Heel in Cancer. *Transl. Oncol.* 2019.

104. Xie, J.; Murone, M.; Luoh, S.M.; Ryan, A.; Gu, Q.; Zhang, C.; Bonifas, J.M.; Lam, C.W.; Hynes, M.; Goddard, A.; et al. Activating Smoothened mutations in sporadic basal-cell carcinoma. *Nature* 1998.

105. Gupta, S.K.; Meiri, K.F.; Mahfooz, K.; Bharti, U.; Mani, S. Coordination between Extrinsic Extracellular Matrix Cues and Intrinsic Responses to Orient the Centrosome in Polarizing Cerebellar Granule Neurons. *J. Neurosci.* 2010.

106. Tostar, U.; Malm, C.J.; Meis-Kindblom, J.M.; Kindblom, L.G.; Toftgård, R.; Undén, A.B. Deregulation of the hedgehog signalling pathway: A possible role for the PTCH and SUFU genes in human rhabdomyoma and rhabdomyosarcoma development. *J. Pathol.* 2006.

107. Wang, Y.; Jin, G.; Li, Q.; Wang, Z.; Hu, W.; Li, P.; Li, S.; Wu, H.; Kong, X.; Gao, J.; et al. Hedgehog signaling non-canonical activated by pro-inflammatory cytokines in pancreatic ductal adenocarcinoma. *J. Cancer* 2016.

108. Colavito, S.A.; Zou, M.R.; Yan, Q.; Nguyen, D.X.; Stern, D.F. Significance of glioma-associated oncogene homolog 1 (GLI1) expression in claudin-low breast cancer and crosstalk with the nuclear factor kappa-light-chain-enhancer of activated B cells (NFκB) pathway. *Breast Cancer Res.* 2014.

109. Stecca, B.; Mas, C.; Clement, V.; Zbinden, M.; Correa, R.; Piguet, V.; Beermann, F.; Ruiz I Altaba, A. Melanomas require HEDGEHOG-GLI signaling regulated by interactions between GLI1 and the RAS-MEK/AKT pathways. *Proc. Natl. Acad. Sci. U. S. A.* 2007.

110. Skoda, A.M.; Simovic, D.; Karin, V.; Kardum, V.; Vranic, S.; Serman, L. The role of the hedgehog signaling pathway in cancer: A comprehensive review. *Bosn. J. Basic Med. Sci.* 2018, *18*, 8–20.

111. Thayer, S.P.; Di Magliano, M.P.; Heiser, P.W.; Nielsen, C.M.; Roberts, D.J.; Lauwers, G.Y.; Qi, Y.P.; Gysin, S.; Fernández-del Castillo, C.; Yajnik, V.; et al. Hedgehog is an early and late mediator of pancreatic cancer tumorigenesis. *Nature* 2003.

112. Berman, D.M.; Karhadkar, S.S.; Maitra, A.; De Oca, R.M.; Gerstenblith, M.R.; Briggs, K.; Parker, A.R.; Shimada, Y.; Eshleman, J.R.; Watkins, D.N.; et al. Widespread requirement for Hedgehog ligand stimulation in growth of digestive tract tumours. *Nature* 2003.

113. Ma, X.; Sheng, T.; Zhang, Y.; Zhang, X.; He, J.; Huang, S.; Chen, K.; Sultz, J.; Adegboyega, P.A.; Zhang, H.; et al. Hedgehog signaling is activated in subsets of esophageal cancers. *Int. J. Cancer* 2006.

114. Karhadkar, S.S.; Bova, G.S.; Abdallah, N.; Dhara, S.; Gardner, D.; Maitra, A.; Isaacs, J.T.; Berman, D.M.; Beachy, P.A. Hedgehog signalling in prostate regeneration, neoplasia and metastasis. *Nature* 2004.

115. Mukherjee, S.; Frolova, N.; Sadlonova, A.; Novak, Z.; Steg, A.; Page, G.P.; Welch, D.R.; Lobo-Ruppert, S.M.; Michael Ruppert, J.; Johnson, M.R.; et al. Hedgehog signaling and response to cyclopamine differ in epithelial and stromal cells in benign breast and breast cancer. *Cancer Biol. Ther.* 2006.

116. Gulino, A.; Ferretti, E.; De Smaele, E. Hedgehog signalling in colon cancer and stem cells. *EMBO Mol. Med.* 2009.

117. Bhattacharya, R.; Kwon, J.; Ali, B.; Wang, E.; Patra, S.; Shridhar, V.; Mukherjee, P. Role of hedgehog signaling in ovarian cancer. *Clin. Cancer Res.* 2008.

118. Theunissen, J.W.; De Sauvage, F.J. Paracrine hedgehog signaling in cancer. *Cancer Res.* 2009.

119. Yauch, R.L.; Gould, S.E.; Scales, S.J.; Tang, T.; Tian, H.; Ahn, C.P.; Marshall, D.; Fu, L.; Januario, T.; Kallop, D.; et al. A paracrine requirement for hedgehog signalling in cancer. *Nature* 2008, *455*, 406–410.

120. Fan, L.; Pepicelli, C. V.; Dibble, C.C.; Catbagan, W.; Zarycki, J.L.; Laciak, R.; Gipp, J.; Shaw, A.; Lamm, M.L.G.; Munoz, A.; et al. Hedgehog signaling promotes prostate xenograft tumor growth. *Endocrinology* 2004, *145*, 3961–3970.

121. Theunissen, J.W.; De Sauvage, F.J. Paracrine hedgehog signaling in cancer. *Cancer Res.* 2009.

122. Fendrich, V.; Oh, E.; Bang, S.; Karikari, C.; Ottenhof, N.; Bisht, S.; Lauth, M.; Brossart, P.; Katsanis, N.; Maitra, A.; et al. Ectopic Overexpression of Sonic Hedgehog (Shh) Induces Stromal Expansion and Metaplasia in the Adult Murine Pancreas. *Neoplasia* 2011.

123. Tian, H.; Callahan, C.A.; DuPree, K.J.; Darbonne, W.C.; Ahn, C.P.; Scales, S.J.; de Sauvage, F.J. Hedgehog signaling is restricted to the stromal compartment during pancreatic carcinogenesis. *Proc. Natl. Acad. Sci.* 2009.

124. Lee, J.J.; Perera, R.M.; Wang, H.; Wu, D.-C.; Liu, X.S.; Han, S.; Fitamant, J.; Jones, P.D.; Ghanta, K.S.; Kawano, S.; et al. Stromal response to Hedgehog signaling restrains pancreatic cancer progression. *Proc. Natl. Acad. Sci.* 2014.

125. Incardona, J.P.; Gaffield, W.; Kapur, R.P.; Roelink, H. The teratogenic Veratrum alkaloid cyclopamine inhibits Sonic hedgehog signal transduction. *Development* 1998.

126. Talpale, J.; Chen, J.K.; Cooper, M.K.; Wang, B.; Mann, R.K.; Milenkovic, L.; Scott, M.P.; Beachy, P.A. Effects of oncogenic mutations in Smoothened and Patched can be reversed by cyclopamine. *Nature* 2000.

127. Gonnissen, A.; Isebaert, S.; Haustermans, K. Targeting the Hedgehog signaling pathway in cancer: beyond Smoothened. *Oncotarget* 2015, *6*, 13899–13913.

128. Maun, H.R.; Wen, X.; Lingel, A.; De Sauvage, F.J.; Lazarus, R.A.; Scales, S.J.; Hymowitz, S.G. Hedgehog pathway antagonist 5E1 binds hedgehog at the pseudo-active site. *J. Biol. Chem.* 2010.

129. Stanton, B.Z.; Peng, L.F.; Maloof, N.; Nakai, K.; Wang, X.; Duffner, J.L.; Taveras, K.M.; Hyman, J.M.; Lee, S.W.; Koehler, A.N.; et al. A small molecule that binds Hedgehog and blocks its signaling in human cells. *Nat. Chem. Biol.* 2009.

130. Petrova, E.; Rios-Esteves, J.; Ouerfelli, O.; Glickman, J.F.; Resh, M.D. Inhibitors of Hedgehog acyltransferase block Sonic Hedgehog signaling. *Nat. Chem. Biol.* 2013.

131. Tremblay, M.R.; Lescarbeau, A.; Grogan, M.J.; Tan, E.; Lin, G.; Austad, B.C.; Yu, L.C.; Behnke, M.L.; Nair, S.J.; Hagel, M.; et al. Discovery of a potent and orally active hedgehog pathway antagonist (IPI-926). *J. Med. Chem.* 2009.

132. Rimkus, T.K.; Carpenter, R.L.; Qasem, S.; Chan, M.; Lo, H.W. Targeting the sonic hedgehog signaling pathway: Review of smoothened and GLI inhibitors. *Cancers (Basel).* 2016, *8*.

133. Pan, S.; Wu, X.; Jiang, J.; Gao, W.; Wan, Y.; Cheng, D.; Han, D.; Liu, J.; Englund, N.P.; Wang, Y.; et al. Discovery of NVP-LDE225, a potent and selective smoothened antagonist. *ACS Med. Chem. Lett.* 2010.

134. Bender, M.H.; Hipskind, P.A.; Capen, A.R.; Cockman, M.; Credille, K.M.; Gao, H.; Bastian, J.A.; Clay, J.M.; Lobb, K.L.; Sall, D.J.; et al. Abstract 2819: Identification and characterization of a novel smoothened antagonist for the treatment of cancer with deregulated hedgehog signaling.; 2011.

135. Munchhof, M.J.; Li, Q.; Shavnya, A.; Borzillo, G. V.; Boyden, T.L.; Jones, C.S.; Lagreca, S.D.; Martinez-Alsina, L.; Patel, N.; Pelletier, K.; et al. Discovery of PF-04449913, a potent and orally bioavailable inhibitor of smoothened. *ACS Med. Chem. Lett.* 2012.

136. Kim, J.; Tang, J.Y.; Gong, R.; Kim, J.; Lee, J.J.; Clemons, K. V.; Chong, C.R.; Chang, K.S.; Fereshteh, M.; Gardner, D.; et al. Itraconazole, a Commonly Used Antifungal that Inhibits Hedgehog Pathway Activity and Cancer Growth. *Cancer Cell* 2010.

137. Lauth, M.; Bergstrom, A.; Shimokawa, T.; Toftgard, R. Inhibition of GLI-mediated transcription and tumor cell growth by small-molecule antagonists. *Proc. Natl. Acad. Sci.* 2007, *104*, 8455–8460.

138. Wang, Z.Y.; Chen, Z. Differentiation and apoptosis induction therapy in acute promyelocytic leukaemia. *Lancet Oncol.* 2000.

139. Axelson, M.; Liu, K.; Jiang, X.; He, K.; Wang, J.; Zhao, H.; Kufrin, D.; Palmby, T.; Dong, Z.; Russell, A.M.; et al. U.S. Food and Drug Administration approval: Vismodegib for recurrent, locally advanced, or metastatic basal cell carcinoma. *Clin. Cancer Res.* 2013.

140. Robarge, K.D.; Brunton, S.A.; Castanedo, G.M.; Cui, Y.; Dina, M.S.; Goldsmith, R.; Gould, S.E.; Guichert, O.; Gunzner, J.L.; Halladay, J.; et al. GDC-0449-A potent inhibitor of the hedgehog pathway. *Bioorganic Med. Chem. Lett.* 2009.

141. Jain, S.; Song, R.; Xie, J. Sonidegib: Mechanism of action, pharmacology, and clinical utility for advanced basal cell carcinomas. *Onco. Targets. Ther.* 2017.

142. Pricl, S.; Cortelazzi, B.; Dal Col, V.; Marson, D.; Laurini, E.; Fermeglia, M.; Licitra, L.; Pilotti, S.; Bossi, P.; Perrone, F. Smoothened (SMO) receptor mutations dictate resistance tovismodegib in basal cell carcinoma. *Mol. Oncol.* 2015.

143. Agyeman, A.; Jha, B.K.; Mazumdar, T.; Houghton, J.A. Mode and specificity of binding of the small molecule GANT61 to GLI determines inhibition of GLI-DNA binding. *Oncotarget* 2014.

144. Benvenuto, M.; Masuelli, L.; De Smaele, E.; Fantini, M.; Mattera, R.; Cucchi, D.; Bonanno, E.; Di Stefano, E.; Frajese, G.V.; Orlandi, A.; et al. In vitro and in vivo inhibition of breast cancer cell growth by targeting the Hedgehog/GLI pathway with SMO (GDC-0449) or GLI (GANT-61) inhibitors.

Oncotarget 2016, *7*, 9250–9270.

145. Latuske, E.M.; Stamm, H.; Klokow, M.; Vohwinkel, G.; Muschhammer, J.; Bokemeyer, C.; Jücker, M.; Kebenko, M.; Fiedler, W.; Wellbrock, J. Combined inhibition of GLI and FLT3 signaling leads to effective anti-leukemic effects in human acute myeloid leukemia. *Oncotarget* 2017.

146. Huang, L.; Walter, V.; Hayes, D.N.; Onaitis, M. Hedgehog-GLI signaling inhibition suppresses tumor growth in squamous lung cancer. *Clin. Cancer Res.* 2014.

147. Petrova, E.; Matevossian, A.; Resh, M.D. Hedgehog acyltransferase as a target in pancreatic ductal adenocarcinoma. *Oncogene* 2015.

148. Bosanac, I.; Maun, H.R.; Scales, S.J.; Wen, X.; Lingel, A.; Bazan, J.F.; De Sauvage, F.J.; Hymowitz, S.G.; Lazarus, R.A. The structure of SHH in complex with HHIP reveals a recognition role for the Shh pseudo active site in signaling. *Nat. Struct. Mol. Biol.* 2009, *16*, 691–697.

149. Chang, Q.; Foltz, W.D.; Chaudary, N.; Hill, R.P.; Hedley, D.W. Tumor-stroma interaction in orthotopic primary pancreatic cancer xenografts during hedgehog pathway inhibition. *Int. J. Cancer* 2013, *133*, 225–234.

150. Coon, V.; Laukert, T.; Pedone, C. a; Laterra, J.; Kim, K.J.; Fults, D.W. Molecular therapy targeting Sonic hedgehog and hepatocyte growth factor signaling in a mouse model of medulloblastoma. *Mol Cancer Ther* 2010.

151. Folkman, J. What is the evidence that tumors are angiogenesis dependent? *J. Natl. Cancer Inst.* 1990, *82*, 4–7.

152. Eichhorn, M.E.; Kleespies, A.; Angele, M.K.; Jauch, K.W.; Bruns, C.J. Angiogenesis in cancer: Molecular mechanisms, clinical impact. *Langenbeck's Arch. Surg.* 2007, *392*, 371–379.

153. Algire, G.H.; Chalkley, H.W.; Legallais, F.Y.; Park, H.D. Vasculae reactions of normal and malignant tissues in vivo. i. vascular reactions of mice to wounds and to normal and neoplastic transplants. *J. Natl. Cancer Inst.* 1945, *6*, 73–85.

154. Sherwood, L.M.; Parris, E.E.; Folkman, J. Tumor Angiogenesis: Therapeutic Implications. *N. Engl. J. Med.* 1971.

155. Hanahan, D.; Folkman, J. Patterns and emerging mechanisms of the angiogenic switch during tumorigenesis. *Cell* 1996, *86*, 353–364.

156. Bergers, G.; Benjamin, L.E. Tumorigenesis and the angiogenic switch. *Nat. Rev. Cancer* 2003.

157. Kerbel, R.S. Tumor angiogenesis: Past, present and the near future. *Carcinogenesis* 2000.

158. Carmeliet, P.; Jain, R.K. Angiogenesis in cancer and other diseases. *Nature* 2000.

159. Ferrara, N.; Kerbel, R.S. Angiogenesis as a therapeutic target. *Nature* 2005, *438*, 967–974.

160. Leung, D.W.; Cachianes, G.; Kuang, W.J.; Goeddel, D. V.; Ferrara, N. Vascular endothelial growth factor is a secreted angiogenic mitogen. *Science (80-.).* 1989, *246*, 1306–1309.

161. Carmeliet, P.; Ferreira, V.; Breier, G.; Pollefeyt, S.; Kieckens, L.; Gertsenstein, M.; Fahrig, M.; Vandenhoeck, A.; Harpal, K.; Eberhardt, C.; et al. Abnormal blood vessel development and lethality in embryos lacking a single VEGF allele. *Nature* 1996.

162. Ferrara, N.; Carver-Moore, K.; Chen, H.; Dowd, M.; Lu, L.; O'Shea, K.S.; Powell-Braxton, L.; Hillan, K.J.; Moore, M.W. Heterozygous embryonic lethality induced by targeted inactivation of the VEGF gene. *Nature* 1996, *380*, 439–442.

163. Ferrara, N.; Gerber, H.P.; LeCouter, J. The biology of VEGF and its receptors. *Nat. Med.* 2003, *9*, 669–676.

164. Mendelsohn, J.; Howley, P.M.; Israel, M.A.; Gray, J.W.; Thompson, C.B. *The Molecular Basis of Cancer*; 2008; ISBN 9781416037033.

165. Forsten, K.E.; Fannon, M.; Nugent, M.A. Potential mechanisms for the regulation of growth factor binding by heparin. *J. Theor. Biol.* 2000.

166. Whitaker, G.B.; Limberg, B.J.; Rosenbaum, J.S. Vascular Endothelial Growth Factor Receptor-2 and Neuropilin-1 Form a Receptor Complex that is Responsible for the Differential Signaling Potency of VEGF165 and VEGF121. *J. Biol. Chem.* 2001.

167. Ashikari-Hada, S.; Habuchi, H.; Kariya, Y.; Kimata, K. Heparin regulates vascular endothelial growth factor165- dependent mitogenic activity, tube formation, and its receptor phosphorylation of human endothelial cells: Comparison of the effects of heparin and modified heparins. *J. Biol. Chem.* 2005.

168. Gitay-Goren, H.; Soker, S.; Vlodavsky, I.; Neufeld, G. The binding of vascular endothelial growth factor to its receptors is dependent on cell surface-associated heparin-like molecules. *J. Biol. Chem.* 1992, *267*, 6093–6098.

169. Tessler, S.; Rockwell, P.; Hicklin, D.; Cohen, T.; Levi, B.Z.; Witte, L.; Lemischka, I.R.; Neufeld, G. Heparin modulates the interaction of VEGF165 with soluble and cell associated flk-1 receptors. *J. Biol. Chem.* 1994.

170. Maureen Dougher, A.; Wasserstrom, H.; Torley, L.; Shridaran, L.; Westdock, P.; Hileman, R.E.; Fromm, J.R.; Anderberg, R.; Lyman, S.; Linhardt, R.J.; et al. Identification of a heparin binding peptide on the extracellular domain of the KDR VEGF receptor. *Growth Factors* 1997.

171. Chiang, M.K.; Flanagan, J.G. Interactions between the flk-1 receptor, vascular endothelial growth factor, and cell surface proteoglycan identified with a soluble receptor reagent. *Growth Factors* 1995.

172. Teran, M.; Nugent, M.A. Synergistic binding of vascular endothelial growth factor-a and its receptors to heparin selectively modulates complex affinity. *J. Biol. Chem.* 2015, *290*, 16451–16462.

173. Beenken, A.; Mohammadi, M. The FGF family: Biology, pathophysiology and therapy. *Nat. Rev. Drug Discov.* 2009, *8*, 235–253.

174. Cao, Y.; Cao, R.; Hedlund, E.M. R Regulation of tumor angiogenesis and metastasis by FGF and PDGF signaling pathways. *J. Mol. Med.* 2008.

175. Cook, K.M.; Figg, W.D. Angiogenesis Inhibitors: Current Strategies and Future Prospects. *CA. Cancer J. Clin.* 2010.

176. Uriel, S.; Brey, E.M.; Greisler, H.P. Sustained low levels of fibroblast growth factor-1 promote persistent microvascular network formation. *Am. J. Surg.* 2006.

177. Ware, A.; Simons, M. Angiogenesis in ischemic heart disease Inducing. *Nature* 1997, *3*, 158–164.

178. Shing, Y.; Folkman, J.; Sullivan, R.; Butterfield, C.; Murray, J.; Klagsbrun, M. Heparin affinity: Purification of a tumor-derived capillary endothelial cell growth factor. *Science (80-.).* 1984.

179. Korc, M.; Friesel, R. The Role of Fibroblast Growth Factors in Tumor Growth. *Curr. Cancer Drug Targets* 2009, *9*, 639–651.

180. Thisse, B.; Thisse, C. Functions and regulations of fibroblast growth factor signaling during embryonic development. *Dev. Biol.* 2005.

181. Murakami, M.; Simons, M. Fibroblast growth factor regulation of neovascularization. *Curr. Opin. Hematol.* 2008.

182. Deng, C.X.; Wynshaw-Boris, A.; Shen, M.M.; Daugherty, C.; Ornitz, D.M.; Leder, P. Murine FGFR-1 is required for early postimplantation growth and axial organization. *Genes Dev.* 1994.

183. Arman, E.; Haffner-Krausz, R.; Chen, Y.; Heath, J.K.; Lonai, P. Targeted disruption of fibroblast growth factor (FGF) receptor 2 suggests a role for FGF signaling in pregastrulation mammalian development. *Proc. Natl. Acad. Sci. U. S. A.* 1998.

184. Tabata, H.; Silver, M.; Isner, J.M. Arterial gene transfer of acidic fibroblast growth factor for therapeutic angiogenesis in vivo: Critical role of secretion signal in use of naked DNA. *Cardiovasc. Res.* 1997.

185. Presta, M.; Dell'Era, P.; Mitola, S.; Moroni, E.; Ronca, R.; Rusnati, M. Fibroblast growth factor/fibroblast growth factor receptor system in angiogenesis. *Cytokine Growth Factor Rev.* 2005.

186. Vlodavsky, I.; Goldshmidt, O.; Zcharia, E.; Atzmon, R.; Rangini-Guatta, Z.; Elkin, M.; Peretz, T.;

Friedmann, Y. Mammalian heparanase: Involvement in cancer metastasis, angiogenesis and normal development. *Semin. Cancer Biol.* 2002, *12*, 121–129.

187. Parish, C.R.; Freeman, C.; Hulett, M.D. Heparanase: A key enzyme involved in cell invasion. *Biochim. Biophys. Acta - Rev. Cancer* 2001.

188. Vlodavsky, I.; Mohsen, M.; Lider, O.; Svahn, C.M.; Ekre, H.P.; Vigoda, M.; Ishai-Michaeli; Peretz, T. Inhibition of tumor metastasis by heparanase inhibiting species of heparin. *Invasion and Metastasis* 1994.

189. Vlodavsky, I.; Friedmann, Y. Molecular properties and involvement of heparanase in cancer metastasis and angiogenesis. *J. Clin. Invest.* 2001, *108*, 341–347.

190. Vlodavsky, I.; Miao, H.Q.; Medalion, B.; Danagher, P.; Ron, D. Involvement of heparan sulfate and related molecules in sequestration and growth promoting activity of fibroblast growth factor. *Cancer Metastasis Rev.* 1996.

191. Klein, U.; von Figura, K. Partial purification and characterization of a heparan sulfate specific endoglucuronidase. *Biochem. Biophys. Res. Commun.* 1976.

192. Ogren, S.; Lindahl, U. Cleavage of macromolecular heparin by an enzyme from mouse mastocytoma. *J. Biol. Chem.* 1975.

193. Hulett, M.D.; Freeman, C.; Hamdorf, B.J.; Baker, R.T.; Harris, M.J.; Parish, C.R. Cloning of mammalian heparanase, an important enzyme in tumor invasion and metastasis. *Nat. Med.* 1999.

194. Kussie, P.H.; Hulmes, J.D.; Ludwig, D.L.; Patel, S.; Navarro, E.C.; Seddon, A.P.; Giorgio, N.A.; Bohlen, P. Cloning and functional expression of a human heparanase gene. *Biochem. Biophys. Res. Commun.* 1999.

195. Toyoshima, M.; Nakajima, M. Human heparanase. Purification, characterization, cloning, and expression. *J. Biol. Chem.* 1999.

196. Vlodavsky, I.; Friedmann, Y.; Elkin, M.; Aingorn, H.; Atzmon, R.; Ishai-Michaeli, R.; Bitan, M.; Pappo, O.; Peretz, T.; Michal, I.; et al. Mammalian heparanase: Gene cloning, expression and function in tumor progression and metastasis. *Nat. Med.* 1999.

197. Mohan, C.D.; Hari, S.; Preetham, H.D.; Rangappa, S.; Barash, U.; Ilan, N.; Nayak, S.C.; Gupta, V.K.; Basappa; Vlodavsky, I.; et al. Targeting Heparanase in Cancer: Inhibition by Synthetic, Chemically Modified, and Natural Compounds. *iScience* 2019.

198. Vlodavsky, I.; Singh, P.; Boyango, I.; Gutter-Kapon, L.; Elkin, M.; Sanderson, R.D.; Ilan, N. Heparanase: From basic research to therapeutic applications in cancer and inflammation. *Drug Resist. Updat.* 2016.

199. Ferro, V. Heparan sulfate inhibitors and their therapeutic implications in inflammatory illnesses. *Expert Opin. Ther. Targets* 2013.

200. Mao, Y.; Huang, Y.; Buczek-Thomas, J.A.; Ethen, C.M.; Nugent, M.A.; Wu, Z.L.; Zaia, J. A liquid chromatography-mass spectrometry-based approach to characterize the substrate specificity of mammalian heparanase. *J. Biol. Chem.* 2014.

201. Wilson, J.C.; Laloo, A.E.; Singh, S.; Ferro, V. 1H NMR spectroscopic studies establish that heparanase is a retaining glycosidase. *Biochem. Biophys. Res. Commun.* 2014.

202. Matsuno, H.; Kozawa, O.; Okada, K.; Ueshima, S.; Matsuo, O.; Uematsu, T. Plasmin generation plays different roles in the formation and removal of arterial and venous thrombus in mice. *Thromb. Haemost.* 2002.

203. Pikas, D.S.; Li, J.P.; Vlodavsky, I.; Lindahl, U. Substrate specificity of heparanases from human hepatoma and platelets. *J. Biol. Chem.* 1998.

204. Nakajima, M.; Irimura, T.; Nicolson, G.L. Heparanases and tumor metastasis. *J. Cell. Biochem.* 1988.

205. Vreys, V.; David, G. Mammalian heparanase: What is the message? *J. Cell. Mol. Med.* 2007, *11*, 427–452.

206. McKenzie, E.A. Heparanase: A target for drug discovery in cancer and inflammation. *Br. J. Pharmacol.* 2007.

207. Vlodavsky, I.; Beckhove, P.; Lerner, I.; Pisano, C.; Meirovitz, A.; Ilan, N.; Elkin, M. Significance of heparanase in cancer and inflammation. *Cancer Microenviron.* 2012.

208. Ilan, N.; Elkin, M.; Vlodavsky, I. Regulation, function and clinical significance of heparanase in cancer metastasis and angiogenesis. *Int. J. Biochem. Cell Biol.* 2006.

209. Edovitsky, E.; Elkin, M.; Zcharia, E.; Peretz, T.; Vlodavsky, I. Heparanase gene silencing, tumor invasiveness, angiogenesis, and metastasis. *J. Natl. Cancer Inst.* 2004, *96*, 1219–1230.

210. Friedmann, Y.; Vlodavsky, I.; Aingorn, H.; Aviv, A.; Peretz, T.; Pecker, I.; Pappo, O. Expression of heparanase in normal, dysplastic, and neoplastic human colonic mucosa and stroma: Evidence for its role in colonic tumorigenesis. *Am. J. Pathol.* 2000.

211. Elkin, M.; Ilan, N.; Ishai-Michaeli, R.; Friedmann, Y.; Papo, O.; Pecker, I.; Vlodavsky, I. Heparanase as mediator of angiogenesis: mode of action. *FASEB J.* 2001.

212. Cohen, I.; Pappo, O.; Elkin, M.; San, T.; Bar-Shavit, R.; Hazan, R.; Peretz, T.; Vlodavsky, I.; Abramovitch, R. Heparanase promotes growth, angiogenesis and survival of primary breast tumors. *Int. J. Cancer* 2006.

213. Kelly, T.; Miao, H.Q.; Yang, Y.; Navarro, E.; Kussie, P.; Huang, Y.; MacLeod, V.; Casciano, J.; Joseph, L.; Zhan, F.; et al. High Heparanase Activity in Multiple Myeloma Is Associated with Elevated Microvessel Density. *Cancer Res.* 2003.

214. Fux, L.; Ilan, N.; Sanderson, R.D.; Vlodavsky, I. Heparanase: busy at the cell surface. *Trends Biochem. Sci.* 2009.

215. Lin, Z.; Zhang, Q.; Luo, W. Angiogenesis inhibitors as therapeutic agents in cancer: Challenges and future directions. *Eur. J. Pharmacol.* 2016.

216. Ferrara, N.; Hillan, K.J.; Gerber, H.P.; Novotny, W. Discovery and development of bevacizumab, an anti-VEGF antibody for treating cancer. *Nat. Rev. Drug Discov.* 2004.

217. Zhao, Y.; Adjei, A.A. Targeting Angiogenesis in Cancer Therapy: Moving Beyond Vascular Endothelial Growth Factor. *Oncologist* 2015.

218. Giuliano, S.; Pagès, G. Mechanisms of resistance to anti-angiogenesis therapies. *Biochimie* 2013.

219. Casu, B.; Vlodavsky, I.; Sanderson, R.D. Non-anticoagulant heparins and inhibition of cancer. *Pathophysiol. Haemost. Thromb.* 2008.

220. Chen, P.-J.; Lee, P.-H.; Han, K.-H.; Fan, J.; Cheung, T.T.; Hu, R.-H.; Paik, S.W.; Lee, W.-C.; Chau, G.-Y.; Jeng, L.-B.; et al. 624PDA phase III trial of muparfostat (PI-88) as adjuvant therapy in patients with hepatitis virus related hepatocellular carcinoma (HV-HCC) after resection. *Ann. Oncol.* 2017.

221. Chow, L.Q.M.; Gustafson, D.L.; O'Bryant, C.L.; Gore, L.; Basche, M.; Holden, S.N.; Morrow, M.C.; Grolnic, S.; Creese, B.R.; Roberts, K.L.; et al. A phase I pharmacological and biological study of PI-88 and docetaxel in patients with advanced malignancies. *Cancer Chemother. Pharmacol.* 2008.

222. Lewis, K.D.; Robinson, W.A.; Millward, M.J.; Powell, A.; Price, T.J.; Thomson, D.B.; Walpole, E.T.; Haydon, A.M.; Creese, B.R.; Roberts, K.L.; et al. A phase II study of the heparanase inhibitor PI-88 in patients with advanced melanoma. *Invest. New Drugs* 2008.

223. Basche, M.; Gustafson, D.L.; Holden, S.N.; O'Bryant, C.L.; Gore, L.; Witta, S.; Schultz, M.K.; Morrow, M.; Levin, A.; Creese, B.R.; et al. A phase I biological and pharmacologic study of the heparanase inhibitor PI-88 in patients with advanced solid tumors. *Clin. Cancer Res.* 2006.

224. Joyce, J.A.; Freeman, C.; Meyer-Morse, N.; Parish, C.R.; Hanahan, D. A functional heparan sulfate mimetic implicates both heparanase and heparan sulfate in tumor angiogenesis and invasion in a mouse model of multistage cancer. *Oncogene* 2005.

225. Ferro, V.; Fewings, K.; Palermo, M.C.; Li, C. Large-scale preparation of the oligosaccharide phosphate fraction of Pichia holstii NRRL Y-2448 phosphomannan for use in the manufacture of PI-88. *Carbohydr. Res.* 2001.

226. Liang, X.J.; Yuan, L.; Hu, J.; Yu, H.H.; Li, T.; Lin, S.F.; Tang, S.B. Phosphomannopentaose sulfate (PI-88) suppresses angiogenesis by downregulating heparanase and vascular endothelial growth factor in an oxygen-induced retinal neovascularization animal model. *Mol. Vis.* 2012.

227. Dredge, K.; Hammond, E.; Handley, P.; Gonda, T.J.; Smith, M.T.; Vincent, C.; Brandt, R.; Ferro, V.; Bytheway, I. PG545, a dual heparanase and angiogenesis inhibitor, induces potent anti-tumour and anti-metastatic efficacy in preclinical models. *Br. J. Cancer* 2011.

228. Jung, D.B.; Yun, M.; Kim, E.O.; Kim, J.; Kim, B.; Jung, J.H.; Wang, E.; Mukhopadhyay, D.; Hammond, E.; Dredge, K.; et al. The heparan sulfate mimetic PG545 interferes with Wnt/β-catenin signaling and significantly suppresses pancreatic tumorigenesis alone and in combination with gemcitabine. *Oncotarget* 2015.

229. Winterhoff, B.; Freyer, L.; Hammond, E.; Giri, S.; Mondal, S.; Roy, D.; Teoman, A.; Mullany, S.A.; Hoffmann, R.; Von Bismarck, A.; et al. PG545 enhances anti-cancer activity of chemotherapy in ovarian models and increases surrogate biomarkers such as VEGF in preclinical and clinical plasma samples. *Eur. J. Cancer* 2015.

230. Hammond, E.; Brandt, R.; Dredge, K. PG545, a Heparan Sulfate Mimetic, Reduces Heparanase Expression In Vivo, Blocks Spontaneous Metastases and Enhances Overall Survival in the 4T1 Breast Carcinoma Model. *PLoS One* 2012.

231. Zhou, H.; Roy, S.; Cochran, E.; Zouaoui, R.; Chu, C.L.; Duffner, J.; Zhao, G.; Smith, S.; Galcheva-Gargova, Z.; Karlgren, J.; et al. M402, a novel Heparan sulfate mimetic, targets multiple pathways implicated in tumor progression and metastasis. *PLoS One* 2011.

232. Galli, M.; Magen, H.; Einsele, H.; Chatterjee, M.; Grasso, M.; Specchia, G.; Barbieri, P.; Paoletti, D.; Pace, S.; Sanderson, R.D.; et al. Roneparstat (SST0001), an Innovative Heparanase (HPSE) Inhibitor for Multiple Myeloma (MM) Therapy: First in Man Study. *Blood* 2015.

233. Pala, D.; Rivara, S.; Mor, M.; Milazzo, F.M.; Roscilli, G.; Pavoni, E.; Giannini, G. Kinetic analysis and molecular modeling of the inhibition mechanism of roneparstat (SST0001) on human heparanase. *Glycobiology* 2016.

234. Ritchie, J.P.; Ramani, V.C.; Ren, Y.; Naggi, A.; Torri, G.; Casu, B.; Penco, S.; Pisano, C.; Carminati, P.; Tortoreto, M.; et al. SST0001, a chemically modified heparin, inhibits myeloma growth and angiogenesis via disruption of the heparanase/syndecan-1 axis. *Clin. Cancer Res.* 2011.

235. Dredge, K.; Hammond, E.; Davis, K.; Li, C.P.; Liu, L.; Johnstone, K.; Handley, P.; Wimmer, N.; Gonda, T.J.; Gautam, A.; et al. The PG500 series: Novel heparan sulfate mimetics as potent angiogenesis and heparanase inhibitors for cancer therapy. *Invest. New Drugs* 2010.

236. Johnstone, K.D.; Karoli, T.; Liu, L.; Dredge, K.; Copeman, E.; Li, C.P.; Davis, K.; Hammond, E.; Bytheway, I.; Kostewicz, E.; et al. Synthesis and Biological Evaluation of Polysulfated Oligosaccharide Glycosides as Inhibitors of Angiogenesis and Tumor Growth. *J. Med. Chem.* 2010.

237. Hossain, M.M.; Hosono-Fukao, T.; Tang, R.; Sugaya, N.; van Kuppevelt, T.H.; Jenniskens, G.J.; Kimata, K.; Rosen, S.D.; Uchimura, K. Direct detection of HSulf-1 and HSulf-2 activities on extracellular heparan sulfate and their inhibition by PI-88. *Glycobiology* 2009.

238. Demir, M.; Iqbal, O.; Hoppensteadt, D.A.; Piccolo, P.; Ahmad, S.; Schultz, C.L.; Fareed, J.; Linhardt, R.J. Anticoagulant and antiprotease profiles of a novel natural heparinomimetic mannopentaose phosphate sulfate (PI-88). *Clin. Appl. Thromb.* 2001.

239. Ferro, V.; Liu, L.; Johnstone, K.D.; Wimmer, N.; Karoli, T.; Handley, P.; Rowley, J.; Dredge, K.; Li, C.P.; Hammond, E.; et al. Discovery of PG545: A highly potent and simultaneous inhibitor of angiogenesis, tumor growth, and metastasis. *J. Med. Chem.* 2012.

240. Mulloy, B.; Hogwood, J.; Gray, E.; Lever, R.; Page, C.P. Pharmacology of Heparin and Related Drugs. *Pharmacol. Rev.* 2015.

241. Türk, H.; Haag, R.; Alban, S. Dendritic Polyglycerol Sulfates as New Heparin Analogues and Potent Inhibitors of the Complement System. *Bioconjug. Chem.* 2004.

242. Sunder, A.; Frey, H.; Mülhaupt, R. Hyperbranched polyglycerols by ring-opening multibranching polymerization. In Proceedings of the Macromolecular Symposia; 2000.

243. Sunder, A.; Mülhaupt, R.; Haag, R.; Frey, H. Chiral hyperbranched dendron analogues. *Macromolecules* 2000.

244. Kainthan, R.K.; Janzen, J.; Levin, E.; Devine, D. V.; Brooks, D.E. Biocompatibility testing of branched and linear polyglycidol. *Biomacromolecules* 2006.

245. Rades, N.; Licha, K.; Haag, R. Dendritic polyglycerol sulfate for therapy and diagnostics. *Polymers (Basel).* 2018.

246. Dernedde, J.; Rausch, A.; Weinhart, M.; Enders, S.; Tauber, R.; Licha, K.; Schirner, M.; Zugel, U.; von Bonin, A.; Haag, R. Dendritic polyglycerol sulfates as multivalent inhibitors of inflammation. *Proc. Natl. Acad. Sci.* 2010.

247. Silberreis, K.; Niesler, N.; Rades, N.; Haag, R.; Dernedde, J. Sulfated Dendritic Polyglycerol Is a Potent Complement Inhibitor. *Biomacromolecules* 2019.

248. Weinhart, M.; Gröger, D.; Enders, S.; Riese, S.B.; Dernedde, J.; Kainthan, R.K.; Brooks, D.E.; Haag, R. The Role of Dimension in Multivalent Binding Events: Structure-Activity Relationship of Dendritic Polyglycerol Sulfate Binding to L-Selectin in Correlation with Size and Surface Charge Density. *Macromol. Biosci.* 2011.

249. Paulus, F.; Schulze, R.; Steinhilber, D.; Zieringer, M.; Steinke, I.; Welker, P.; Licha, K.; Wedepohl, S.; Dernedde, J.; Haag, R. The effect of polyglycerol sulfate branching on inflammatory processes. *Macromol. Biosci.* 2014.

250. Gröger, D.; Kerschnitzki, M.; Weinhart, M.; Reimann, S.; Schneider, T.; Kohl, B.; Wagermaier, W.; Schulze-Tanzil, G.; Fratzl, P.; Haag, R. Selectivity in Bone Targeting with Multivalent Dendritic Polyanion Dye Conjugates. *Adv. Healthc. Mater.* 2014.

251. Reimann, S.; Schneider, T.; Welker, P.; Neumann, F.; Licha, K.; Schulze-Tanzil, G.; Wagermaier, W.; Fratzl, P.; Haag, R. Dendritic polyglycerol anions for the selective targeting of native and inflamed articular cartilage. *J. Mater. Chem. B* 2017.

252. Schneider, T.; Welker, P.; Licha, K.; Haag, R.; Schulze-Tanzil, G. Influence of dendritic polyglycerol sulfates on knee osteoarthritis: An experimental study in the rat osteoarthritis model. *BMC Musculoskelet. Disord.* 2015.

253. Licha, K.; Welker, P.; Weinhart, M.; Wegner, N.; Kern, S.; Reichert, S.; Gemeinhardt, I.; Weissbach, C.; Ebert, B.; Haag, R.; et al. Fluorescence imaging with multifunctional polyglycerol sulfates: Novel polymeric near-IR probes targeting inflammation. *Bioconjug. Chem.* 2011.

254. Biffi, S.; Dal Monego, S.; Dullin, C.; Garrovo, C.; Bosnjak, B.; Licha, K.; Welker, P.; Epstein, M.M.; Alves, F. Dendritic Polyglycerolsulfate Near Infrared Fluorescent (NIRF) Dye Conjugate for Non-Invasively Monitoring of Inflammation in an Allergic Asthma Mouse Model. *PLoS One* 2013, *8*.

255. Pant, K.; Gröger, D.; Bergmann, R.; Pietzsch, J.; Steinbach, J.; Graham, B.; Spiccia, L.; Berthon, F.; Czarny, B.; Devel, L.; et al. Synthesis and biodistribution studies of ^{3}H- and ^{64}Cu-Labeled dendritic polyglycerol and dendritic polyglycerol sulfate. *Bioconjug. Chem.* 2015.

256. Reimann, S.; Gröger, D.; Kühne, C.; Riese, S.B.; Dernedde, J.; Haag, R. Shell Cleavable Dendritic Polyglycerol Sulfates Show High Anti-Inflammatory Properties by Inhibiting L-Selectin Binding and Complement Activation. *Adv. Healthc. Mater.* 2015.

257. Gröger, D.; Paulus, F.; Licha, K.; Welker, P.; Weinhart, M.; Holzhausen, C.; Mundhenk, L.; Gruber, A.D.; Abram, U.; Haag, R. Synthesis and biological evaluation of radio and dye labeled amino functionalized dendritic polyglycerol sulfates as multivalent anti-inflammatory compounds. *Bioconjug. Chem.* 2013.

258. Sousa-Herves, A.; Würfel, P.; Wegner, N.; Khandare, J.; Licha, K.; Haag, R.; Welker, P.; Calderón, M. Dendritic polyglycerol sulfate as a novel platform for paclitaxel delivery: Pitfalls of ester linkage. *Nanoscale* 2015.

259. Ferber, S.; Tiram, G.; Sousa-Herves, A.; Eldar-Boock, A.; Krivitsky, A.; Scomparin, A.; Yeini, E.; Ofek, P.; Ben-Shushan, D.; Vossen, L.I.; et al. Co-targeting the tumor endothelium and P-selectin-expressing glioblastoma cells leads to a remarkable therapeutic outcome. *Elife* 2017.

260. Zhong, Y.; Dimde, M.; Stöbener, D.; Meng, F.; Deng, C.; Zhong, Z.; Haag, R. Micelles with Sheddable Dendritic Polyglycerol Sulfate Shells Show Extraordinary Tumor Targetability and Chemotherapy in Vivo. *ACS Appl. Mater. Interfaces* 2016.

261. L. Bolognesi, M. Polypharmacology in a Single Drug: Multitarget Drugs. *Curr. Med. Chem.* 2013.

262. Nikolaou, M.; Pavlopoulou, A.; Georgakilas, A.G.; Kyrodimos, E. The challenge of drug resistance in cancer treatment: a current overview. *Clin. Exp. Metastasis* 2018.

263. Ramsay, R.R.; Popovic-Nikolic, M.R.; Nikolic, K.; Uliassi, E.; Bolognesi, M.L. A perspective on multi-target drug discovery and design for complex diseases. *Clin. Transl. Med.* 2018.

264. Bolognesi, M.L.; Cavalli, A. *ChemMedChem*. 2016,.

265. Piccinini, F.; Tesei, A.; Arienti, C.; Bevilacqua, A. Cancer multicellular spheroids: Volume assessment from a single 2D projection. *Comput. Methods Programs Biomed.* 2015.

266. Koskela, E. V.; Frey, A.D. Homologous Recombinatorial Cloning Without the Creation of Single-Stranded Ends: Exonuclease and Ligation-Independent Cloning (ELIC). *Mol. Biotechnol.* 2015.

267. Ziem, B.; Thien, H.; Achazi, K.; Yue, C.; Stern, D.; Silberreis, K.; Gholami, M.F.; Beckert, F.; Gröger, D.; Mülhaupt, R.; et al. Highly Efficient Multivalent 2D Nanosystems for Inhibition of Orthopoxvirus Particles. *Adv. Healthc. Mater.* 2016.

268. Hammond, E.; Li, C.P.; Ferro, V. Development of a colorimetric assay for heparanase activity suitable for kinetic analysis and inhibitor screening. *Anal. Biochem.* 2010.

269. Friedrich, J.; Seidel, C.; Ebner, R.; Kunz-Schughart, L.A. Spheroid-based drug screen: Considerations and practical approach. *Nat. Protoc.* 2009.

270. Schirrmacher, V. From chemotherapy to biological therapy: A review of novel concepts to reduce the side effects of systemic cancer treatment (Review). *Int. J. Oncol.* 2019.

271. Montero, A.J.; Escobar, M.; Lopes, G.; Glück, S.; Vogel, C. Bevacizumab in the treatment of metastatic breast cancer: Friend or foe? *Curr. Oncol. Rep.* 2012.

272. Harrison, P.T.; Huang, P.H. Exploiting vulnerabilities in cancer signalling networks to combat targeted therapy resistance. *Essays Biochem.* 2018.

273. Licha, K.; Welker, P.; Weinhart, M.; Wegner, N.; Kern, S.; Reichert, S.; Gemeinhardt, I.; Weissbach, C.; Ebert, B.; Haag, R.; et al. Fluorescence imaging with multifunctional polyglycerol sulfates: Novel polymeric near-IR probes targeting inflammation. *Bioconjug. Chem.* 2011.

274. Couvé-Privat, S.; Le Bret, M.; Traiffort, E.; Queille, S.; Coulombe, J.; Bouadjar, B.; Avril, M.F.; Ruat, M.; Sarasin, A.; Daya-Grosjean, L. Functional analysis of novel sonic hedgehog gene mutations identified in basal cell carcinomas from xeroderma pigmentosum patients. *Cancer Res.* 2004.

275. Ohlig, S.; Farshi, P.; Pickhinke, U.; van den Boom, J.; Höing, S.; Jakuschev, S.; Hoffmann, D.; Dreier, R.; Schöler, H.R.; Dierker, T.; et al. Sonic hedgehog shedding results in functional activation of the solubilized protein. *Dev. Cell* 2011.

276. Zhang, F.; McLellan, J.S.; Ayala, A.M.; Leahy, D.J.; Linhardt, R.J. Kinetic and structural studies on interactions between heparin or heparan sulfate and proteins of the hedgehog signaling pathway. *Biochemistry* 2007.

277. Chen, J.K.; Taipale, J.; Young, K.E.; Maiti, T.; Beachy, P.A. Small molecule modulation of Smoothened activity. *Proc. Natl. Acad. Sci.* 2002, *99*, 14071–14076.

278. Spinella-Jaegle, S.; Rawadi, G.; Kawai, S.; Gallea, S.; Faucheu, C.; Mollat, P.; Courtois, B.; Bergaud, B.; Ramez, V.; Blanchet, A.M.; et al. Sonic hedgehog increases the commitment of pluripotent mesenchymal cells into the osteoblastic lineage and abolishes adipocytic differentiation. *J. Cell Sci.* 2001.

279. Katsuura, M.; Hosono-Sakuma, Y.; Wagatsuma, M.; Yanagisawa, S.; Okazaki, M.; Kimura, M. The NH2-terminal region of the active domain of sonic hedgehog is necessary for its signal transduction. *FEBS Lett.* 1999.

280. Kinto, N.; Iwamoto, M.; Enomoto-Iwamoto, M.; Noji, S.; Ohuchi, H.; Yoshioka, H.; Kataoka, H.; Wada, Y.; Yuhao, G.; Takahashi, H.E.; et al. Fibroblasts expressing Sonic hedgehog induce osteoblast differentiation and ectopic bone formation. *FEBS Lett.* 1997.

281. Nakamura, T.; Aikawa, T.; Iwamoto-Enomoto, M.; Iwamoto, M.; Higuchi, Y.; Maurizio, P.; Kinto, N.; Yamaguchi, A.; Noji, S.; Kurisu, K.; et al. Induction of osteogenic differentiation by hedgehog proteins. *Biochem. Biophys. Res. Commun.* 1997.

282. Lauth, M.; Bergström, Å.; Shimokawa, T.; Toftgård, R. Inhibition of GLI-mediated transcription and tumor cell growth by small-molecule antagonists. *Proc. Natl. Acad. Sci. U. S. A.* 2007.

283. Lin, G.L.; Hankenson, K.D. Integration of BMP, Wnt, and notch signaling pathways in osteoblast differentiation. *J. Cell. Biochem.* 2011.

284. Rahman, M.S.; Akhtar, N.; Jamil, H.M.; Banik, R.S.; Asaduzzaman, S.M. TGF-β/BMP signaling and other molecular events: Regulation of osteoblastogenesis and bone formation. *Bone Res.* 2015.

285. Zhao, M.; Qiao, M.; Harris, S.E.; Chen, D.; Oyajobi, B.O.; Mundy, G.R. The Zinc Finger Transcription Factor Gli2 Mediates Bone Morphogenetic Protein 2 Expression in Osteoblasts in Response to Hedgehog Signaling. *Mol. Cell. Biol.* 2006.

286. Hu, H.; Hilton, M.J.; Tu, X.; Yu, K.; Ornitz, D.M.; Long, F. Sequential roles of Hedgehog and Wnt signaling in osteoblast development. *Development* 2005.

287. Rawadi, G.; Vayssière, B.; Dunn, F.; Baron, R.; Roman-Roman, S. BMP-2 Controls Alkaline Phosphatase Expression and Osteoblast Mineralization by a Wnt Autocrine Loop. *J. Bone Miner. Res.* 2003.

288. Smith, R.A.A.; Murali, S.; Rai, B.; Lu, X.; Lim, Z.X.H.; Lee, J.J.L.; Nurcombe, V.; Cool, S.M. Minimum structural requirements for BMP-2-binding of heparin oligosaccharides. *Biomaterials* 2018.

289. Ruppert, R.; Hoffmann, E.; Sebald, W. Human bone morphogenetic protein 2 contains a heparin-binding site which modifies its biological activity. *Eur. J. Biochem.* 1996.

290. Binari, R.C.; Staveley, B.E.; Johnson, W.A.; Godavarti, R.; Sasisekharan, R.; Manoukian, A.S. Genetic evidence that heparin-like glycosaminoglycans are involved in wingless signaling. *Development* 1997.

291. Malinauskas, T.; Aricescu, A.R.; Lu, W.; Siebold, C.; Jones, E.Y. Modular mechanism of Wnt signaling inhibition by Wnt inhibitory factor 1. *Nat. Struct. Mol. Biol.* 2011.

292. Konitsiotis, A.D.; Chang, S.C.; Jovanovic, B.; Ciepla, P.; Masumoto, N.; Palmer, C.P.; Tate, E.W.; Couchman, J.R.; Magee, A.I. Attenuation of hedgehog acyltransferase-catalyzed sonic hedgehog palmitoylation causes reduced signaling, proliferation and invasiveness of human carcinoma cells. *PLoS One* 2014.

293. Singh, B.N.; Fu, J.; Srivastava, R.K.; Shankar, S. Hedgehog signaling antagonist GDC-0449 (Vismodegib) inhibits pancreatic cancer stem cell characteristics: Molecular mechanisms. *PLoS One* 2011.

294. Matevossian, A.; Resh, M.D. Hedgehog Acyltransferase as a target in estrogen receptor positive, HER2 amplified, and tamoxifen resistant breast cancer cells. *Mol. Cancer* 2015.

295. Koga, K.; Nakamura, M.; Nakashima, H.; Akiyoshi, T.; Kubo, M.; Sato, N.; Kuroki, S.; Nomura, M.; Tanaka, M.; Katano, M. Novel link between estrogen receptor α and hedgehog pathway in breast cancer. *Anticancer Res.* 2008.

296. Bermudez, O.; Hennen, E.; Koch, I.; Lindner, M.; Eickelberg, O. Gli1 Mediates Lung Cancer Cell Proliferation and Sonic Hedgehog-Dependent Mesenchymal Cell Activation. *PLoS One* 2013.

297. Singh, S.; Wang, Z.; Fei, D.L.; Black, K.E.; Goetz, J.A.; Tokhunts, R.; Giambelli, C.; Rodriguez-Blanco, J.; Long, J.; Lee, E.; et al. Hedgehog-producing cancer cells respond to and require autocrine hedgehog activity. *Cancer Res.* 2011.

298. Single, A.; Beetham, H.; Telford, B.J.; Guilford, P.; Chen, A. A comparison of real-time and endpoint cell viability assays for improved synthetic lethal drug validation. *J. Biomol. Screen.* 2015.

299. Hoarau-Véchot, J.; Rafii, A.; Touboul, C.; Pasquier, J. Halfway between 2D and animal models: Are

3D cultures the ideal tool to study cancer-microenvironment interactions? *Int. J. Mol. Sci.* 2018.

300. Lin, R.Z.; Chang, H.Y. Recent advances in three-dimensional multicellular spheroid culture for biomedical research. *Biotechnol. J.* 2008.

301. Weiswald, L.B.; Bellet, D.; Dangles-Marie, V. Spherical Cancer Models in Tumor Biology. *Neoplasia (United States)* 2015.

302. Costa, E.C.; Moreira, A.F.; de Melo-Diogo, D.; Gaspar, V.M.; Carvalho, M.P.; Correia, I.J. 3D tumor spheroids: an overview on the tools and techniques used for their analysis. *Biotechnol. Adv.* 2016.

303. Nederman, T.; Glimelius, B.; Norling, B.; Carlsson, J.; Brunk, U. Demonstration of an Extracellular Matrix in Multicellular Tumor Spheroids. *Cancer Res.* 1984.

304. Bai, C.; Yang, M.; Fan, Z.; Li, S.; Gao, T.; Fang, Z. Associations of chemo- and radio-resistant phenotypes with the gap junction, adhesion and extracellular matrix in a three-dimensional culture model of soft sarcoma. *J. Exp. Clin. Cancer Res.* 2015.

305. GLIMELIUS, B.; NORLING, B.; NEDERMAN, T.; CARLSSON, J. Extracellular matrices in multicellular spheroids of human glioma origin: Increased incorporation of proteoglycans and flbronectin as compared to monolayer cultures. *APMIS* 1988.

306. Powan, P.; Luanpitpong, S.; He, X.; Rojanasakul, Y.; Chanvorachote, P. Detachment-induced E-cadherin expression promotes 3D tumor spheroid formation but inhibits tumor formation and metastasis of lung cancer cells. *Am. J. Physiol. - Cell Physiol.* 2017.

307. Loessner, D.; Stok, K.S.; Lutolf, M.P.; Hutmacher, D.W.; Clements, J.A.; Rizzi, S.C. Bioengineered 3D platform to explore cell-ECM interactions and drug resistance of epithelial ovarian cancer cells. *Biomaterials* 2010.

308. Bewersdorff, T.; Vonnemann, J.; Kanik, A.; Haag, R.; Haase, A. The influence of surface charge on serum protein interaction and cellular uptake: Studies with dendritic polyglycerols and dendritic polyglycerol-coated gold nanoparticles. *Int. J. Nanomedicine* 2017.

309. Reichert, S.; Welker, P.; Calderón, M.; Khandare, J.; Mangoldt, D.; Licha, K.; Kainthan, R.K.; Brooks, D.E.; Haag, R. Size-dependant cellular uptake of dendritic polyglycerol. *Small* 2011.

310. MacDonald, A.; Priess, M.; Curran, J.; Guess, J.; Farutin, V.; Oosterom, I.; Chu, C.L.; Cochran, E.; Zhang, L.; Getchell, K.; et al. Necuparanib, a multitargeting heparan sulfate mimetic, targets tumor and stromal compartments in pancreatic cancer. *Mol. Cancer Ther.* 2019.

311. Krause, S.; Weyers, A.; Loveluck, K.; Schultes, B. Abstract 5499: Necuparanib affects tumor progression and invasion in a 3D co-culture system of pancreatic cancer cells and stellate cells.; 2015.

312. Blumlein, A.; Williams, N.; McManus, J.J. The mechanical properties of individual cell spheroids. *Sci. Rep.* 2017.

313. Gaskell, H.; Sharma, P.; Colley, H.E.; Murdoch, C.; Williams, D.P.; Webb, S.D. Characterization of a functional C3A liver spheroid model. *Toxicol. Res. (Camb).* 2016.

314. Edmondson, R.; Broglie, J.J.; Adcock, A.F.; Yang, L. Three-dimensional cell culture systems and their applications in drug discovery and cell-based biosensors. *Assay Drug Dev. Technol.* 2014.

315. Karlsson, H.; Fryknäs, M.; Larsson, R.; Nygren, P. Loss of cancer drug activity in colon cancer HCT-116 cells during spheroid formation in a new 3-D spheroid cell culture system. *Exp. Cell Res.* 2012.

316. Mach, H.; Middaugh, C.R. Probing the Affinity of Polyanions for Acidic Fibroblast Growth Factor by Unfolding Kinetics. *Arch. Biochem. Biophys.* 1994.

317. Kamei, K.; Wu, X.; Xu, X.; Minami, K.; Huy, N.T.; Takano, R.; Kato, H.; Hara, S. The analysis of heparin-protein interactions using evanescent wave biosensor with regioselectively desulfated heparins as the ligands. *Anal. Biochem.* 2001.

318. Francis, D.J.; Parish, C.R.; McGarry, M.; Santiago, F.S.; Lowe, H.C.; Brown, K.J.; Bingley, J.A.; Hayward, I.P.; Cowden, W.B.; Campbell, J.H.; et al. Blockade of vascular smooth muscle cell proliferation and intimal thickening after balloon injury by the sulfated oligosaccharide PI-88: phosphomannopentaose sulfate directly binds FGF-2, blocks cellular signaling, and inhibits

proliferation. *Circ. Res.* 2003.

319. Shiga, M.; Saito, M.; Hattori, M.; Torii, C.; Kosaki, K.; Kiyono, T.; Suda, N.; Iancu, E.M.; Speiser, D.E.; Rufer, N.; et al. Characteristic phenotype of immortalized periodontal cells isolated from a Marfan syndrome type I patient\rAssessing ageing of individual T lymphocytes: Mission impossible?\rFacile Synthesis of Naphthoquinone Spiroketals by Diastereoselective Oxidative [3. *Cell Tissue Res* 2007.

320. Cochran, S.; Li, C.P.; Ferro, V. A surface plasmon resonance-based solution affinity assay for heparan sulfate-binding proteins. *Glycoconj. J.* 2009.

321. Nakajima, M.; DeChavigny, A.; Johnson, C.E.; Hamada, J.I.; Stein, C.A.; Nicolson, G.L. Suramin: A potent inhibitor of melanoma heparanase and invasion. *J. Biol. Chem.* 1991.

322. Irimura, T.; Nakaiima, M.; Nicolson, G.L. Chemically Modified Heparins as Inhibitors of Heparan Sulfate Specific Endo-β-glucuronidase (Heparanase) of Metastatic Melanoma Cells. *Biochemistry* 1986.

323. Parish, C.R.; Coombe, D.R.; Jakobsen, K.B.; Bennett, F.A.; Underwood, P.A. Evidence that sulphated polysaccharides inhibit tumour metastasis by blocking tumour-cell-derived heparanases. *Int. J. Cancer* 1987.

324. Loka, R.S.; Yu, F.; Sletten, E.T.; Nguyen, H.M. Design, synthesis, and evaluation of heparan sulfate mimicking glycopolymers for inhibiting heparanase activity. *Chem. Commun.* 2017.

325. Bompais, H.; Chagraoui, J.; Canron, X.; Crisan, M.; Liu, X.H.; Anjo, A.; Tolla-Le Port, C.; Leboeuf, M.; Charbord, P.; Bikfalvi, A.; et al. Human endothelial cells derived from circulating progenitors display specific functional properties compared with mature vessel wall endothelial cells. *Blood* 2004.

326. Sahni, A.; Francis, C.W. Vascular endothelial growth factor binds to fibrinogen and fibrin and stimulates endothelial cell proliferation. *Blood* 2000.

327. Selbonne, S.; Azibani, F.; Iatmanen, S.; Boulaftali, Y.; Richard, B.; Jandrot-Perrus, M.; Bouton, M.-C.; Arocas, V. In Vitro and In Vivo Antiangiogenic Properties of the Serpin Protease Nexin-1. *Mol. Cell. Biol.* 2012.

328. Jih, Y.J.; Lien, W.H.; Tsai, W.C.; Yang, G.W.; Li, C.; Wu, L.W. Distinct regulation of genes by bFGF and VEGF-A in endothelial cells. *Angiogenesis* 2001.

329. Ferro, V.; Dredge, K.; Liu, L.; Hammond, E.; Bytheway, I.; Li, C.; Johnstone, K.; Karoli, T.; Davis, K.; Copeman, E.; et al. PI-88 and novel heparan sulfate mimetics inhibit angiogenesis. In Proceedings of the Seminars in Thrombosis and Hemostasis; 2007.

8 List of publications

Presentation

"Dendritic polyglycerol sulfates as modulators of Sonic Hedgehog signaling pathway". International conference Biobarrier 2018, Saarbrücken, Germany. August 2018.

"Dendritic polyglycerol sulfates: modulators of cancer signaling pathways". Doktorandentag SFB 765. Berlin, Germany. March 2017.

Posters

Rossi S., Chowdhury S., Kühne C., Kumari S., Donskyi I., Haag R. & Dernedde J. "Tumorigenesis inhibition via dendritic polyglycerol sulfate: interfering with Shh-signaling pathway and angiogenesis." 5th International Symposium of SFB765 "Multivalency in Chemistry and Biology". Berlin, Germany. October 2019.

Rossi S., Chowdhury S., Kühne C., Albring K. F., Reimann S., Haag R. & Dernedde J. "Dendritic Polyglycerol Sulfates as potential Hedgehog pathway inhibitors" International conference Biobarrier 2018, Saarbrücken, Germany. August 2018.

Rossi S., Chowdhury S., Kühne C., Albring K. F., Reimann S., Haag R. & Dernedde "Dendritic polyglycerol sulfates as potential Sonic Hedgehog pathway´s inhibitors". Doktorandentag SF765. Berlin, Germany, March 2018

Rossi S., Kühne C., Albring K. F., Reimann S., Haag R. & Dernedde J. Dendritic Polyglycerol Sulfates as potential Hedgehog pathway inhibitors". International conference "Sharing radically novel visions in Cancer", Berlin, Germany. June 2017.

Publications

Serena Rossi, Ievgen Donskyi, Raineer Haag & Jens Dernedde. "Dendritic polyglycerol sulfate targets multiple pathways involved in tumor progression and angiogenesis". *In preparation*

9 Curriculum vitae

For reasons of data protection,

the curriculum vitae is not published in the electronic version

For reasons of data protection,

the curriculum vitae is not published in the electronic version

For reasons of data protection,

the curriculum vitae is not published in the electronic version

10 Acknowledgments

A long and difficult journey, with many ups and downs, comes to an end. This would not have been possible without the precious help and the support of my first supervisor Dr. Jens Dernedde, who guided me thought this intricated path. As well fundamental is the contribution of Prof. Dr. Rainer Haag, my second supervisor, who gave me the opportunity to pursue my Ph.D. and always offered many good suggestions for my research. I would like to profoundly thank Dr. Nicole Niesler for her constant support, scientifically, emotionally, as a friend, as a valuable scientist. My scientific development counted as well on the help of Dr. Kai Frederik Albring, who initially designed the Shh project and helped me incredibly during the beginning of my research to build up the base of my scientific method. My formal colleagues Dr. Christian Kühne and Dr. Sebastian Reise contributed as well to this work and to my scientific development, giving me important advice, introducing me to many new techniques and overall bringing joy and laughs to the lab! I would like to thank my friend and colleague, Dr. Shalini Kumari, for her help with the SPR, for the long talks about life, science, and yoga, for being one of the purest and toughest person I have ever met!

Many times, during this journey, I lost my strengths. In those moments there were always my friends Carlotta and Valeria. To say that they supported me is reductive. I can just say I´m lucky I have met these two beautiful persons and I am extremely honored to share life with them. Mamma and Babbo were also always there, they gave me strength, they supported me incredibly. They loved me and just wanted my joy overall. No matter what!

And finally, to the biggest contributor to this work: my partner Jonas. He does not like to hear it, but again, this would have not been possible without you.

To all of you, to the stranger who gave me a smile, to myself: THANKS!

Declaration

I, Serena Rossi, declare that the doctoral thesis entitled " Evaluation of dendritic polyglycerol sulfate as inhibitor of sonic hedgehog and further pro-tumorigenic factors" contains no material that has been submitted previously, in whole or in part, for the award of any other academic degree or diploma. I would hereby like to confirm that there is no conflict of interest in the present study of any kind. Except where otherwise indicated, this thesis is my own original work.

Serena Rossi

Berlin, 2020